multi-Risk sciEnce for resilienT commUnities undeR a changiNgclimate

Codice progetto MUR: **PE00000005** – CUP LEAD PARTNER H93C22000610002

Deliverable title

Data processing and analysis by the implementation of a geodatabase in advanced computing cloud systems

Deliverable ID: DV 2.2.4

Due date: May 31, 2024

Submission date: May 29, 2024

AUTHORS

Mario Parise (UNIBA); Matteo Berti (UNIBO); Giuseppe Ciccarese (UNIBO); Riccardo Fanti (UNIFI); Isabella Serena Liso (UNIBA); Giovanni Forte (UNINA); Elena Scacchia (UniRoma1); partecipants to TK 2.2.2

1. Technical references

Project Acronym	RETURN
Project Title	multi-Risk sciEnce for resilienT commUnities undeR a changiNg climate
Project Coordinator	Domenico Calcaterra UNIVERSITA DEGLI STUDI DI NAPOLI FEDERICO II domcalca@unina.it
Project Duration	December 2022 – November 2025 (36 months)

Deliverable No.	DV2.2.4
Dissemination level*	PU
Work Package	WP2 - State of the art and knowledge base to define impact-oriented hazard indicators
Task	T2.2.2 - Quantitative analysis of predisposition to ground instabilities through: (a) geological, geomorphological (including erosion, transport, deposition processes), and geotechnical parameters; (b) factors controlling coastal and seafloor environment, geomorphological setting, submarine mass wasting
Lead beneficiary	UNIBA
Contributing beneficiary/ies	UNIFI, UNIBO.

* PU = Public

PP = Restricted to other programme participants (including the Commission Services)

RE = Restricted to a group specified by the consortium (including the Commission Services)

CO = Confidential, only for members of the consortium (including the Commission Services)

Document history

Version	Date	Lead contributor	Description
0.1	15.05.2024	Mario Parise (UNIBA) Matteo Berti (UNIBO) Giuseppe Ciccarese (UNIBO) Riccardo Fanti (UNIFI) Isabella Serena Liso (UNIBA) Giovanni Forte (UNINA) Elena Scacchia (Uniroma1)	First draft
0.2	24.05.2024	Riccardo Fanti (UniFI) Matteo Berti (UNIBO)	Internal Spoke review
0.3	27.05.2024	Salvatore Martino (UniRoma1) Francesca Bozzano (UniRoma1) Domenico Calcaterra (UNINA) Diego Di Martire (UNINA)	Spoke leader review
0.4	29.05.2024	Mario Parise (UNIBA) Matteo Berti (UNIBO) Riccardo Fanti (UNIFI)	Critical review and proofreading
0.5	30.05.2024	Participants to TK2.2.2	Final version

2. Abstract

This Deliverable, part of **Milestone 2.3** of Spoke 2 in the Extended Partnership RETURN Project, deals with the theme "Identification of impact-oriented indicators" as outlined in the Executive Work Plan – Milestone 2.1. It summarizes the scientific research activities conducted from November 2023 to May 2024 by Task 2.2.2 ("Quantitative analysis of predisposition to ground instabilities") of Work Package 2.2 ("State of the art and knowledge base to define impact-oriented hazard indicators"). This task is a component of the vertical spoke VS2, "Ground Instabilities", and involves 57 researchers from various institutions.

The focus of WP2 is on detecting and analysing predisposing factors to ground instabilities, while WP3 and WP4 concentrate on preparatory factors, and triggering and multiple geohazards cascading scenarios (MULTI-HAZARD), respectively. These work packages collectively aim to quantify the effects of ground instabilities on territories, buildings, and communities, and to develop an IT platform for the spatial and temporal analysis of these instabilities.

A significant phase within Task 2.2.2 involved defining Ground Instability categories, which were categorized initially into landslides, subsidence, liquefaction, and sinkholes. A more detailed differentiation was later made, particularly distinguishing between slow and fast types of ground instability in subaerial phenomena. These categories have been detailed in DV 2.2.3 and DV 2.2.5, and are fundamental in guiding the project's direction.

This Deliverable had as an overarching goal the identification of reasons, based on specific learning examples from the literature, for the identification of both soil instabilities by macro-categories of factors (predisposing, precursory, triggering) and the construction of analytical tools that can be used in a specific logical-executive order (tool chain) to design an IT platform for the recovery of spatial overlap (multiple hazard) or temporal sequence (multiple hazard, i.e. chain effects) of soil instabilities, in the PoC. This will make it possible to quantify the effects of ground instabilities in terms of their impact on buildings and communities and to assess their suitability and reliability. Further, this assessment aims to understand the extent to which soil instability can jeopardise the safety and stability of building structures and affect the well-being of the people living there. Using appropriate models and methods, experts can then assess the likelihood and extent of potential damage and develop strategies to mitigate the associated risks. Essentially, the analysis of this DV provides an empirical basis for informed decisions regarding land planning and emergency management, contributing to the safety and sustainability of communities.

3. Table of contents

1. Technical references 2

Document history 3

2. Abstract 4

3. Table of contents 5

4. Introduction 6

4.1 Project framework 6

5. Internal validation 9

5.1 Methods 9

5.2 Internal validation - Tuscany 10

5.3 Internal validation – Messina area 14

5.4 Internal validation – Assi landslides (Calabria) 17

5.5 Internal validation – Crotone mega-landslide (Calabria) 21

5.6 Internal validation – Gioia Tauro (Calabria) 25

5.7 Internal validation – Guidonia – Bagni di Tivoli Plain (central Italy) 27

5.8 Internal validation – Altamura sinkholes (Apulia) 31

5.9 Internal validation – Liquefaction in Emilia-Romagna 35

5.10 Insight on submarine landslides 41

5.10.1 Review of landslide susceptibility methods in marine environments 41

5.10.2 Feasibility of the selected methods for susceptibility assessment in the marine environment 42

5.10.3. From predisposing factors to susceptibility maps input data 43

6. Conclusions 47

7. References 49

Addendum 55

4. Introduction

This Deliverable was created as part of **Milestone 2.3** of Spoke 2, which has the topic (from the Executive Work Plan) "Identification of impact-oriented indicators". The deliverables of Spoke 2 for this milestone have therefore set as an overarching goal the identification of reasons, based on specific learning examples from the literature, for the identification of both soil instabilities by macro-categories of factors (predisposing, precursory, triggering) and the construction of analytical tools that can be used in a specific logical-executive order (tool chain) to design an IT platform for the recovery of spatial overlap (multiple hazard) or temporal sequence (multiple hazard, i.e. chain effects) of soil instabilities, in the PoC. This will make it possible to quantify the effects of ground instabilities on the area in terms of their impact on buildings and communities and to assess their suitability and reliability. Further, this assessment aims to understand the extent to which soil instability can jeopardise the safety and stability of building structures and affect the well-being of the people living there. Using appropriate models and methods, experts can then assess the likelihood and extent of potential damage and develop strategies to mitigate the associated risks. Essentially, the analysis of this DV provides an empirical basis for informed decisions regarding land planning and emergency management, contributing to the safety and sustainability of communities.

4.1 Project framework

This report summarizes the scientific research activities carried out in the period November 2023 – May 2024 by the **Task 2.2.2** *"Quantitative analysis of predisposition to ground instabilities through: (a) geological, geomorphological (including erosion, transport, deposition processes), and geotechnical parameters; (b) factors controlling coastal and seafloor environment, geomorphological setting, submarine mass wasting"* (hereinafter referred to as **TK2**) of the **Work Package 2.2** *"State of the art and knowledge base to define impact-oriented hazard indicators"* (hereinafter referred to as **WP2**) within the vertical spoke **VS2** "Ground Instabilities" of the Extended Partnership RETURN.

It should be noted that VS2 structured the work packages WP2, WP3 and WP4 by identifying the following areas of interest for each of them:

- WP2 focuses on the detection and analysis of **PREDISPOSING** factors to ground instabilities;
- WP3 targets **PREPARATORY** factors to ground instability;
- WP4 is centered on **TRIGGERING** and multiple geohazards cascading scenarios (**MULTI-HAZARD**).

In accordance with the definitions given within the VS2, the distinction between predisposing, preparatory and triggering factors/processes is made on a temporal basis: the predisposing factors are considered invariable on the observation scale, while the preparatory factors show changes or cyclical trends during the same period. As a consequence, a trigger is considered as a process that acts in a very short and well-defined time.

The partners involved in the **WP2** are ENEA, OGS, POLITO, UNIBA, UNIBO, UNIFI, UNIGE, UNINA, UNIPA, UNIPD and UNIROMA1. **WP2** leaders are Riccardo Fanti (UNIFI) and Mario Parise (UNIBA), **TK1** leader is Francesco Latino Chiocci (UNIROMA1), **TK2** leader is Mario Parise (UNIBA), **TK3** leader is Matteo Berti (UNIBO). 70 researchers participate in the activities of **WP2/TK2** (i.e., TK 2.2.3): 5 from ENEA, 4 from OGS, 5 from POLITO, 6 from UNIBA, 6 from UNIBO, 7 from UNIFI, 4 from UNIGE, 7 from UNINA, 12 from UNIPA, 6 from UNIPD and 8 from UNIROMA1.

The goal of **TK2** (*Quantitative analysis of predisposition to ground instabilities through: (a) geological, geomorphological (including erosion, transport, deposition processes), and geotechnical parameters; (b) factors controlling coastal and seafloor environment, geomorphological setting, submarine mass wasting*) and the issue of **DV 2.2.4** (*Data processing and analysis by the implementation of a geodatabase in advanced computing cloud systems*) have been interpreted within the framework of the entire Spoke work process.

In line with the core concept of the Project and **VS2**, the learning phase aimed to establish a framework for preparatory processes to serve as input for the Proof of Concept (PoC). This phase unfolded in three stages: firstly, compiling an inventory of Learning Examples (LEs); secondly, identifying the preparatory processes examined in each LE; and finally, formulating a rationale for each process based on the available LEs. **DV 2.2.3** (*Rationale for quantifying parameters measuring the susceptibility to ground instabilities in offshore and onshore areas*) and **DV 2.2.5** (*Rationale for selecting and scale-dependent weighting of predisposing factors*) represented the transitional descriptions from the aforementioned phases.

Following the submission of the two Rationales, our focus shifted towards developing and implementing a Proof of Concept (PoC) prototype aimed at conducting susceptibility analysis for ground instabilities. This prototype was informed by the outcomes of the internal validation of the Learning Examples (LEs) detailed in this **DV** (*Data processing and analysis through the implementation of a geodatabase in advanced computing cloud systems*).

After the delivery of the two Rationales, therefore, we started to move toward the design, set-up and tuning of scale-dependent methods, to analyze and rank the relevance of predisposing and preparatory factors based on different approaches for the quantitative assessment of the susceptibility to geo-hydrological processes, and to develop models at different scales for the forecasting of ground instability phenomena, through the hybridization of statistical and physically-based methods, and standardization of the validation procedures. The main goal is to determine the spatial proneness to ground instabilities, that should have the following features:

- be implemented for different types of Ground Instabilities;
- use methods of proven reliability, from the international literature;
- allow to include different geo-spatial data (in terms of type, resolution, scale, etc.), that were identified in the previous DVs as relevant for the specific category of ground instability;
- allow the user to personalize the analysis in a simple way, without the need to have specific knowledge of coding;
- do not use commercial software;
- be easily implemented in the PoC.

To achieve this goal, we progressed through an internal phase of validation, aimed at identifying, among the experiences of **TK2** participants, those LEs containing a sufficient amount of data to produce susceptibility maps, and that could be used, at the same time, to produce other maps through different approaches. This latter objective is fully presented in the **DV 2.2.6.** Meetings were therefore organized among the project partners in order to select some LEs for each process of Ground Instability, and to examine specific case studies at a greater detail, from which data to start for the definition of susceptibility analysis. Thus, a phase of data collection on test sites for an internal validation has been developed (going forward with respect to the initial LEs), including the basic data originally used by the individual partner to define the susceptibility maps. Aimed at data collection, a dedicated form was established by the Task Leaders for the internal validation; the form includes the following fields:

- Description of ground instability type and test area/site;
- Description of available data (type, formats, etc.);
- Description of the methodologies used to define/map susceptibility;
- Methods used for validation;
- Overall discussion: key strengths and areas for improvement;
- Figures and/or Tables (optional);
- References.

As already pointed out in the previous activities of **TK2**, the uniqueness of the theme of submerged environments was highlighted in some of the cases analyzed through internal validation in this DV. This is in accordance with the fact that **TK2** includes, at the same level, the two types of ground instability

(*"Quantitative analysis of predisposition to ground instabilities through: (a) geological, geomorphological (including erosion, transport, deposition processes), and geotechnical parameters; (b) factors controlling coastal and seafloor environment, geomorphological setting, submarine mass wasting"*).

The material included in this DV is part of the overall analysis of all ground instabilities dealt with in the Spoke, albeit with a more in-depth analysis in relation to landslides, especially the subaerial ones. The DV should be seen as preparatory and complementary to **DV 2.2.6**, which focused on the development of an interface for vulnerability analysis with user-uploaded data, as a synthesis effort to develop a proof-of-concept prototype based on the above-mentioned analysis work. The analysis and synthesis properties of spatial vulnerability to ground instability can be summarized in the following aspects, as further described in **DV 2.2.6**: a) they are applicable to all types of soil instabilities; b) they use methods whose validity has been demonstrated in the literature; c) they allow the use of different spatial data considered important for the process in question; d) they allow the user to customize the analysis in a simple way, without requiring knowledge in coding; e) they do not use commercial software or proprietary codes; f) they are easily implementable in the future Proof of Concept (PoC).

5. Internal validation

5.1 Methods

As anticipated in the introduction of this document, to determine the spatial proneness to ground instabilities we progressed through an internal phase of validation, aimed at identifying, among the experiences of **TK2** participants, those LEs containing a sufficient amount of data to produce susceptibility maps, and that could be used, at the same time, to produce other maps through different approaches (this objective is fully presented in the **DV 2.2.6).** Meetings have been organized among the project partners in order to select some LEs for each process of Ground Instability, and to examine at a greater detail specific case studies, from which data to start for the definition of susceptibility analysis. Thus, a phase of data collection on test sites for an internal validation has been developed (going forward with respect to the initial LEs), including the basic data originally used by the individual partner to define the susceptibility maps. Aimed at data collection, a dedicated form was established by the Task Leaders for the internal validation; the form includes the following fields:

- Description of ground instability type and test area/site;
- Description of available data (type, formats, etc.);
- Description of the methodologies used to define/map susceptibility;
- Methods used for validation;
- Overall discussion: key strengths and areas for improvement;
- Figures and/or Tables (optional);
- References.

Eight forms were compiled as follows:

- Different typologies of slope movements in Tuscany
- Assi landslide (Calabria)
- Submarine landslide at Gioia Tauro (Calabria)
- Crotone mega-landslide (Calabria)
- Landslides in the Messina area (Sicily)
- Sinkholes in the Guidonia – Bagni di Tivoli plain (central Italy)
- Sinkholes at Altamura (Apulia)
- Seismically-induced liquefaction in Emilia-Romagna.

In the following sections, the main data obtained from the phase of internal validation are presented. These will represent the databases on which to build the procedure shown in detail in **DV 2.2.6** *(Procedures to map the areal distribution of values of predisposing parameters)*.

5.2 Internal validation - Tuscany

The internal validation form on landslides in Tuscany was produced by colleagues from the University of Florence, that shared their experience and the work done with participants to TK 2.2.2 during the meetings held on February 29, 2024. After that meeting, and the selection of the sites for internal validation, more detailed information was provided on analysis of slope movements in Tuscany region, central Italy, and is summarized in this section.

The Region Tuscany extends over 22.994 km^2 and is characterized by extremely various landscapes in terms of morphology, from the Thyrrenian coastal plains, in the western part, to the Apennines ridge running on the border of the region from NW to SE, reaching elevation even above 2000 m a.s.l. (Monte Prado, 2054 m a.s.l.), where the topography pattern is typical of mountainous areas. The central part of the region includes hilly areas and flat territories or wide valley floors where the main rivers flow. As a whole, the climate of Tuscany is typically Mediterranean (Köppen classification, Csa), characterized by mild and moist winters and hot and dry summers. The highest values of rainfall and snowfall concentrate in the northern sector of the region, along the Apennine ridge leading to mean annual precipitations up to 2000 mm/year. In southern Tuscany, low rainfall amounts are instead recorded, and the amounts are usually lower than 600 mm/year, with low peaks of ca. 400 mm/year.

The geological setting of the region is strictly correlated with the overlapping of three main geological units: the Ligurian unit (containing deposits of Jurassic oceanic lithosphere) overlapping the Tuscan unit (composed by the Metamorphic Tuscan Units and the Non-Metamorphic Tuscan Units), that, in turn, overlaps the Umbro-Marchigian unit (consisting in a sedimentary sequence).

The landslides inventory consists of ca. 91,700 landslides, mainly slides (39%), followed by flows (14%) and fall (1%), with 46% of unclassified landslides.

As concerns the available data, it should be pointed out that an initial, expert-driven selection of the input parameters is not necessary for this area, since the feature selection procedure will automatically sort landslide conditioning variables (LCVs) according to importance ranking. Initially, two main kinds of input parameters have been used: morphometric attributes, and thematic attributes.

- Elevation (ELE). Elevation is commonly used in landslide susceptibility assessments as different altitudes may be related to different environmental settings (e.g. vegetation, temperature, rainfall regime, etc.). File .tiff (50 m of resolution).
- Slope (SLO). Slope angle is one of the most important predisposing factors as it strongly controls the shear forces acting on hillslopes, therefore it has been widely used in landslide susceptibility mapping. File .tiff (50 m of resolution).
- Profile curvature (CPR) expresses the rate at which the slope gradient changes towards the direction of maximum slope. It affects the acceleration/deceleration of superficial flux and thus the erosion/deposition of the hillslope's loose material. File .tiff (50 m of resolution).
- Plan curvature (CPL) is calculated orthogonally to the direction of the maximum slope and it can be used to characterize the convergence and divergence of flow, and to discriminate between watersheds and hollows channelized by a 0th order hydraulic network as well. File .tiff (50 m of resolution).
- Aspect (ASP). Aspect represents the orientation in the space of each pixel composing the landscape. This variable can play a key role in landslide susceptibility as it may influence the exposition of the terrain to different amounts of rainfall and solar radiation, thus conditioning the terrain humidity and the vegetation growth. In this study the aspect was used as a categorical variable after reclassifying its angular values on the basis of the facing direction with respect to the eight main cardinal directions. File .tiff (50 m of resolution).
- TWI (TWI). Topographic wetness index (TWI) is defined as $\ln(A/\tan\beta)$, where A is the aforementioned upslope contributing area (or flow accumulation) and β is the slope angle. This index is commonly used to characterize the spatial distribution of soil moisture, therefore it is used in landslide susceptibility assessments. File .tiff (50 m of resolution).

- Lithology (LIT). Lithology is largely acknowledged as one of the most important driving variables in susceptibility assessments, since it directly reflects the geo-mechanical and hydraulic properties of the bedrock and influences the characteristics of the soil coverage. A 1:100,000 litho-technical map was used in the study. File .tiff (50 m of resolution).
- Land cover (COV). Landslide susceptibility is highly influenced by the vegetation cover and the use of land may be used to indirectly account for the human interference on hillslopes. A land use map in nine classes (urban fabric; crops and permanent cultivations; grasslands; heterogeneous cultivated lands; forests; rangelands; scrublands; wetlands) was devised starting form a 1:50,000 scale land cover map. As for the lithology, the variety of land cover classes in a 3 pixel×3 pixel window was included amongst the susceptibility variables as well. File .tiff (50 m of resolution).
- Distance to rivers (RIV). The stream network is an important feature in the geomorphological setting of an area and may directly or indirectly be linked to landslides. Similarly to roads and faults, a shapefile of existing streams (Strahler order > 0) was extracted from 1:25,000 technical maps, and a raster of distances from the hydraulic network was set up. File .tiff (50 m of resolution).
- Logarithm of the drained area (LOGF). File .tiff (50 m of resolution).
- Stream Power Index (SPI). It is the amount of energy the water is exerting on the sides and bottom of a slope, and represents a measure of the superficial flux erosion capacity. File .tiff (50 m of resolution).
- Geomorphological domain. It is a qualitative information about the environmental domain in term of geomorphological slope energy. It separates the plain areas (generally with altitudes lower than 200 m above sea level) from the hilly/mountainous areas. File .tiff (50 m of resolution).
- Landslide inventory. Polygonal shapefile .shp.

As a basic model for landslide susceptibility maps (LSM), a random forest implementation based on Matlab was used. Random forest (RF) classification is basically a machine-learning algorithm for non-parametric multi-variate classification. The algorithm exploits random binary trees which use a subset of the observations through bootstrapping techniques: from the original data set a random selection of the training data is sampled and used to build the model, and the data not included are referred to as "out-of-bag" (OOB). Furthermore, a random selection of predictor variables is used to split each node of the trees. Each tree is developed so as to minimize classification errors but the random selection influences the results, thus making a single-tree classification very unstable. For this reason, the RF-type methods make use of an ensemble of trees (the so-called "forest"), thereby ensuring model stability.

A single realization of a RF model ends up in a forest structure whose tree number T# is usually established by the user. There is no specific rule, nor a best a priori value for T# and, even with complex classification or regression models, there is no guarantee that the accuracy of the results would increase proportionally with T#. In the case of prediction of landslide susceptibility at the regional scale, there is in general a problem of unknown a priori complexity which demands a strong computational effort. Therefore, in applying a RF-type method, a preliminary exploratory step has to be performed in order to evaluate a T# value ensuring an optimal cost-benefit ratio. A technique to find the optimal range of T# is based on the run of a basic model performance test with increasing structure complexity (increasing T#). This technique was applied to the study case plotting the overall accuracy of the prediction (in terms of out-of-bag classification errors, OOBE) versus the number of grown trees (T#). The working T# should be chosen at the value at which the OOBE stops decreasing and starts oscillating around a stabilized value.

In order to identify the minimum number of trees required to minimize OOBE, the training sequence was repeatedly run, and the OOBE were calculated as a function of increasing T#. Figure 1 shows that the OOBE stabilizes starting from T# = 100. Considering that the calculation time depends on T#, 200 trees were chosen as the optimal configuration of the model. Considering a 10 m resolution and the full parameters set, for each LCV the OOBE was calculated executing 1, 10 and 100 runs. The results show

that the value obtained with one run is almost always comparable to the other values, falling within the range identified by ±3 standard deviations.

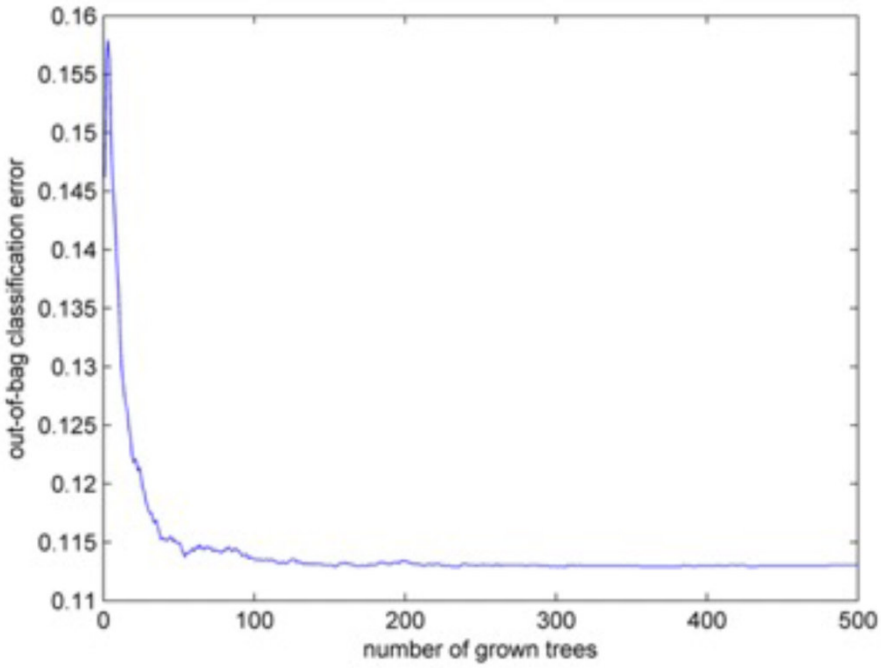

Figure 5.1: plot showing the decrease of OOBE with increasing number of trees T# in the RF structure. A sill value is reached for T#>100. A working value of T# = 200 was chosen for the RFtb model structure.

Furthermore, in order to compare mean values obtained with 10 and 100 runs, a t test was implemented to compare the results coming out from different number of runs: the calculated value is always lower than the critical value, so that the null hypothesis that the two values (10 and 100 runs averages in Table 1) belong to the same distributions can never be rejected (in Table 1 the corresponding probability value is also shown). It can be asserted that the number of model runs does not affect the OOBE. In Table 1 the variation coefficient (CV) considering the mean and std value calculated for 10 and 100 runs are also reported. The highest values are obtained for RND and LIT_VAR: the first one did not affect the classification result, while the last one makes little sense at 10 m resolution, being derived from a 1:100,000 scale map.

An interesting feature of RF is the internal procedure of weighting of variables: the out-of-bag samples are used to calculate the prediction error (out-of-bag error) that would be committed if a variable was excluded from the modelling. In this way, the RF algorithm can be used to get, at the same time, a susceptibility mapping, validation of its predictive accuracy, and a study on the sensitivity of the results to the explanatory variables used in the model.

Table 1. Out-of-bag errors (OOBE) relative to the used LCVs for different numbers of model runs. Results show that the number of runs does not seem to influence the LCV impact on classification.

	1 run	10 runs			100 runs			t test	
	OOBE	meanOOBE	Std dev	CV	meanOOBE	Std dev	CV	t value	p value
ASP	0.095	0.070	0.058	0.828	0.076	0.078	1.020	−0.319	$< t(p = 10\,\%)$
ASP_VAR	0.471	0.375	0.055	0.146	0.382	0.072	0.189	−0.391	$< t(p = 10\,\%)$
CPL_STD	1.391	1.380	0.072	0.053	1.355	0.084	0.062	1.006	$< t(p = 10\,\%)$
CPR_STD	1.606	1.510	0.081	0.054	1.498	0.114	0.076	0.442	$< t(p = 10\,\%)$
CUR_STD	1.611	1.447	0.119	0.082	1.410	0.104	0.074	0.943	$< t(p = 10\,\%)$
CUR	1.294	1.357	0.115	0.085	1.318	0.118	0.090	1.018	$< t(p = 10\,\%)$
CPL	1.200	1.206	0.058	0.048	1.187	0.099	0.083	1.000	$< t(p = 10\,\%)$
CPR	1.185	1.150	0.113	0.098	1.145	0.101	0.088	0.106	$< t(p = 10\,\%)$
FTS	0.947	1.081	0.096	0.089	1.056	0.095	0.090	0.779	$< t(p = 10\,\%)$
RIV	0.280	0.328	0.052	0.160	0.308	0.070	0.228	1.134	$< t(p = 10\,\%)$
RDS	0.639	0.711	0.066	0.093	0.709	0.067	0.095	0.077	$< t(p = 10\,\%)$
ELE	1.748	1.737	0.112	0.064	1.756	0.099	0.056	−0.511	$< t(p = 10\,\%)$
ELE_STD	1.312	1.378	0.138	0.100	1.360	0.117	0.086	0.398	$< t(p = 10\,\%)$
FLA_STD	1.049	1.088	0.153	0.141	1.134	0.112	0.099	−0.907	$< t(p = 10\,\%)$
FLA	1.090	0.923	0.057	0.062	0.934	0.073	0.079	−0.575	$< t(p = 10\,\%)$
LIT_VAR	−0.005	0.023	0.083	3.578	0.034	0.071	2.126	−0.373	$< t(p = 10\,\%)$
LIT	0.919	0.900	0.044	0.049	0.874	0.052	0.060	1.802	$< t(p = 5\,\%)$
LFA	1.054	0.877	0.059	0.067	0.924	0.080	0.086	−2.380	$< t(p = 1\,\%)$
LFA_STD	0.942	1.000	0.143	0.143	1.034	0.121	0.117	−0.719	$< t(p = 10\,\%)$
RND	−0.044	0.019	0.068	3.641	−0.002	0.074	−35.091	0.921	$< t(p = 10\,\%)$
SLO	1.208	1.201	0.092	0.077	1.219	0.111	0.091	−0.596	$< t(p = 10\,\%)$
SLO_STD	1.354	1.322	0.117	0.089	1.361	0.092	0.068	−0.980	$< t(p = 10\,\%)$
CCU	0.725	0.595	0.048	0.081	0.618	0.079	0.129	−1.405	$< t(p = 10\,\%)$
CCU_VAR	0.172	0.219	0.077	0.353	0.209	0.080	0.385	0.407	$< t(p = 10\,\%)$
TWI	0.665	0.550	0.056	0.102	0.547	0.076	0.139	0.167	$< t(p = 10\,\%)$
TWI_STD	0.693	0.596	0.069	0.116	0.614	0.074	0.121	−0.797	$< t(p = 10\,\%)$
COV	0.806	0.859	0.063	0.073	0.862	0.071	0.083	−0.125	$< t(p = 10\,\%)$
COV_VAR	0.109	0.052	0.058	1.114	0.040	0.067	1.692	0.631	$< t(p = 10\,\%)$
Rp_100_24	1.443	1.435	0.097	0.068	1.471	0.088	0.060	−1.104	$< t(p = 10\,\%)$
Rp _100_72	1.631	1.517	0.071	0.047	1.533	0.097	0.063	−0.704	$< t(p = 10\,\%)$
Rp_24_24	1.500	1.604	0.067	0.044	1.593	0.095	0.060	0.476	$< t(p = 10\,\%)$
Rp_300_72	1.519	1.536	0.078	0.051	1.542	0.091	0.059	−0.221	$< t(p = 10\,\%)$
Rp_30_1	1.559	1.477	0.072	0.049	1.471	0.075	0.051	0.281	$< t(p = 10\,\%)$
Rp_50_6	1.398	1.501	0.082	0.054	1.515	0.088	0.058	−0.501	$< t(p = 10\,\%)$
Rp_600_120	1.425	1.418	0.063	0.044	1.433	0.090	0.062	−0.715	$< t(p = 10\,\%)$

Table 5.1: out-of-bag errors (OOBE) relative to the used LCVs for different numbers of model runs. Results show that the number of runs does not seem to influence the LCV impact in classification.

The validation of the susceptibility assessment was performed in terms of AUC (area under receiver-operator characteristic curves), a quantitative index widely used in landslide susceptibility studies to quantify the overall predictive effectiveness of a model. AUC is a cutoff-independent index with an operating range from 0.5 (completely random predictions) to 1.0 (perfection). The relative importance of each parameter used within a model configuration is quantitatively expressed by the OOBE (out-of-bag error), an estimation of the relative error that the model would commit if a given parameter was omitted.

As concerns the key strengths of the model used for Tuscany, and the areas for improvement, it should be pointed out that the RF technique has several advantages with respect to other, more used, multi-variate regression or classification methods. Firstly, it does not require assumptions on the distribution of explanatory variables; secondly, it allows for the mixed use of categorical and numerical variables without recurring to the use of indicator (or dummy) variables; and, thirdly, it is capable of accounting for interactions and non-linearities between variables. These are big advantages that limit the generation of outliers, especially when working with terrain variables with a high frequency of missing data and an intrinsic uncertainty in the assignment to the correct class also in surveyed areas (see e.g. the case correctly defining the type of soil for a given areal extent for which only a few point locations have been directly surveyed).

A further advantage is the ability of RFtb models to provide information on the statistical weight of each single variable on the overall result. The algorithm estimates the importance of a variable by looking at how much the prediction error increases when OOB data for that variable is permuted while all others are left unchanged. This capability can be fruitfully exploited to study the relative importance of the different explanatory variables, a quite important but often neglected aspect of LSM. In the Matlab implementation of RFtb, the model output is a membership probability to one of the 2 possible classes "landslide" and "no-landslide". An estimator of the ensemble error is the "out-of-bag error" (OOBE), which is computed comparing the out-of-bag predicted responses against the true responses.

The overall performance of the model, instead, can be assessed through the misclassification probability (MP) given by the average classification errors (commission and omission) after a given number of runs on a specific RF configuration.

The main areas of improvement concern two main aspects:

- First, the flexibility of the methodology poses virtually no limits on type and characteristics of the input variables to be used. Consequently, the methodology can be applied using any predisposing and preparatory variable. Indeed, also dynamic triggering variables can be incorporated in the modeling to perform a dynamic susceptibility mapping.
- Second, the main critique to similar machine learning methods is that they are traditionally conceived like "black box" models, where the user has little to no control on the results and on the way they are obtained. However, recently, different features have been made available that can be used to visualize intermediate result and to quantify some indicators, in order to fully understand how the artificial intelligence of the algorithm "thinks", the weight it gives to all factors, how they are treated and how each of them contributes to the final susceptibility assessment.

5.3 Internal validation – Messina area

The internal validation form on landslides in the Messina area was produced by colleagues from ENEA and the University of Palermo, who shared their experience and the work done with participants to TK 2.2.2 during the meetings held on February 29, 2024. After that meeting, and the selection of the sites for internal validation, more detailed information was provided on analysis of slope movements in the Messina area, Sicily, and is summarized in this section.

The Messina area is characterised by the Peloritani Mountain Belt, the southern extremity of the Calabride-Peloritan Arc in North-Eastern Sicily, composed by a SE-verging pile of nappes. The main geologic bedrock is made of various grade metamorphic rocks, with a geomorphological setting strongly controlled by recent and on-going uplifting, with very steep slopes heading toward small stream valleys. The combination of the presence of a thick weathered mantle and of the intense rainfall forcing is responsible for recent multiple landslide events, as that which stroke the area in 2009, with the activation of thousands of debris-mud flows and debris avalanches phenomena, whose tracks crossed roads and inhabited fraction/villages, resulting in near 40 deaths and millions of euros of economic losses. The landslides activate mainly as debris flow s.s. (loss of cohesion) or debris slide (increase in pore pressure), evolving into debris flows or avalanches depending on the morphological setting (linear/convex/concave) of the slopes and the geomorphic control. The failure zones or surface are limited to the weathered mantle or to the regolith/bedrock limit, respectively, typically involving even a less than one-meter-thick slab. At the same time, the source area of the landslides frequently involves few hundreds of square meters. However, the magnitude of the phenomena rather relies on the multiple and coupled activations, resulting in multiple converging landslide with fast propagation, thus affecting the main drainage lines. The same mass/volume amplification can be produced by damming of the track channels.

Orographic and morphologic characteristics as a whole directly influence the climatic features of the Messina territory, that is typically Mediterranean with hot and dry summers, and precipitation falling mostly in the period from October to January. In recent years shallow rapid landslides have been more recurrent in the late summer early autumn season, due to high sea temperature and slow atmospheric circulation linked with climate change. The Mediterranean region may experience an escalation of shallow landslide hazards due

to intense cyclones, known as Medicanes, acquiring tropical characteristics accompanied by extreme winds and rainfall.

Both the Ionian and the Tyrrhenian sides of the Peloritani Mountains have undergone significant urban development since the post-Second World War period. The area now features a continuous urban landscape along the coastline, where the population migrated in past decades, leaving the outback original settlements. Moreover, several critical linear infrastructures are located along the coastline, such as main highways, railway, pipelines, and telecommunications features.

Regarding the submarine sector, the study area (especially in the coastal stretch encompassed between S. Margherita Marina and Ali Terme) is characterised by a tight network of narrow canyons, often geographically linked with the subaerial water courses. These canyon heads are in shallow water (15-30 m depth), indenting the edge of a submarine depositional terrace, whose formation can be related to the present sea-level highstand (< ~5 ka). The possibility to compare bathymetric data collected before and after the 2009 event in the study area, allowed to recognize significant sea-floor changes only in two submarine canyons facing the Racinazzo and Giampilieri catchment basins. These seafloor changes can be related to both the deposition of flood-related deposits and to instability processes affecting the canyon head and sidewalls. Specifically, a 130 m-wide landslide scar occurred at Scaletta Canyon head offshore the Racinazzo basin, producing a maximum excavation of about 15 m, and the canyon head retreat of 50 m upslope, with an estimated mobilized volume of 65,000 m^3.

In recent years, the subaerial landslides in the Ionian Peloritan area have been more frequent in the late summer - early autumn season, due to high sea temperature and slow atmospheric circulation. In this sense, the learning site is relevant for setting study approaches suitable for modelling this type of highly hazardous phenomena.

Given the relevance of the 2009 landslides, and the impacts on society, different research groups have been active in the area. Therefore, the following data are available:

- VECTOR
  - Landslide Identification Points (LIPs) for the 2009 event (initiation point): Briga (752 cases), Giampilieri (916 cases), Itala (753 cases) catchments (source: remotely recognized from post-event LIDAR Civil Protection).
  - Landslide Identification Points (LIPs) for 2007 (initiation point): Briga (21 cases), Giampilieri (91 cases) and Itala (82 cases) catchments (source: remotely recognized from orthophoto 2007/2008 ARTA 25cm).
  - 1583 Landslide Identification Points (LIPs) and source areas for the 2009 event (distinguished in channelized and non-channelized phenomena): Briga, Giampilieri, Itala catchments (source: orthophoto by post-event flight of Civil Defense for Sicily Region).
  - 1539 Landslide Identification Points (LIPs) and source areas for 2012 events (distinguished in channelized and non-channelized phenomena): Castroreale, Scaletta, Calvaruso, Saponara, Fiumedinisi catchments (source: Google Maps/Google Earth).
  - 13 Landslide Identification Points (LIPs) for 2023 events: Roccafiorita, Antillo and Limina areas (source: field survey).
  - Outcropping lithology (derived from CARG)
  - Outcropping lithology (Geological map of the Messina Province, in raster format)
- RASTER
  - DTM 2007-2008 2m pixel size
  - DTM 2012-2013 2m pixel size
  - Orthophoto 25cm 2007/2008 and 2012-2013, on demand.
  - DTM for the 2005-2007 and 2009 multibeam bathymetries 1 m cell-size
  - Seafloor samplings of the marine area.

Two different approaches have been applied by the institutions that worked in the area (ENEA and UNIPA).

The method used by ENEA is based on a mixed heuristic-statistic approach, by assigning weights and coefficients to the predisposing factors classes on the basis of the frequency distribution of known activation cases through the factor domain. The considered predisposing factors (in polygon vector or raster format) are: aspect, lithology, land use, slope, ruggedness index and topographic wetness index (TWI). The areal extension of each class, for each predisposing factor, was calculated and normalized to the total extension of the study area. Each phenomenon present in the inventory was attributed to a class for each predisposing factor. The normalized frequency of each class of each predisposing factor is calculated in relation to the total study area. The equation used to attribute susceptibility is:

$$S = \frac{\sum_n (i_n * P_n)}{\sum_n P_n}$$

where S is the susceptibility value and i_n and P_n are the index and the weight of the nth predisposing factor, respectively. The weight of each predisposing factor was attributed between the values of 1 and 5, on the basis of the observation of the frequency distribution of the different classes of each predisposing factor: a greater value was attributed heuristically to distributions with evident Gaussian patterns, than to flat and homogeneous. The index of each class of each predisposing factor was attributed between the values of 1 and 10, on the basis of the normalized frequency of each class, calculated in relation to the value of the maximum frequency class.

The UNIPA approach, on the other hand, was based on the application of different statistical methods (Binary logistic regressions, Stocasting Gradient Boosting, Maximum Entropy), testing different pixel size data frames and model building and validation strategies. A number of potential predictors was taken into consideration and tested for multi-collinearity. All the researches were based on model suite generation by means of multi-random splitting. Models and maps were validated both in terms of accuracy and precision indexes (both in the cut-off independent and dependent domains), as well as in terms of stability of the set selected predictors and of their role.

Based on the widespread recognition in the submarine area of scar morphologies similar to that generated by the flash flood at the Scaletta Canyon headwalls, and considering the volume mobilized during this event, from a statistic point of view it was roughly estimated the occurrence of 90–180 landslides in the last 5 ky, i.e., one landslide every 25–50 years in a sector of coast as long as 5.5 km, or one landslide each km every 125–250 years, compatible with the recurrence time of the largest flood events recognized in the area, so becoming a predisposing/triggering factors for their development.

As regards the assessment of landslide susceptibility, the UNIPA studies adopted different validation design scheme, including temporal partition (calibrating and validating in the same area, based on ante and post 1/X/2009 inventories), spatial partition (calibrating in a source area and validating in a target area, based on the same post 1/X/2009 inventory) and typical random partition (calibrating and validating in the same area, with the same post 1/X/2009 inventory). The validation scheme included accuracy and reliability (both with cut-off dependent and independent metrics), as well as the evaluation of the inner structure of the models (importance and role of the model controlling factors). In the case of the ENEA method, a goodness of fit between multiparametric scores and landslides was estimated.

No validation was carried out for the submarine sector.

As concerns the key strengths of the model used for the Messina area, and the areas for improvement, it should be pointed out that:

- a massive number of cases under different triggering events and in different areas was observed;
- some of the inventoried cases are already distinguished into channelized and non-channelized phenomena, so that could be later constitute a basis for propagation studies within the framework of the activities of WP4;
- the applied methods for susceptibility assessment demonstrated to be suitable for obtaining reliable and accurate models and maps.

Based on the experiences carried out in the area, the following points can be established as positive:

- to include soil thickness and wetness conditions maps among the predictors for statistical susceptibility assessment;
- to couple statical modelling with deterministic physically-based approaches, for downscaling from catchment areas to slopes;
- to link susceptibility models and maps to rainfall forcing for exploring preparation and triggering conditions (WP3 and WP4 activities);
- to link the morphogenesis of submarine canyon head to riverine dynamics and flash-flood events.

Retrogressive evolution of canyon head in shallow-water can imply interception of longshore drift and modification of sedimentary budget along the shoreface, with implications on coastal erosion too.

5.4 Internal validation – Assi landslides (Calabria)

The internal validation form on the Assi landslides was produced by colleagues from OGS, who shared their experience and the work done with participants to TK 2.2.2 during the meetings held on February 29, 2024. After that meeting, and the selection of the sites for internal validation, more detailed information was provided on analysis of slope movements in the Assi area, Calabria, and is summarized in this section.

The tectonically active Ionian margin of Calabria is affected by repeated sediment failures, recorded by slide scars at the seabed and stacked slide deposits. A reconstruction of the geometry and dynamics of one of the largest examples of multiple retrogressive landslide events, the Assi failure, is presented, which consists of three distinct landslides and occurred on the relatively steep slope (average 5°) off southern Calabria (Fig. 2). Morphometric parameters (source area, run out, volume of deposit mobilized) were used as inputs to apply numerical modeling to evaluate the potential tsunamigenic hazard.

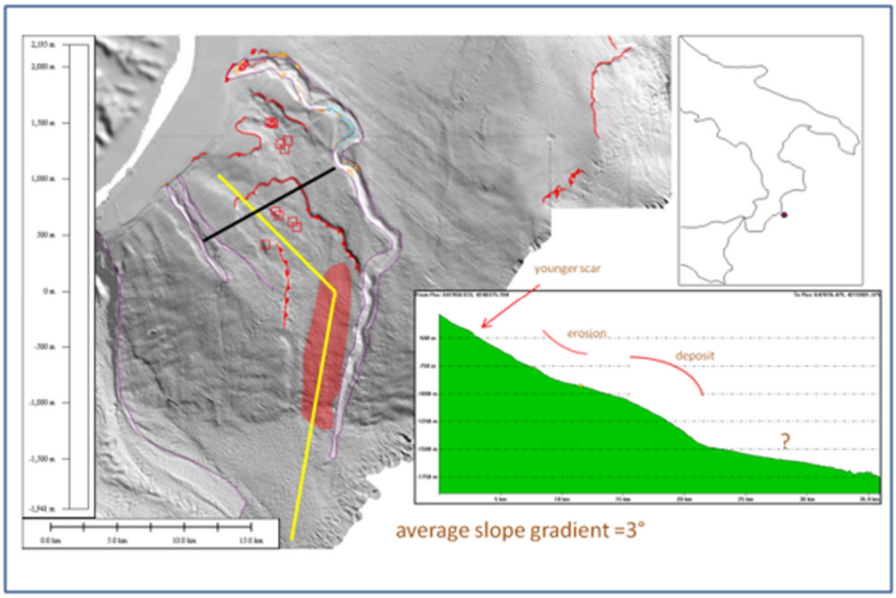

Figure 5.2: Study area location on the Ionian margin of Calabria. Main figure: shaded relief from DEM of multi-beam data acquired by OGS; submarine canyons are indicated in white, red lines denote seabed scarps, the elongated red area indicates deposited material. Inset shows a bathymetric profile along the axis of the Assi landslide (yellow line). Black line shows location of Fig. 5.3.

The oldest scarp of the Assi failure lies only 6 km away from today's coastline, at about 200 water depth, and is about 1 km wide and 4 km long (Fig. 2). The second landslide lies 10 km far from the coast, at 450 m

water depth and is about 5 km wide and 4.5 km long. The main landslide is up to 6 km wide and at least 18 km long and involves the displacement of c. 2 km^3 of sediment. The main landslide event is inferred to have taken place within the last 4,000 years in two main phases.

The three landslide events are used as input to the tsunami modeling, on the assumption that each slide moved in a single step as a coherent mass, with volumes respectively of about 50 million m^3, 0.7 km^3 and 1.85 km^3, in order to evaluate the most disruptive possible consequences. The results indicate that within 8 minutes waves with an amplitude of more than 1.5 m could affect the southern Calabrian coast between Monasterace and Roccella Jonica, where their capacity to cause damage could be amplified when reaching small harbors. This proves that tsunamis represent a hazard for Ionian coastal areas, and call for accurate monitoring and further study.

As concerns the available data, high-resolution geophysical data were used to reconstruct the retrogressive failures dynamic and to define the parameters used for numerical modelling the consequent tsunami such failures could have generated. High-resolution geophysical swath and profile data were acquired by the r/v OGS Explora during campaigns in 2005 and 2009. Swath bathymetric data were acquired over an area of about 30,000 km^2 using Reson 8150 (12 kHz) and 8111 (100k Hz) multi-beam systems, to obtain DEMs of variable cell size (5-50 m). Sub-bottom profiles consist of about 10,000 line-km of Chirp data (2-7 kHz).

The interpretive method consists of integrating seabed morpho-bathymetric elements with acoustic facies recognized on the sub-bottom profiles, in order to identify the major predisposing and trigger factors and reconstruct the failure dynamics. The data were collected aboard the research vessel OGS Explora in the framework of the MAGIC Project (Marine Geohazards along the Italian Coasts), funded by the Italian Civil Protection agency. The geophysical data provide evidence that the ICM has experienced a history of failure events. Here the most recent failure, referred to as the Assi Slide, is examined.

Numerical code simulating landslide motion provides the complete time history of the sliding body geometry and sliding dynamics, allowing to quantify the deposit position and run-out; the tsunami simulation code produces the snapshots of wave propagation at different time steps, the maximum water amplitude for each point of the computational grid, the tsunami arrival time and velocity, and a set of virtual marigrams allowing to quantify tsunami period at the coast. These data allow to quantify coastal geohazards for the Calabrian margin (small scale) and extrapolates results to adjacent margins of the Mediterranean basin (large scale).

The bathymetric data and maps were analyzed to identify morphologies and bedforms associated to the landslide (scars, run out, deposits, channels) and to establish their sizes. A seismo-stratigraphic analysis based on seismic features recognizable on multi-channel seismic profiles and high-resolution sub-bottom data was performed in order to recognize seismic facies and units. A tectono-stratigraphic analysis allowed to recognize unconformities as well as the main detachment horizons that have been assumed to behave as weak layers, characterizing the gravity-driven body.

The tsunami simulation code provides, among the many outputs, the possibility to evaluate the maximum water amplitude at the coast (Fig. 3). This can be used as an indicator of the tsunami impact, allowing to identify the coastal stretches potentially more affected by the waves.

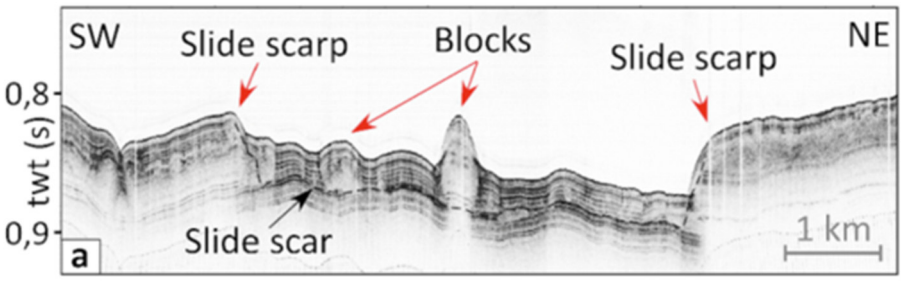

Figure 5.3: Chirp sub-bottom profile across the Assi landslide (location in Fig. 5.2). Black dashed line marks the low-angle unconformity at the base of the landslide deposits.

At present, susceptibility maps are not available.

This part of the slope under study seems to have been affected by at least three phases of failure (Fig. 5.4). The oldest phase (SLIDE 1) is that associated with scarps on the upper slope (Fig. 5.2) and unstratified deposits on the slope below that are truncated by the Assi slide (Fig. 5.3). The Assi slide itself provides evidence of two phases of failure: the N-S oriented lower slide (SLIDE 2), which was inferred to be older, and the NW-SE oriented upper slide (SLIDE 3). The Assi slide as a whole extends over an area of about 90 km^2 and it was estimated that it mobilised in total about 2 km^3 of sediment during the two events (Fig. 5.4).

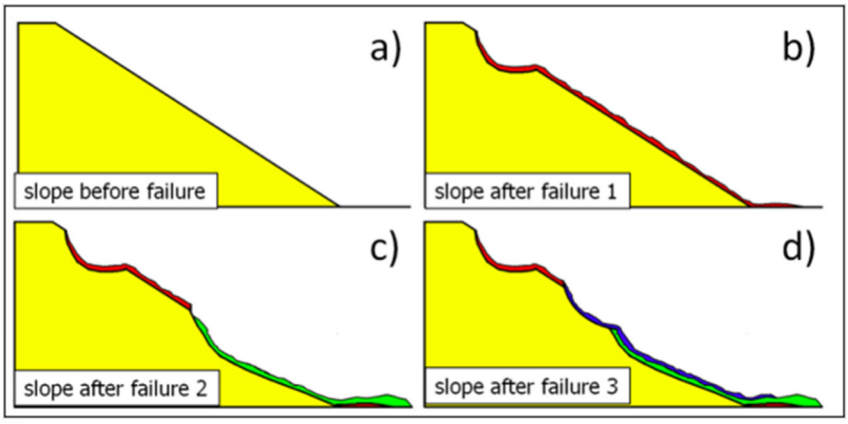

Figure 5.4: Reconstruction of failure dynamics along the Ionian Calabrian Margin.

The age of the three slide events (Fig. 5.4) has been estimated from the thickness of a layer of sediment observed on sub-bottom profiles to overlie the slide deposits across the slope (e.g. Fig. 5.3). On the upper slope above SLIDE 1, this deposit is 6 m thick, whereas downslope above both SLIDES 2 and 3 it is 4 m thick. Post-LGM sedimentation rates for this area are taken from Zecchin et al. (2011) to be about 1.4 mm/yr. This yields an estimated age of about 4300 yr for SLIDE 1 and an age of about 2850 yr for SLIDES 2 and 3. The comparable thickness of this deposit across SLIDES 2 and 3 supports their interpretation as linked events, with SLIDE 3 having formed by retrogressive failure after the larger SLIDE 2 (Fig. 5.4).

The first phase of the Assi slide (SLIDE 2, Fig. 5.4c) is the largest of all the failures to have affected this steep open slope. In the following, the focus is on SLIDE 2 in order to model the failure dynamics and evaluate its tsunamigenic potential.

The numerical codes applied to the landslide-tsunami scenarios have been applied to many different cases of submarine and subaerial landslides with good results when compared to observations (see for example Tinti et al., 2006; Zaniboni et al., 2016). The model simulating the landslide considers the mass split into different portions, which motion equation is determined considering the forces acting on them and is solved through numerical methods. The landslide motion evolution provides the impulse for tsunami generation. The propagation of the wave is computed adopting the shallow-water approximation, meaning that the wavelength is much bigger than the sea depth.

As concerns the key strengths of the model used for the Assi landslides, and the areas for improvement, the following points should be pointed out. The morpho-bathymetric data reveal a seabed slide scar up to 50 m high, that extends downslope at least 18 km across water depths of 700-1400 m (Fig. 5.2); sub-bottom profiles indicate stacked slide deposits at and near seabed, with older deposits truncated by stratified and unstratified sediments of the Assi Slide (Fig. 5.3). It was estimated that the failure mobilized ca. 2 km^3 of sediment, over an area of at least 90 km^2.

The landslide dynamics has been reconstructed in three steps (Fig. 5.4). The material mobilized during SLIDE 2 has been used for the tsunami modeling, considering the material to be failed in one single step (more dramatic scenario). On the basis of the most dramatic scenario, an attempt was made to mathematically model the failure and simulate the tsunami that would have been generated by the considered volume of sediment.

The preconditioning factors that have contributed to increasing instability in this area are inferred to be the rapid tectonic uplift (1mm/yr) that began in the Pleistocene, combined with the high sedimentation rate (1.4 mm/yr) during the Pliocene and Pleistocene, which made the margin rapidly inclined and stacked with sediments. Two main unconformities have been observed on sub-bottom data that represent the slide planes for the inferred landslides and may have functioned as weak layers. It was inferred that fluids might have played a role in destabilizing the slope. They have been observed on the continental shelf at the back of the examined slide scars: erosion (active in glacial periods) may have decreased the pressure in pores, facilitating the migration of fluids through pre-existing discontinuities, decreasing the resistance to slipping (especially during seismic events), and eventually making mass movements possible.

The coastal areas along the southern part of the margin near the village of Riace Marina (Fig. 5.2), and more in general in the coastal stretch between Monasterace and Roccella Jonica, are found to be the most susceptible to tsunamis generated by the Assi slides: within 8 minutes they are affected by waves with maximum peak-to-peak elevations that can exceed 3.5 m (see Fig. 5.5). The waves are not catastrophic, but able to provoke damage, especially in the small harbors along the coast, where resonance and multiple reflections, amplifying the wave effects, can take place. Further, the wave can pose a threat to coastal populations, especially if occurring during the season of major tourism flow.

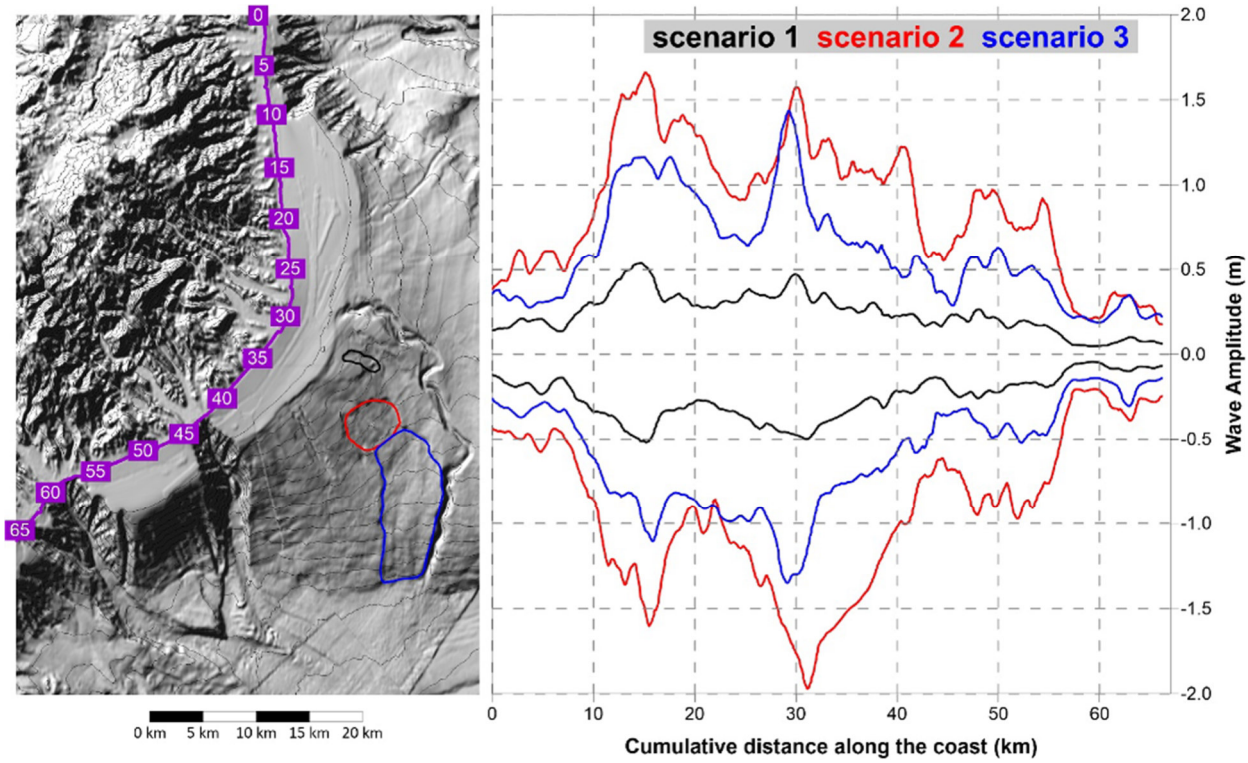

Figure 5.5: Left plot: Cumulative distance along the coast in the studied coastal stretch. The black, red and blue contours mark respectively Scenario 1, Scenario 2 and Scenario 3 initial mass boundaries. Notice the presence of canyons, in the southern part, nearly reaching the coastline. Right plot: Maximum and minimum wave amplitude measured along the coast. The distance is cumulative starting from the northern extreme of the domain and is shown on the left. The black, red and blue lines recall the three landslide scenarios, which boundary is shown on the left.

More generally, the unpredictability of the sliding phenomena, their proximity to the coast and the corresponding shortness of the lead time (in this case about 7 minutes), the large number of possible tsunami sources related to evidence of repeated episodes of failure along the margin, suggest that tsunamis represent a recurrent hazard for Ionian coastal areas and thus need accurate monitoring and further study.

There is currently an active collaboration with the Department of Mathematics, Informatics, and Geosciences of the University of Trieste on artificial intelligence and machine learning for the automated classification of the seabed. The aim is to train a computer to the automatic recognition and labeling of morphological

features, given only bathymetric data. The aim of this collaboration is to develop a tool to support stakeholders for visualization of marine data and recognition of underwater geomorphic features.

5.5 Internal validation – Crotone mega-landslide (Calabria)

The internal validation form on the Crotone mega-landslide was produced by colleagues from the University of Rome, who shared their experience and the work done with participants to TK 2.2.2 during the meetings held on February 29, 2024. After that meeting, and the selection of the sites for internal validation, more detailed information was provided on analysis of the Crotone mega-landslide, along the Tyrrhenian margin of Calabria, and is summarized in this section.

The Crotone mega-landslide, on the Ionian side of the Calabria region, covers a large part of the Crotone basin (ca. 1500 km^2) and involves up to 1.6 km thick succession composed of upper Messinian and Plio-Pleistocene sediments (mainly silt and clay with minor sand) (Figs. 5.6-5.8). It glides seaward (SE) at variable velocities due to the presence of a Messinian halite layer that acts as a basal detachment surface. The mega-landslide consists of a downdip offshore compressional domain including thrusts/reverse faults, which form the Crotone Swell in the Ionian Sea, connected via the basal detachment surface to an updip extensional domain onland represented by seaward-dipping arcuate normal faults linked to the basal detachment (Figs. 5.6-5.8). Gravitative listric normal faults are located in the northern part of the Crotone Basin, where they form the mega-scar of the landslide (Fig. 5.6). The detachment surface is inclined seaward up to 3-4° (Fig. 5.7). Both the compressional and extensional domains are the result of a long-term seaward movement of the gravity-driven landmass since Zanclean time. While the sedimentary succession that forms the landmass in the compressional domain appears to be strongly deformed due to the movement of secondary structures (Fig. 5.7), most of the succession that lies onland appears to be largely undeformed. The mega-landslide is bounded to the north and the south by the active NW-SE trending regional shear zone called Petilia-Sosti and Rossano- San Nicola, respectively (Fig. 5.6).

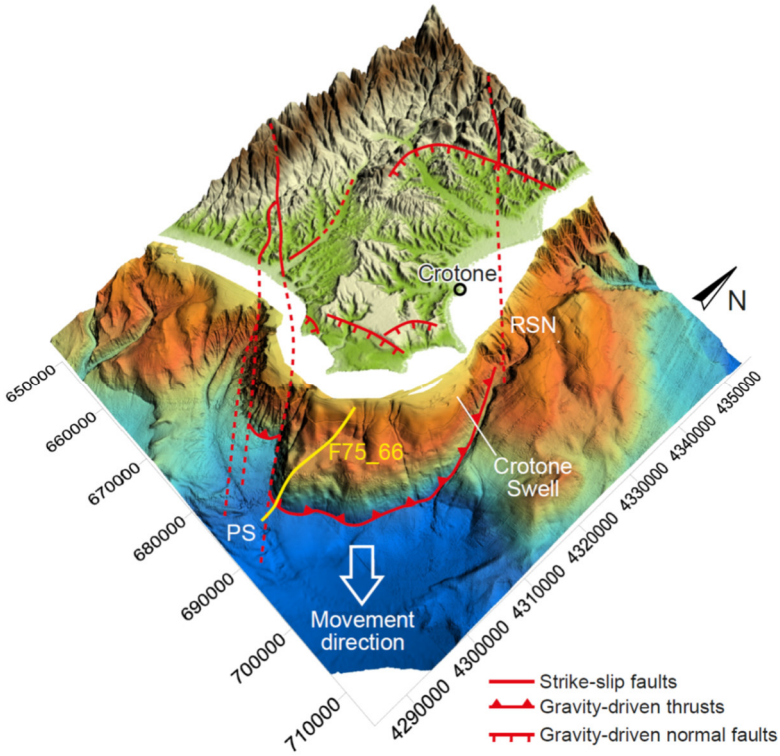

Figure 5.6: Three-dimensional view of the Crotone basin highlighting the Crotone Mega-landslide (modified after Zecchin et al., 2018).

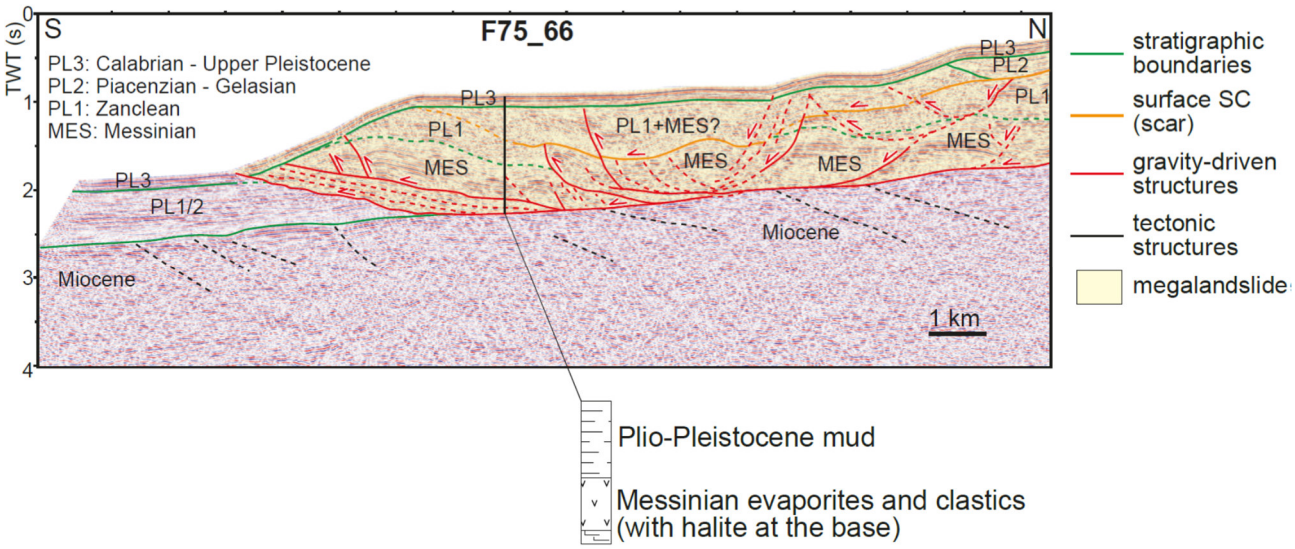

Figure 5.7: Interpreted seismic profile cross-cutting the marine part of the Crotone Mega-landslide (see Fig. 5.6 for location; after Zecchin et al., 2018). SW-verging tectonic structures (in black) are truncated by SE-verging, gravity-driven structures (in red), which are dominated by a basal detachment surface and a thrust front that reaches the seafloor. The gravity-driven phenomenon involves Late Miocene and Plio-Pleistocene deposits, which in seismic profiles correspond to seismic units (Units MES and PL1-3) separated by unconformities.

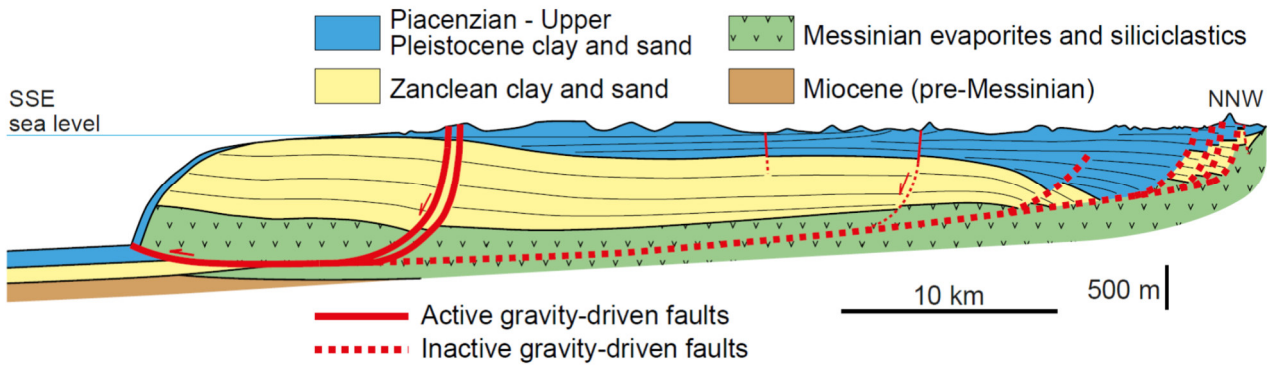

Figure 5.8: Simplified onshore-offshore geologic section of the Crotone Mega-landslide (after Zecchin et al., 2018).

Two main gliding stages were recognized in the evolution of the mega-landslide: 1) a late Zanclean – late Gelasian stage, triggered by trans-pressional tectonics, which affected the Calabrian Arc, plus uplift and involving the whole landmass, and 2) a middle Pleistocene to Holocene stage, inferred to be driven by the regional uplift of Calabria and mainly involving the Crotone Peninsula plus the compressional domain in the offshore area. Based on the observed displacements related to the basal detachment surface, the first stage was associated with a rate of movement of at least 7 mm/yr, whereas the second one was associated with a rate of ca. 1 mm/yr. Currently, the non-homogeneous GPS and interferometric SAR data indicate that an overall SE-ward migration of the onshore part of the mega-landslide does not occur (Fig. 5.9). Significant eastward movements (up to 4–5 mm/ yr) were only detected along the coastal area between Crotone and Capo Colonna using the interferometric SAR-data (Fig. 5.9).

In brief, the predisposing factor favoring the large-scale movement is the presence of a halite layer overlain by a thick, mainly muddy succession, and this, together with tectonic uplift possibly accompanied by seismic events, led to the long-term gliding of the landmass.

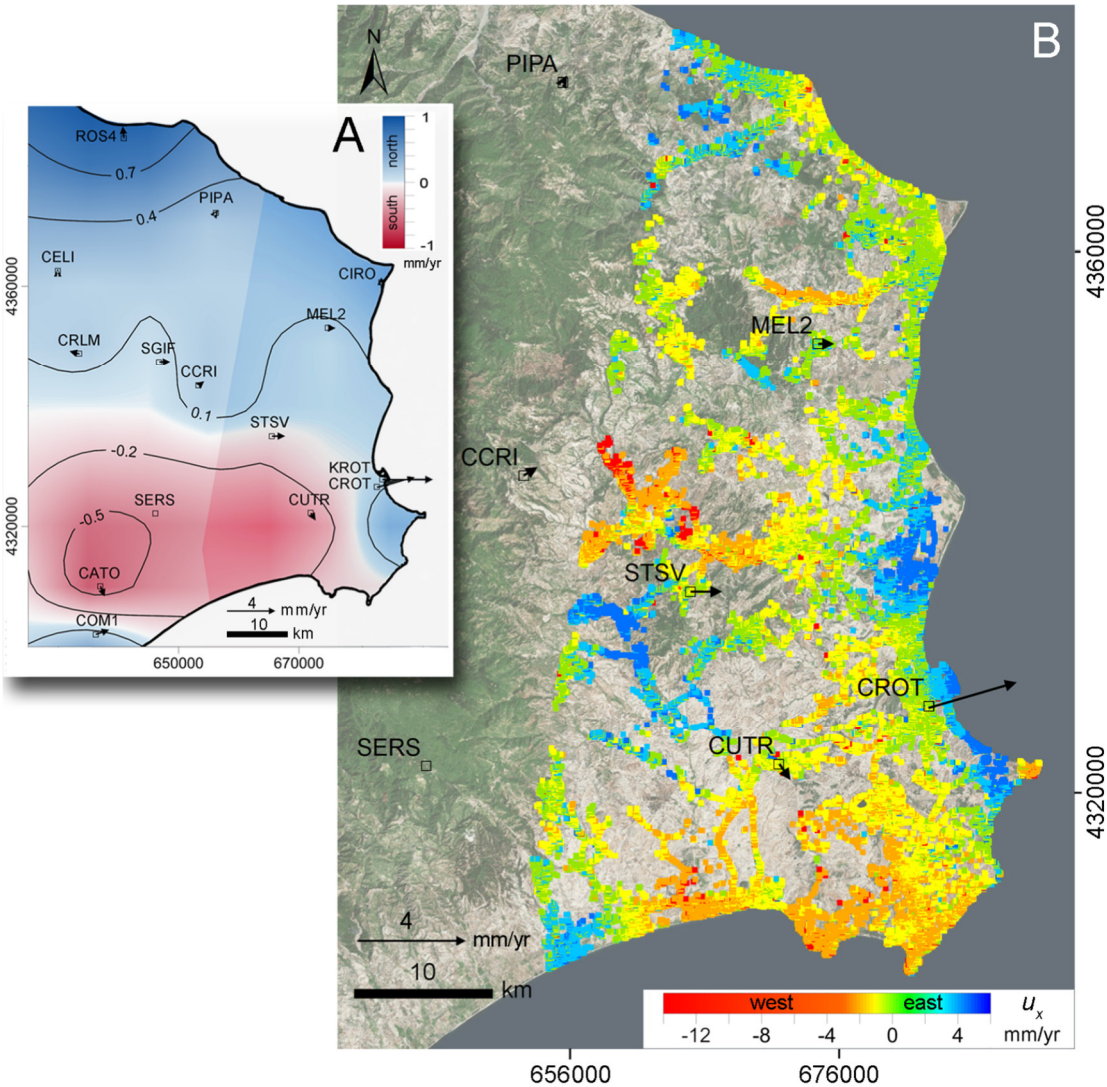

Figure 5.9: Maps of the ground movements (after Zecchin et al., 2018). (A) GPS velocities superposed to the interpolated map of south-north displacements referred to SERS. (B) Average west-east ground movements obtained by SAR-based interferometry over the 2011–2014 period. Black squares show the positions of the GPS stations, with the arrows providing the direction and magnitude of the horizontal displacement rate. Satellites base map used is from Esri, DigitalGlobe, GeoEye, Earthstar Geographics, CNES/Airbus DS, USDA, USGS, AeroGRID, IGN, and the GIS User Community.

The data used to characterize the Crotone mega-landslide consist of:

- 2D multi-channel seismic reflection profiles and exploration wells made available in PDF format by the Ministry of the Economic Development in the framework of the project "Visibility of Petroleum Exploration Data in Italy" (ViDEPI) (http://unmig.sviluppoeconomico.gov.it/videpi/). The seismic lines were converted to SEG-Y format files and afterwards the SEG-Y header was edited in order to assign the CMP (Common-Mid-Points) to the corresponding geographic coordinates. In order to reconstruct the seismic section as faithfully as possible, band-pass filters were applied to the SEG-Y files following the processing information contained in the original file. A post-stack time migration was applied to the SEG-Y files obtained from the files (PDF format) to remove artefacts such as hyperbolas and to better define the slope of the reflections.
- High-resolution morpho-bathymetric data and sub-bottom profiles acquired by OGS in the frame of the MaGIC (Marine Geohazards along the Italian Coasts) project. The sub-bottom profiles were acquired during a geophysical campaign onboard of the R/V OGS Explora in April 2009 using the

CHIRP II Benthos CAP-6600 system, comprising 16 hull-mounted transducers operating at frequencies of 2–7 kHz (sub-metric vertical resolution);

- Public DTM data available at https://www2.jpl.nasa.gov/srtm/;
- The land movements are based on the Persistent Scatterer Interferometry (PSI) products made available by the Italian Ministry of the Environment and Protection of Land and Sea (http://www.pcn.minambiente.it) and Copernicus. Specifically, the following datasets are available: Envisat 2003-2010; COSMO-SkyMed 2011-2014; and Sentinel 1 2015-2022. The interferometric products require extensive work to calibrate the interferometric output by the use of correction planes modeled through ground truths consisting of the velocities time series data recorded by some permanent local GNSS stations. GNSS velocities are available from the MAGNET GPS network (http://geodesy.unr.edu).

A seismic-stratigraphic analysis based on seismic features recognizable on multi-channel seismic profiles, high-resolution sub-bottom and well information was performed in order to recognize seismic facies and units and correlate them with litho-formations (Fig. 5.7). The correlation between the boreholes and the seismic profiles was performed using a time-depth relationship based on the interval velocities provided in the seismic profiles. A tectono-stratigraphic analysis has allowed to recognize normal and reverse faults and to define compressional and extensional domains, as well as main detachment horizons, characterizing the gravity-driven body.

The bathymetric data were analysed to identify bedforms associated to the mega-landslide (scars, active faults, counterslope areas, terraces, channels) and to establish its size.

The knowledge of the onland sedimentary succession deriving by several geological-structural surveys, obtained through several geological-structural surveys also carried out within the CARG project (sheets 571 Crotone and 577 Isola di Capo Rizzuto), greatly helps in reconstructing the succession and the architecture of the mega-landslide.

At present, susceptibility maps are not available.

The methods used for validation were:

- Field analysis of faults associated with the large-scale gravity-driven phenomenon;
- Analysis of gravity-driven structures and of sedimentary units based on seismic profiles and wells in the marine part of the mega-landslide;
- Permanent GNSS stations that were not used for the calibration of the interferometric outcomes will be used for the validation of the ground velocity maps.

As concerns the key strengths of the model used for the Crotone mega-landslide, and the areas for improvement, the following points should be pointed out. The Ionian margin of Calabria represents a unique in Italy for the analysis of geological risk phenomena due to its morphological and geological peculiarities, which are closely linked to the very significant uplift occurred since the middle Pleistocene. In this context, the Crotone mega-landslide represents the largest landslide recognized in the Italian offshore. Moreover, it also involves a densely populated area in which the city of Crotone is located. For this reason, a monitoring of the large-scale gravity-driven phenomenon and of associated structures is necessary.

The areas for improvement are as follows:

- A more accurate measurement of land movements based on new data sets from multi-sensor SAR-based interferometry and permanent GPS stations located in critical sites and will significantly improve the interpretation of the data.
- Specific sites should be established in critical areas for ground- and satellite- the inter-calibration measurements.

5.6 Internal validation – Gioia Tauro (Calabria)

The internal validation form on the Gioia Tauro area was produced by colleagues from the University of Rome, who shared their experience and the work done with participants to TK 2.2.2 during the meetings held on February 29, 2024. After that meeting, and the selection of the sites for internal validation, more detailed information was provided on analysis of the slope movements at Gioia Tauro (Calabria), and is summarized in this section.

The Italian peninsula is characterized by numerous shelf-indenting canyons carving the continental margins for tens or hundreds of kilometers, connecting the bathyal plain to the coastal environment. Submarine canyons are extremely dynamic environments that naturally evolves retrogressively (i.e. upslope), causing the progressive approaching towards the coast of the canyon heads. The proximity of canyon heads to the coast makes these environments extremely dangerous for coastal infrastructure and society since occasionally tsunamigenic landslides occur at the canyon head. In the Mediterranean Sea, there are at least two very well-known events that caused tsunamis due to submarine landslides occurring at canyon head: in 1977 at Gioia Tauro (Southern Italy) during harbor construction (Colantoni et al., 1992). and in 1979 during the seaward expansion of the Nice airport (Cote d'Azur, France; Ioualalen et al., 2010).

Specifically, the test area comprises the head of the submarine Gioia Canyon, located in the south-eastern Tyrrhenian Sea, in front of the Gioia Tauro harbor (Italy). This shelf-indenting canyon is characterized by numerous landslide scars recognized both at its head and flanks; in the upper part, the canyon divides in two branches which cut back in shallow-water, very close to the coast (Fig. 5.10; Casalbore et al., 2019). In particular, the analysis focused on large size tsunamigenic landslides (Mm^3) occurring at the canyon head, since of this kind is the famous and aforementioned event that occurred in Gioia Tauro. On July 12, 1977, a fast submarine landslide of about 5.5 Mm^3 occurred in the northern branch during the dredging operations carried out during the harbor construction. The submarine landslide induced a tsunami wave as high as 5 meters that hit the harbor, causing damage to facilities and infrastructure but fortunately resulting in no casualties. The deposit of the landslide is absent due to the fluidification of the slide mass that generated a turbidity current that broke a submarine cable.

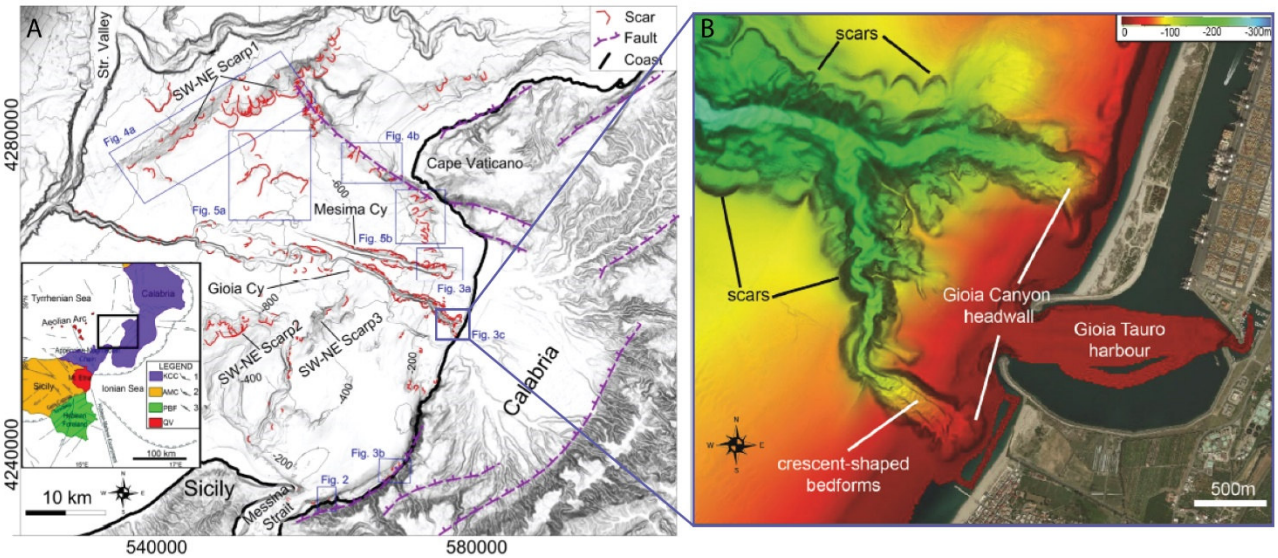

Figure 5.10: A) Shaded relief map of the Calabro-Tyrrhenian continental margin with the indication of the recognized landslide scars (red lines), the inset shows a simplified structural ketch of Southern Italy. B) Zoom of the upper reach of the study area, the Gioia canyon, formed by two branches.

The available data for the site are:

1) Bathymetric maps before and after the slide event that allowed the calculation of the isopach maps;
2) High-resolution seismic data;

3) Geotechnical data and in-situ investigation in the area surrounding the slide

- In-situ investigations:
  - Borings;
  - CPTs;
  - Soil and pore water resistivity tests;
  - SPT tests;
  - 2 Piezometers.
- Laboratory test on sand samples for the determination of soil parameters to assess the susceptibility to liquefaction and the behavior under cyclic loading (seismic conditions)
  - Visual soil descriptions;
  - Grain size distributions;
  - Critical porosity determinations (with dry and wet method);
  - Maximum and minimum porosities determinations;
  - Cell tests on silty samples;
  - Test on cyclic behavior.

4) Foreshore stability analysis previous and after the slide under static and seismic conditions.

In the framework of the RETURN project, the research group of marine geologists has identified different predisposing parameters for submarine landslides occurring at canyon head and classified them into four classes on the basis of their experience and existing bibliography: a) Negligible, when the predisposing factor is absent or considered as irrelevant in predisposing slope to instability; b) Presence: the predisposing factor is considered as relevant for the instability process; c) Determinant: when the predisposing factor plays a very important role in the destabilization and d) Unknown/Not measured: when available information do not permit the exclusion but neither the consideration of the parameter. Moreover, a different combination of predisposing factors has been associated with small-scale (≤1 Mm^3) and large (tsunamigenic) landslide (>1 Mm^3). The main predisposing factors considered for the large events (i.e., tsunamigenic Gioia Tauro slide) are:

- Lithology: unconsolidated sands and gravels (Plio-Quaternary sedimentary succession) → Presence
- Weak layer→ Unknown
- Stratigraphic features: Discontinuity surfaces between folded Trubi formation and the overlying two sedimentary units (Pleistocene and Holocene ages) with basal erosive surfaces → Presence
- Prograding sedimentary wedge → Presence
- Sedimentation rates: 0.67 mm/yr → Determinant
- High seismic activity → Presence
- Site effect → Unknown
- Slope morphology: 1-2° (inner shelf) - 20° (foreset of the prograding wedge) - 2.7° (middle shelf)→ Determinant.
- Previous events/undercutting: retrogressive landslide at the canyon head → Presence
- Littoral transport: 75 m3/yr → Presence
- Presence of fluid/gas → Unknown

No validation method has been applied, as there are no susceptibility maps. Confirming the relevance of the identified predisposing factors, in combination with specific predisposing and triggering factors, is the occurrence of the landslide in Gioia Tauro in 1977.

As concerns the key strengths of the model used for the Gioia Tauro area, and the areas for improvement, it should be pointed out that the site is:

- one of the few examples of submarine landslides occurring at canyon head in Italy, where geophysical and geotechnical data are available;
- there are possibilities to connect WP2, WP3 and WP4;
- there is a high hazard related to its retrogressive evolution and tsunamigenic potential;
- relation with critical infrastructure; it is noteworthy that a similar landslide occurred two years later in the Var Canyon during the harbor construction at Nice Airport, leading to the collapse into the sea of the new harbor and generation of tsunami wave with casualties.

5.7 Internal validation – Guidonia – Bagni di Tivoli Plain (central Italy)

The internal validation form on the sinkholes in the Guidonia – Bagni di Tivoli Plain, in central Italy, was produced by colleagues from the University of Florence, who shared their experience and the work done with participants to TK 2.2.2 during the meetings held on February 29, 2024. After that meeting, and the selection of the sites for internal validation, more detailed information was provided on analysis of the sinkholes in the Guidonia – Bagni di Tivoli Plain, in central Italy, and is summarized in this section.

The study area is the Guidonia-Bagni di Tivoli plain (central Italy), an area historically threatened by sinkholes occurrence (Billi et al. 2016). The geo-hydrogeological and structural features of the Guidonia-Bagni di Tivoli plain make the area prone to various karst and hyperkarst processes (Nisio et al. 2007; Centamore et al. 2009; Floris et al. 2014; Ozdemir 2016). Buried collapse and deep piping sinkholes filled with soil and regolith are common in the travertine bedrock of this geothermal-seismic area. Moreover, travertine quarry activities in the area and the load of buildings due to urbanization accelerate the development of subsurface cavities in the travertine plateau (De Ritis et al. 2020). The selected study area of the work extends over an area of about 38 km^2 within the Guidonia-Bagni di Tivoli plain, located in a Plio-Pleistocene, geothermally- and seismically-active basin, near Rome, in Lazio region (central Italy), also known by the name of Acque Albule basin. This area is characterized by a thick deposit of late Pleistocene thermogenic travertine, which has been historically quarried, and it is threatened by land subsidence and sinkholes, due to collapse for water percolation in karst travertine structures and to dissolution for the upwelling of mineralized high-pressure water (Billi et al. 2016; Ciotoli et al. 2016). The current extraction process is facilitated by an extensive system of sumps and pump stations for dewatering the travertine aquifer and permitting mining operations at the pit floor. Such groundwater abstraction activities contribute to subsidence and thus to potential sinkhole occurrence (Brunetti et al. 2013). Furthermore, seismic shaking due to seismically-active shallow faults could have played a concurrent role in producing sudden ground collapses (Billi et al. 2016).

Sinkholes and similar surface karst phenomena as well as subsidence have been well documented in the Acque Albule Basin since historical times (Nisio et al. 2007). The area is characterized by different sinkhole typologies, mainly cover collapse sinkholes and deep piping sinkholes (Waltham et al. 2005; Nisio et al. 2007; Caramanna et al. 2008; Gutierrez et al., 2014; Parise, 2019, 2022). The cave collapse sinkhole develops in the outcropping lithoid travertines through the brittle deformation of bedrock karst material, while the cover collapse sinkhole refers to the quick sinking of unconsolidated cover deposits. The deep piping sinkholes occur in the travertine and are caused by the rising of pressurized and mineralized waters, which lead to the formation of a conduit or funnel, even at great depth. Many sinkholes in the Guidonia Bagni di Tivoli are buried sinkholes since they are totally filled by unconsolidated deposits and regolith that have been compacted under the load of construction, and thus are hidden and relict.

The mapped sinkholes considered for this study account to 203 elements (points or polygons depending on the data sources). In particular, 191 mapped geometries were derived from the work by Billi et al. (2016) and

converted into points as polygon centroids, while additional 12 sinkholes were collected from the Italian National Institute for Environmental Protection and Research (ISPRA) which manages a database of point-wise sinkhole locations over the whole Italian territory (ISPRA 2022). Eight geo-environmental conditioning factors for sinkhole occurrence were considered. They are seven controlling factors, i.e. lithology, land use, soft soil thickness, travertine thickness, hydrography, groundwater levels, distance to faults, and one precursory factor, i.e. InSAR ground motion rates. These factors, together with the sinkhole inventory map, were used as input parameters for producing the sinkhole susceptibility map on the Guidonia-Bagni di Tivoli area. All the factors, either classified as categorical or numerical discrete data, were computed as thematic layer with the same 10 m cell-size. In particular, those categorical data (lithology, land use, hydrography) that contain a finite number of categories were rasterized. Those maps that contain a spatially discontinuous information (i.e. point-wise and counter-lines maps) were spatially interpolated to obtain a continuous thematic layer: more in detail, such vectorial linear elements (faults, groundwater, soft soil and travertine thickness lines) and point-like elements (ground motion rates of InSAR benchmarks) were converted into continuous surface maps by means of the Inverse Distance Weighted tool in GIS environment.

In detail:

- The geolithological map of the Guidonia-Bagni di Tivoli study area was collected from Lazio Region authority. The lithotypes cropping out in the area have been grouped into 10 lithological classes;
- The land use map of the study area, derived from merging levels 2 and 3 of the CORINE Land Cover map (European Environment Agency 2007);
- Soft soils correspond to compressible recent alluvial deposits that constitute the terrain surface layer throughout the plain. Data referred to the thicknesses of these soils were obtained from Bozzano et al. (2015), who showed that the thickest stratigraphical layers correspond to the areas affected by the highest rates of ground lowering;
- The thickness of the travertine in the area was reproduced as discontinuous thickness contour lines derived from the work of Faccenna et al. (2008), who created a travertine thickness map by interpolating data of 114 boreholes;
- The used thematic layer for the structural setting of the study area is the spatial distance from faults (in meters) represented as an interpolated continuous surface map;
- Hydrographic data were managed as categorical data: indeed, in this case, before converting data into a raster layer, the map was transformed into a matrix of presence-absence of the hydrographic element with an applied buffer of 50 m, without generating a map of the distances from the element since the effect of hydrography is much more limited around the element itself
- The piezometric data were taken from the most recent available cartography of Guidonia-Montecelio municipality that dates back to 2016. The water table contour lines displayed refer to the depth to groundwater of the shallow aquifer from ground level in meters above sea level.

Satellite PSI (Persistent Scatterer Interferometry) InSAR data were decomposed into their horizontal and vertical components, revealing a main vertical direction of displacement.

For this elaboration the MaxEnt software package was exploited (Phillips et al. 2021). The MaxEnt model estimates the spatial distribution of an event by finding the distribution that has the highest entropy and that is subject to a series of environmental conditioning factors characterizing the events (Phillips et al. 2006). In particular, the method compares the probability density functions of each environmental input variable (in this case, the chosen conditioning factors) at the event occurrences (in this case, the sinkhole locations) and at any other location on the study area, and computes the difference as 'relative entropy' (Convertino et al. 2013; Kornejady et al. 2017). Then the MaxEnt algorithm analyses the probability density functions of the environmental variables, transformed into logistic values, and finds the one that maximizes the entropy of information, in order to forecast the sinkhole event by spatially mapping its probability to occur, i.e. the susceptibility. On the Guidonia-Bagni di Tivoli study area, the sinkholes inventory was randomly split into a training set (70% of the total inventory) used for the model itself, and a testing set (30%) employed to validate the predictive capacity of the method. The MaxEnt algorithm was used by elaborating the average of 6 repeat models and 1000 iterations for each model, in order to tune the system performance

and search for the best result. Thus, the result of these elaborations was an average susceptibility map based on six maps each calculated on the result of 1000 iterations. The MaxEnt algorithm allowed the calculation of the weights for each class of every conditioning factor used as an environmental variable in the model by means of response curve graphs. In particular, if the variable is continuous, the output is actually a response curve, while if the variable is categorical, the output is a histogram. These graphs show how the probability of predicted presence changes as the value of each environmental variable changes, while keeping all the other variables at their average value.

The accuracy assessment of the produced sinkhole susceptibility map implies the evaluation of the finest combination map from the processed tests within MaxEnt and was performed by empiric ROC analysis and cross-comparison of the area under curve (AUC) values. Furthermore, a jackknife test was performed to further check the contribution of each environmental variable in the model calculation developed by MaxEnt. Jackknife is a resampling method that estimates the variability of a statistic from the variability of that statistic across subsamples plot (Sinharay 2010). The Jackknife test removes one variable at time and records the change in the chosen AUC evaluation metric. The plot provides two values for each variable: the first one is the AUC value that would be obtained using only that variable, while the second one is the AUC values obtained considering all the other variables except that one. The final susceptibility map, divided into 5 classes, was thus cross-compare with the sinkhole inventory.

As concerns the key strengths of the model used for the Guidonia – Bagni di Tivoli Plain area, and the areas for improvement, it should be pointed out that the sinkhole susceptibility assessment was performed by means of maximum entropy algorithm through the MaxEnt model. This machine learning algorithm is a data-driven model that has been already used for geohazard susceptibility mapping and that has revealed its effectiveness. In scientific literature it has been compared with various other modeling and has been evaluated as an excellent predictive approach, since it provides a continuous distribution model and has a very stable confidence interval system (Phillips et al. 2006; Townsend Peterson et al. 2007; Kaky et al. 2020). The MaxEnt approach is based upon a probabilistic framework and in our work was chosen with the purpose of using a machine learning algorithm that generates predictions from an incomplete set of information. The MaxEnt algorithm is a presence-only model, exploited where presence data are abundant, but absence data are hard to obtain and often unreliable due to insufficient survey effort. To counter the lack of absences, MaxEnt uses a background sample to contrast the distribution of presence data along environmental gradients against the distribution background points, randomly drawing from the study area (Gomes et al. 2018).

The limitation of this open-source tool of managing only point-wise data was, in our case, aligned with the lack of information concerning the actual size of the sinkhole events, so further improvements can be achieved by using the size reconstruction of the sinkholes.

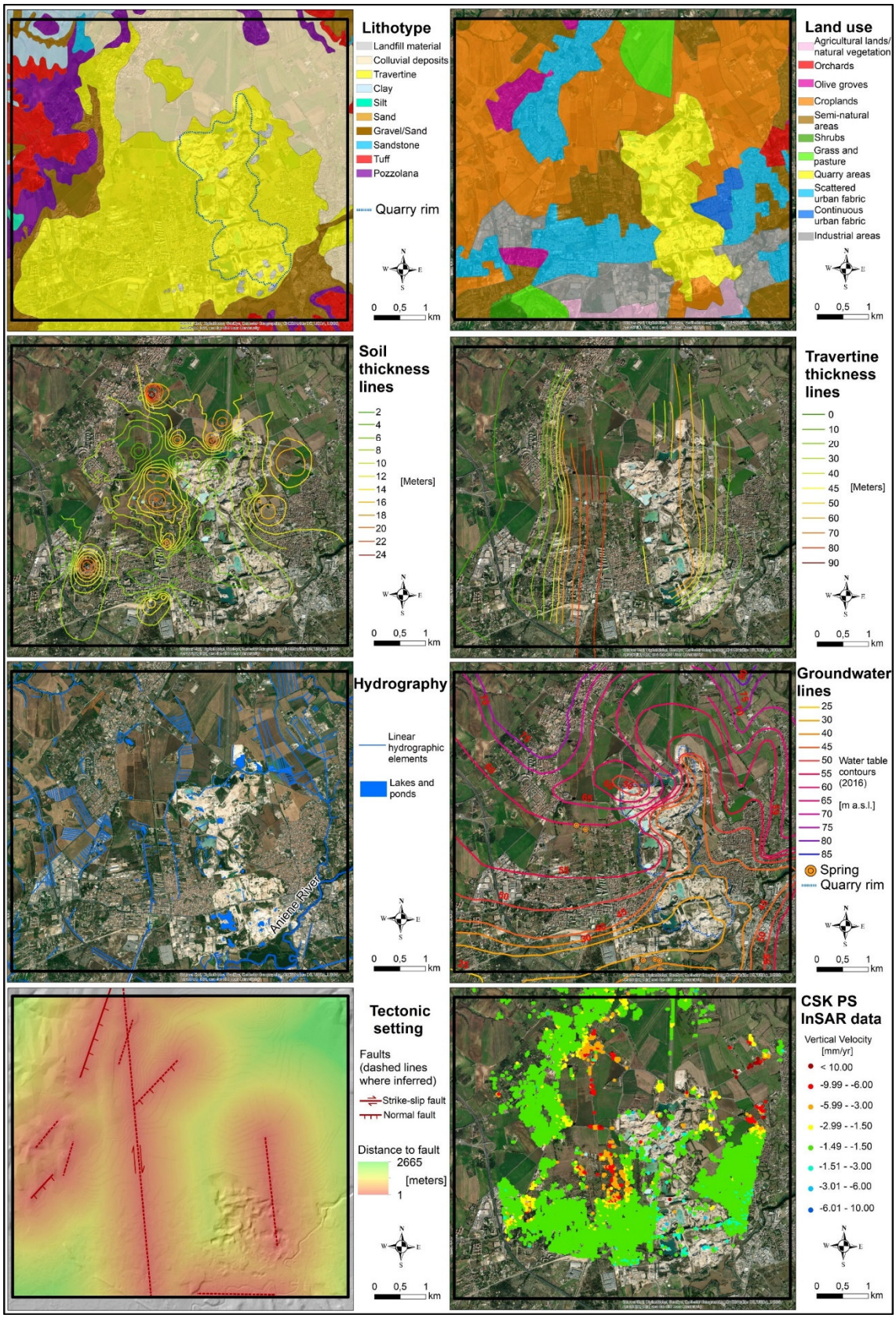

Figure 5.11: Maps of the eight conditioning and precursory factors chosen for assessing the sinkhole susceptibility over the study area. These maps are referred to the categorical and discrete data as they were available over the study area. Then, all the factor maps were converted into continuous surface raster maps with the same 10 m cell-size to be used as input data for MaxEnt algorithm.

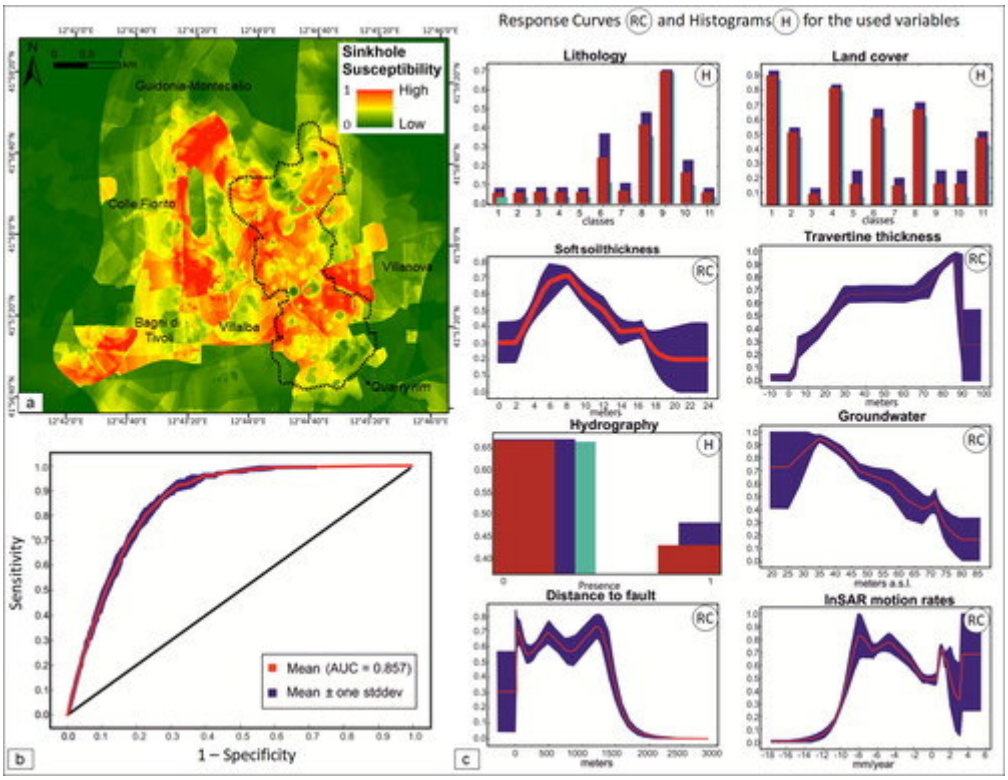

Figure 5.12: (a) Sinkhole susceptibility map of the study area; (b) AUC value of the ROC analysis (stddev = standard deviation); (c) Response curves (RC) and histograms (H) for the used variables. In RC, the red line represents the average value of the computed six repeats of the test, the blue area shows the average value ± stddev. In H, the light blue bar represents the model without the variable. The blue bar represents the model with the only variable. The red bar represents the final output. (Lithology classes: 1= Landfill; 2 = Clay, 3 = Sand, 4 = Tuff, 5 = Silt, 6 = Lithic tuff, 7 = Pozzolana, 8 = Colluvial deposit, 9 = Travertine, 10 = Gravel/Sand, 11 = Sandstone; Land use classes: 1= Continuous urban fabric, 2= Scattered urban fabric; 3= Industrial areas; 4= Quarry areas; 5 = Orchards; 6 = Olive groves; 7= Grass and pasture; 8 = Agricultural areas; 9 = Cropland, 10 = Scrubs; 11 = Semi-natural areas).

5.8 Internal validation – Altamura sinkholes (Apulia)

The internal validation form on the sinkholes at Altamura, Apulia, southern Italy, was produced by colleagues from the University of Bari, who shared their experience and the work done with participants to TK 2.2.2 during the meetings held on February 29, 2024. After that meeting, and the selection of the sites for internal validation, more detailed information was provided on analysis of the sinkholes at Altamura, Apulia, southern Italy, and is summarized in this section.

The study area is the eastern portion of the Altamura town (Apulia, southern Italy), heavily threatened by sinkholes occurrence (Pepe et al. 2013a, b; Fiore & Parise 2013). From a geological point of view, the area is characterized by the outcropping of Gravina calcarenite soft to very soft rock layers overlying a bedrock formed of Altamura limestone. Altamura is one of the largest towns in the High Murge of Apulia (south-east Italy), and is located in a foreland area consisting of carbonate rocks where karst is the main agent shaping the landscape (Parise, 2011). In addition to the many karst caves and surface landforms, there are several cavities of anthropogenic origin at the outskirts of town, in a sector undergoing fast urban expansion. These cavities represent a significant risk to the population. Until 2006, it was commonly believed that the subterranean voids were limited to a few areas near ancient open quarries since abandoned and partly filled with solid waste. However, a number of sinkholes have developed in recent years causing safety concerns. Information on these underground man-made cavities has increased greatly in recent years, with over 16 km of subterranean passages explored and mapped. Their abandonment, and the progressive weathering of the rock, has caused failures in the underground quarries. Eventually, such instabilities propagated upward

until reaching the surface, and producing sinkholes. Many sinkholes in Altamura have occurred within the urban area, and/or in areas of recent or proposed future constructions. A great amount of data has been collected in these studies in recent years, which has been organized and managed in a dedicated geo-database.

The man-made cavities that are the proximate cause of sinkhole formation at Altamura consist of underground quarries located at the north eastern and eastern outskirts of town. Their development may be hazardous in this recently urbanized area, where many buildings have been constructed in the last ten years. Only a small number of the buildings date back before 1990, and have been built using surficial foundations. Construction companies did not take into account the underground cavities until sinkholes began to develop. When cavities were found during construction, foundation piles were used to cross the cavities which often produced rock failures within the quarries.

In 2008, following some sinkhole events, the Altamura Municipality issued decree no. 135/2008 obliging all building owners considered at risk to undertake a detailed geological study to verify, and eventually mitigate, all dangerous situations for both public and private properties. At the same time, the Basin Authority of Basilicata issued specific regulations for any new construction, or modification of structures already existing in the areas at risk (Fiore, 2006; Berardi et al., 2010). These regulations included direct and indirect surveys aimed at ascertaining underground conditions, particularly the presence of voids and instability problems. These regulations included direct and indirect surveys aimed at ascertaining underground conditions, particularly the presence of voids and instability problems.

Documentation and temporal references have been found for eight sinkholes in the Altamura territory.

The main causes of the sinkholes at Altamura are both natural and anthropogenic. Anthropogenic activities have often accelerated processes that were occurring naturally. On the other hand, recent construction activities in the area where the underground quarries are located has highlighted a phenomenon that otherwise would have been less noticed.

In most of the cases, access to the underground quarries has been closed off for two main reasons: man-made solid waste fill and collapse of access points. Runoff water also played a role by transporting and depositing material at the entrances, which in turn produced additional loadings over gallery vaults. Whatever the reason, access closure impeded air circulation in the underground quarries, leading to degradation of the physical and mechanical properties of the calcarenite rock mass.

Rainfall runoff is among the most significant factors producing instability in the underground quarries. It is well documented that runoff from the urban area of Altamura is discharged into the old entrances of underground quarries, or in topographically depressed areas. Transport of solid materials by these waters is erosive and may, over time, change the permeability characteristics of the rock mass.

Pile foundations have likely contributed to the development of cracks and failures in the calcarenite rock mass; at the same time, they also represent preferential pathways for water flow.

In a few cases, boreholes below houses have been found to discharge rainfall runoff collecting in areas around the buildings.

There are several other factors that can contribute to sinkhole formation, although generally subordinate to the previously discussed factors. Leakage from hydric and sewer systems is common. At several areas the sewers directly enter the underground quarries; it is well known that contact between waste waters and soft rocks such as calcarenites may have serious consequences in terms of reduction in the mechanical properties of the rock mass.

Vibrations induced by the traffic may also act in amplifying or accelerating the process of degradation in the rock mass. Eventually, failures and falls from the vault progressively reduce the thickness of the overlying stiff calcarenite, and f ill voids with the breakdown deposits. These latter are frequently of a size that can damage the piles sustaining the buildings above.

Based on the collection of the different data carried out in recent years by the Municipal Authority of Altamura town, the following dataset is available:

- Detailed map of the caves and of the sinkholes occurred (Figure 1)

- Detailed map of the building areas and of the road net
- Detailed geological map and local stratigraphy
- Digital reconstruction of the ground surface via LiDAR technology
- Geotechnical properties of the calcarenite layer and of the overlying clay layer, when existing
- Land cover

Recently, a detailed investigation of the interferometry InSAR ground motion rates has been started by the Municipal Authority throughout the urban area and the corresponding data have been made available.

A GIS-based system was used to manage data associated with the underground quarries (Figure 10), and to highlight the most important data. These include plan views of the cave boundaries, which are basic information for planning any operational activities. The precise locations of narrow passages within the subterranean network are critical to choosing optimal sites for filling of underground voids. Using the dataset available at the Technical Office of the Altamura Municipality, a geo-database was developed. Data have been sub-divided into seven thematic groups (feature datasets) that comprise specific layers of the database. In order to map sinkhole spatial hazards, some criteria of exclusion, repulsion, and attraction (ERA) have been defined by assigning values to the land attributes in the database. In this way thematic maps were created, to which a weight was then given. Such an approach is not only important for describing and characterizing the territory, but is also aimed at determining those areas that are particularly affected by the phenomena and therefore require particular attention, especially with respect to the design of monitoring and/or alert systems.

To summarize, the tools used have been:

• a multi-criteria analysis to identify the most vulnerable areas and develop a zonation based on susceptibility to sinkholes;

• overlay mapping for spatial analysis.

The variables used to define the susceptibility map to sinkholes are:

1. Presence of cavities;
2. Presence of underground failures;
3. Depth of cavities;
4. Lithotypes;
5. Land use;
6. Surface hydrography;
7. Presence of faults;
8. Seismicity.

Some features such as tectonics and seismicity have not been taken into account because they are not available or homogeneous over the whole area.

The multi-criteria analysis (Malczewski, 1999) was carried out using the comparative matrix of coupled informative layers (Saaty, 1980). Through this procedure the following data layers necessary to produce the hazard map were identified:

• Presence of cavities

• Underground failures

• Cavity depths

• Land use

• Hydrogeology

Elaboration and digital overlaying of the individual data layers have produced the sinkhole spatial hazard map. This map is being used to identify the sectors that most need mitigation measures, taking into account all possible interactions between the spatial characteristics and potential susceptibility. Values with respect to criteria of exclusion, repulsion, and attraction were assigned to each theme with respect to its relative contribution in terms of susceptibility. The coupled themes were put into a comparison matrix, in order to determine relative weights. All the maps are in raster format, and, by assigning them weights, it was possible to sum the pixel values and obtain the sinkhole susceptibility map (Figure 2), with a maximum value of 60 (greatest susceptibility).

As concerns the key strengths of the model used for the Altamura area, and the areas for improvement, it should be pointed out that, as key strengths:

the dataset is quite easy to collect, given the co-operation with the Municipality of Altamura (within the framework of a PhD project), and the acceptable level of confidence of the susceptibility analysis results.

Areas for improvement: future attempt to take into account also the mechanical equilibrium conditions of the caves and the mechanical properties of the calcarenite rock to derive a mechanically-based sinkhole susceptibility map, based on previous experiences (see Perrotti et al., 2018, 2019).

Figure 5.13: Map of the anthropogenic cave net in the underground environment of Altamura, along with the sinkholes detected in the same area.

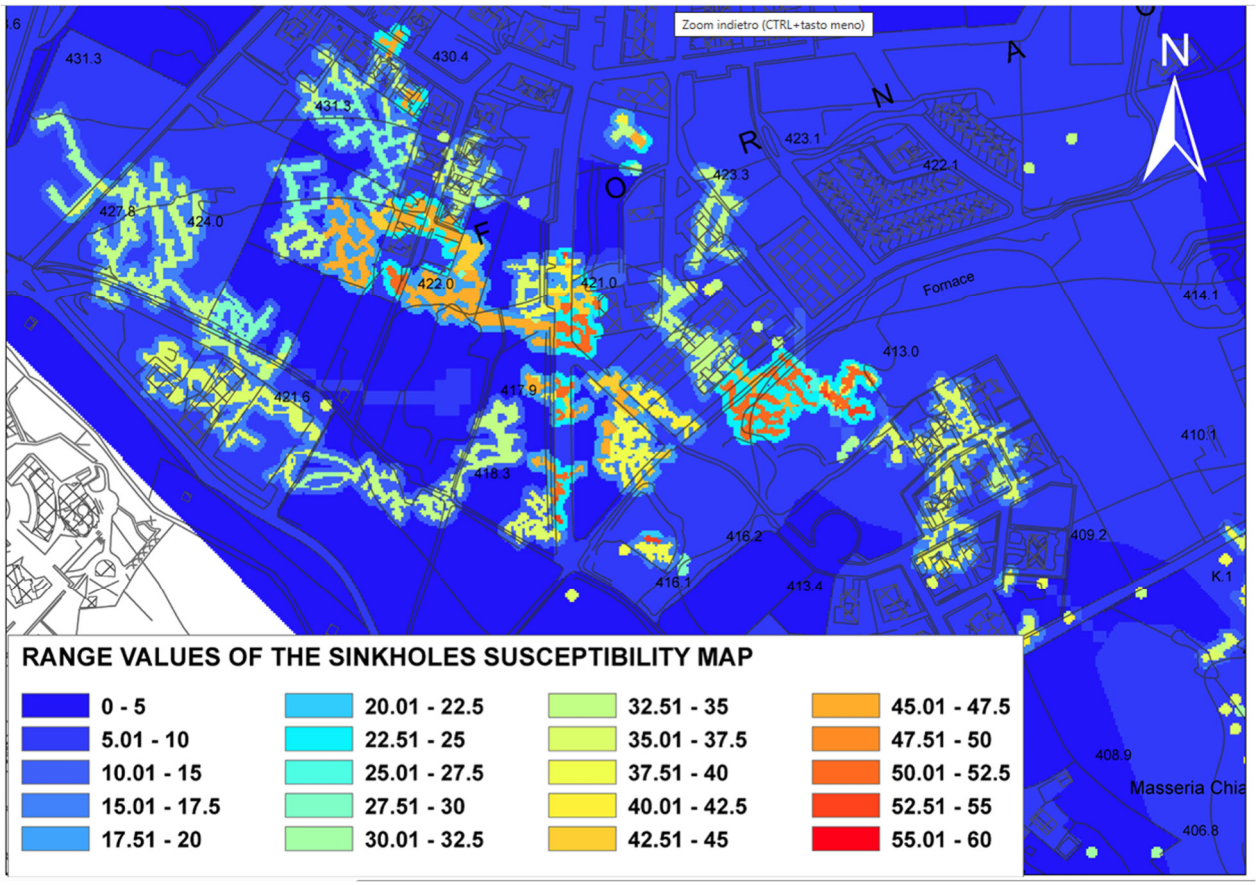

Figure 5.14: Sinkhole susceptibility map of the Altamura area.

5.9 Internal validation – Liquefaction in Emilia-Romagna

The internal validation form on analysis of liquefaction phenomena induced by seismic shaking in Emilia Romagna, was produced by colleagues from the University of Naples, who shared their experience and the work done with participants to TK 2.2.2 during the meetings held on February 29, 2024. After that meeting, and the selection of the sites for internal validation, more detailed information was provided on analysis of liquefaction phenomena induced by seismic shaking in Emilia Romagna, and is summarized in this section.

Liquefaction is a phenomenon marked by a rapid loss of soil strength and stiffness, which can occur in loose, saturated sandy soil deposits subjected to earthquake shaking or other forms of rapid loading. During liquefaction, when the effective stresses approach zero, the soil behaviour switches from that of a solid to that of a fluid, with potentially catastrophic consequences. The detrimental effects on structures and infrastructures put soil liquefaction among the most serious effects of earthquakes and in the last years there has been an increasing demand for improving the knowledge on this topic and, in particular, on the predisposing factors. In order to study these, the Emilia Romagna region, struck on May 2012 by an important seismic sequence, was chosen. The main shock occurred on 20 May 2012 (M_w=6.1) and caused extensive liquefaction phenomena. The part of the country which was affected by these violent shakes was the area of the river Po Valley, in the foreland basin of two mountain chains constituted by the Alps and the northern Apennine, in the Emilia-Romagna Region (Northern Italy). Since 19 May 2012, Emilia Romagna and surrounding sectors of Veneto and Lombardia were hit by a long seismic sequence characterized by about two thousand of shakes. Many buildings collapsed and 27 victims were recorded. The epicenter of the 20 May event (44.89°N latitude and 11.23°E longitude) was located between the provinces of Modena and Ferrara, while the hypocenter was at a depth of 6.3 km, owing to that it is considered a shallow earthquake (Lai et al., 2015). This event was extremely interesting in the Italian seismic literature, due to the rarity of such extended soil liquefaction phenomena in Italy. Although Italy is

a seismic country, liquefaction occurred only in restricted areas, with quite limited induced damage. The most evident effects of liquefaction phenomena following the 2012 earthquake were found in San Carlo (Municipality of Sant'Agostino) and Mirabello, whose subsoil was characterized as alluvial deposits of different depositional environment, consisting of alternated layers of silty-clayey deposits and sandy soils mainly constituting ancient rivers banks (Chiaradonna et al., 2018). The effects of liquefaction induced by the 2012 Northern Italy earthquake have been reported in several works (Sciarra et al., 2012; Vannucchi et al., 2012; Lombardi and Bhattacharya, 2014; Lai et al., 2015). As an example, some photos are shown as figure 5.15 (Vannucchi et al., 2012), where the typical effects of liquefaction may be noted, such as sand boils, vents, sinkholes, craters, surface ruptures, extensional fissures. Many open spaces, as courtyards, gardens and roads, were completely covered by the ejected sand, mud and water.

In this research, Emilia Romagna region was chosen to study in depth the predisposing factors of liquefaction phenomena and to develop susceptibility maps for this area.

Data for *level 1* and *level 2* liquefaction susceptibility map are summarise in Table 5.2, that lists the parameter type, the file format and the availability. In particular, geological, geotechnical and geophysical data are freely provided by Emilia Romagna Region, while seismic data (shakemap or seismic hazard map) from the INGV website. In addition, the point localization of historical liquefaction events (observations of 2012-earthquake) is also available for validation.

Liquefaction susceptibility can be evaluated in four levels as reported in Table 5.3. To define susceptibility in a vast area as Emilia Romagna, *level 1* should be recommended. According to the Italian Technical Standards for Constructions (NTC 2018, Section 7.11.3.4.2), the likelihood of liquefaction occurring in saturated sandy soils is low or zero if at least one of the following conditions occurs:

a. maximum expected accelerations at ground level in the absence of artefacts (free field conditions) less than 0.1g;

b. average seasonal depth of the water table greater than 15 m from ground level, for sub-horizontal ground level with superficial foundations;

c. deposits consisting of clean sands with normalised penetrometer resistance $(N_1)_{60} > 30$ or $q_{c1N} > 180$;

d. particle size distribution outside the zones shown in Fig. 2a in the case of soils with uniformity coefficient $U_c < 3.5$ and in Fig. 2b in the case of soils with uniformity coefficient $U_c > 3.5$.

If the first condition is not verified and, therefore, the maximum acceleration expected at ground level is higher than 0.1 g, the geotechnical investigations must be aimed at determining the parameters necessary to verify the other three conditions. These are all related to soil state or intrinsic parameters, therefore expressing the possibility of having under a seismic action: i) pore pressure build up at shallow depths (condition 2); ii) a state condition loose enough to induce a contractive behaviour, thus leading to positive pore pressure increments in an undrained or quasi-undrained mechanism (condition 3); iii) a granulometric distribution (intrinsic property) poorly graded and included in ranges considered critical based on previous experiences (condition 4).

When none of the four abovementioned conditions is satisfied, the site is potentially susceptible to liquefy (i.e. vulnerable, due to the presence of predisposing elements) and therefore potentially at risk (due to the non-negligible seismic hazard). It could be therefore necessary to assess the liquefaction safety factor (FS) at the depths where potentially liquefiable soils are present (*level 2*; Table 5.3). FS can be estimated by the following relationship:

$$FS = \frac{CRR}{CSR} \qquad (1)$$

Where CRR is the cyclic resistance ratio (evaluated by means of in situ-based or laboratory-based methods) and CSR is the cyclic stress ratio defined as:

$$\mathrm{CSR} = 0.65 \frac{a_{max}}{g} \frac{\sigma_v}{\sigma'_v} r_d \qquad (2)$$

where σ_v and σ'_v are the total and effective lithostatic stress at the generic depth (z), a_{max} is the peak value of the expected horizontal acceleration at the surface, g is the earth's gravitational acceleration and r_d is a reductive factor of the acceleration to take into account the deformability of the soil column and can be estimated empirically or calculated numerically through a local seismic response analysis.

FS values lower than 1 imply the liquefaction susceptibility of site. In this case, the potential consequences of liquefaction can be evaluated with the integral response of the deposit, through the simplified liquefaction index LSN (Tonkin and Taylor, 2013), defined as:

$$LSN = 1000 \int_0^{20} \frac{\varepsilon_v}{z} dz \quad (3)$$

where z is the depth in meters and ε_v is the post-liquefaction volumetric reconsolidation strain (entered as a decimal) that can be calculated according to existing charts (see Ishihara & Yoshimine, 1992). Degree of damage can be estimated as:

- 0<LSN<20: minor;
- 20<LSN<40: major;
- LSN>40: severe.

It is worth mentioning that LSN is not the only indicator proposed in literature, and many alternatives have been suggested in time. From a historical point of view, the first (and most popular) integral indicator is the *Liquefaction Potential Index*, *LPI* (Iwasaki et al., 1984), which represents a measure of the vulnerability of a site as a single value, ranging between 0 (very low risk) and values over 15 (very high risk), defined as:

$$LPI = \int_0^{20} F(z) \cdot W(z) dz \quad (4)$$

where z is the depth in meters, while $F(z)$ and $W(z)$ are respectively:

$$F(z) = \begin{cases} 1 - FS & \text{for } FS < 1 \\ 0 & \text{for } FS \geq 1 \end{cases} \quad (4a)$$

$$W(z) = 10 - 0.5z \quad (4b)$$

in which FS is computed by eq. (1).

Emilia Romagna region was affected by extensive liquefaction phenomena during the 2012 earthquake, which hit North-Italy. Geological and geotechnical data can be used to perform analyses of *level 1* and *2* (Table 5.3). In particular, analyses of *level 1* permits to identify the area susceptible to liquefaction, while those of *level 2* to identify the degree of damage through LSN (eq. 3) and LPI (eq. 4) values.

The procedure can be validated from point observations of the 2012 earthquake liquefaction by means of ROC (receiver operating characteristic) curve analysis for performance of the susceptibility assessment. The ROC is a graphical representation of the model fit. This type of analysis measures, for different thresholds (e.g., different values of Factor of Safety, or Susceptibility Class), the proportion of positive values (i.e., liquefaction presence) that are correctly identified as such (TPR; true positive rate or sensitivity) together with the proportion of negative values (i.e., liquefaction absence) that are erroneously reported as positive (FPR; false positive rate or fall-out). The area under the curve (AUC) is the value that summarizes the expected performance: the larger the area, the better the accuracy of the model.

As concerns the key strengths of the model used for the Emilia Romagna, and the areas for improvement, it should be pointed out, as key strengths, that the consequences of liquefaction in Italy may be catastrophic, as occurred in Japan, New Zealand and recently in Turkey. In order to study the predisposing factors for liquefaction the vast area of Emilia Romagna region has been chosen, thanks to the large amount of available data, that allowed to perform analyses of level 1 and 2, achieving a clear description of area susceptible to liquefaction. This method can be used for forecasting liquefaction susceptibility adopting scenario events for seismic hazard maps.

Although such methods of liquefaction susceptibility assessment provide an estimate of which areas are relatively more susceptible than others, when applied over large areas they have some uncertainties related to the spatialization of point data (geological and geotechnical) that often estimate indices along a vertical profile. To improved results, it is necessary to have a large amount of uniformly distributed data.

(a) (b)

(c) (d)

Figure 5.15: Liquefaction evidences at San Carlo: main roads covered by grey silty sand ejected from the ground in San Carlo (a); garage (b); sand boils (c) and a private house (d) (after Vannucchi et al., 2012).

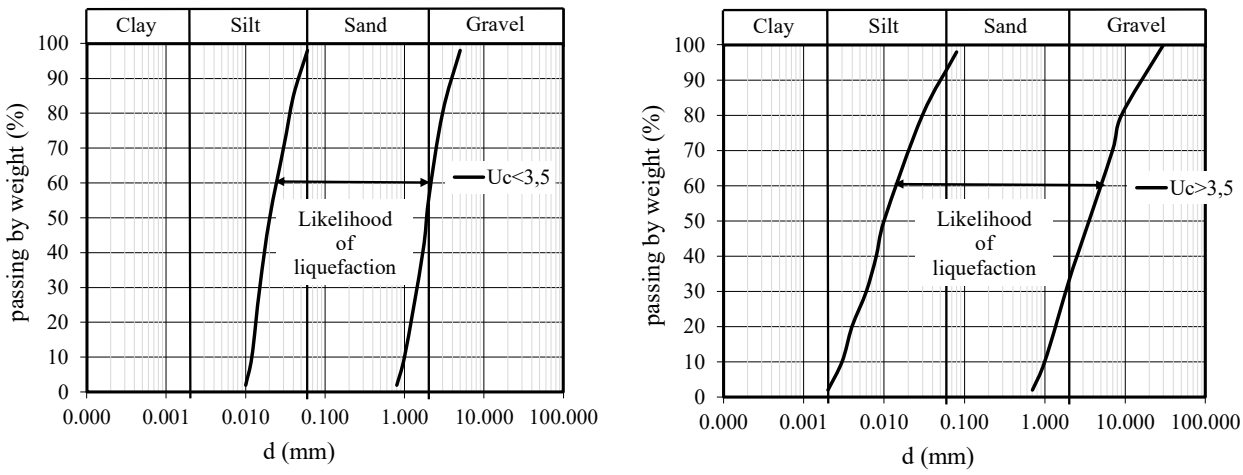

(a) U_c<3.5 (b) U_c>3.5

Figure 5.16: Particle size ranges of soils susceptible to liquefaction (adapted from NTC 2018).

Parameter	Data type	Format	Availability (Y/N)
Geological investigations	Borehole	Localization (shapefile)	Y
		Data (access DB)	Y
Ground water table	Depth of ground water table	-	N
Expected maximum acceleration	PGA map	PGA values (shapefile)	Y
Geotechnical investigations	CPT	Localization (shapefile)	Y
		Data (Excel)	Y
Geophysical investigation	Down Hole and Cross Hole	Localization (shapefile)	Y
		Data (pdf)	Y
Liquefaction events	Point localization	shapefile	Y

Table 5.2. Parameters for liquefaction triggering map.

Level of analysis	Type of analysis	Constitutive model	Calculation approach	Output
Level 1	Screening criteria (qualitative)	-	Evaluation of some parameters (grain size distribution, ground water table and expected maximum acceleration)	Liquefaction yes, no
Level 2	Semi-empirical methods	Elementary	Simplified stress-based	Actions (demand) vs. Resistance (capacity)
Level 2	Simplified dynamic analyses	Simplified (mostly visco-elastic, uncoupled)	Dynamic (with simplified geometry)	Total stresses, shear strains, pore pressure increments*
Level 4	Advanced dynamic analyses	Advanced (elasto-plastic with hardening, coupled)	Dynamic (with complex 3D geometry)	Total and effective stresses, shear strains, pore pressure increments, residual displacements

Table 5.3. Analyses for liquefaction triggering assessment (modified after Silvestri and d'Onofrio, 2014).

5.10 Insight on submarine landslides

5.10.1 Review of landslide susceptibility methods in marine environments

Using Scopus to look for the term "submarine landslide susceptibility" 29 documents are found, of which 16 elements are strictly related to the argument. As can be noted from the bibliographic data reported, landslide susceptibility maps in marine environments are not as frequent as those developed for the subaerial environment. Given the innovative nature of the topic, a brief review of the methods primarily used to generate submarine landslide susceptibility maps to understand which ones are best suited to be proposed within the framework of the RETURN project.

Many methods have been applied to elaborate the susceptibility of terrestrial geohazards, but the review highlighted that only the following three are applied to marine geological disasters: (1) deterministic approach, (2) statistical approach, and (3) heuristic approach. The deterministic approach is a quantitative assessment method based on comprehension of the occurrence mechanism of marine geological disasters and their physical laws. Deterministic methods require the use of sufficient and accurate input parameters in the geotechnical analysis to achieve an accurate assessment of slope stability analysis (Borges et al., 2016; Carlton et al., 2019; Collico et al., 2020; Nian et al., 2019; Strasser et al., 2011; Tan, Liu, et al., 2023). A statistical approach can be used for the qualitative and quantitative evaluation of landslide predisposition based on statistical principles to describe the correlation between condition factors including the slope gradient, lithology, curvature, flow accumulation, etc. Accordingly, this approach includes Wi-index (Avdievitch & Coe, 2022; Borrell et al., 2016; León & Somoza, 2011; Tarazona et al., 2023), information value (IV) (Lapa et al., 2020), logistic regression (LR) (Lapa et al., 2020), and machine learning algorithm such as gradient-boosted decision tree (Dyer et al., 2024), maximum entropy model (Innocenti et al., 2020), XGBoost model (Tan, Zhou, et al., 2023), k-means, spectral clustering, and hierarchical clustering (Du et al., 2022) ; Heuristic approaches, such as the analytic hierarchy process (AHP) (Shan et al., 2021), are indirect and qualitative methods with requirements for data based on prior insight into the causes and instability of geological disasters in the investigation area. The number of papers for each data-driven methods are reported in Table 5.4.

Data-driven methods	Number of papers
Slope stability analysis	6
Wi-index	5
Information value (IV)	1
Logistic regression (LR)	1
Machine learning	4
Analytic hierarchy process (AHP)	1

Table 5.4 "Popularity index" of different data-driven methods (rows) used to perform landslide susceptibility maps in the marine environment according to the number of papers where the methodology is used (column). Colors indicate the three most frequently used methods in red and yellow respectively.

5.10.2 Feasibility of the selected methods for susceptibility assessment in the marine environment

According to Table 5.4, the most popular methodologies for susceptibility assessment in the marine environment are slope stability analysis and Wi-index followed by Machine learning methods. In the case of slope stability analysis, geotechnical data are required to perform this type of analysis; however, these data are quite rare in marine environments and heterogeneous in space. For this reason, despite being a popular methodology in marine environments, we do not recommend its use in marine environments except in spatially limited areas.

The Wi-index (commonly called Frequency Ratio, the extended description of this method is in the **DV 2.2.5**) as well as Machine learning methods necessitate raster files reporting the characteristics of the study area and the mapped landslides with which to instruct the model. These types of data, unlike geotechnical ones, are readily available in the marine environment.

The interface developed for the elaboration of susceptibility maps in the context of the RETURN project includes four methodologies i.e. Logistic Regression (LR), Weight of evidence (WoE), Random Forest (RF) and Flow-R. Those methods have been described in chapter 5; however, they will be here briefly summarized.

LR is a statistical method used to model the probability of a binary event (yes/no, true/false) based on one or more independent variables. The LR method analyzes environmental variables (such as slope, geology, and land use) to determine the contribution of each to the probability of the event quantified with an output between 0 and 1. WoE is a statistical model that calculates the weight of each predisposing factor considering the presence and absence of the considered factors compared to the presence or absence of landslides. The final weight elucidates the spatial relationship of all landslides contributing factors and landslides. The RF method is a machine learning algorithm used for producing landslide susceptibility maps by combining predictions from many decision trees trained on different portions of the dataset. Flow-R method relies on drainage network and flow path analysis to identify areas most susceptible to mass movements. The model allows for automatic source area delineation and for the assessment of the propagation extent based on several published empirical run-out models at local and regional scales. various spreading.

Similarly to the Wi-index, those methodologies need raster files (e.g. DEM, Aspect, Slope, Lithology) and a layer containing the mapped landslides (through points or areas). Specifically, Flow-R requires only a DEM and user-defined source areas as input files. Anyway, Flow-R is an empirical model whose algorithms and simple frictional laws are built on the subaerial context.

For these reasons, we believe that the LR, WoE and RF methods are well-suited for the marine context since those methods do not involve the use of algorithms designed from subaerial data and so they are more easily adaptable to the marine context compared to Flow-R.

5.10.3. From predisposing factors to susceptibility maps input data

Among the literature analyzed, various predisposing factors are considered for the elaboration of susceptibility map. The variety in the selection of factors depends on the data availability by the authors and by the chosen methodology. In the context of the RETURN project, various predisposing factors have emerged through the analysis of case studies. In the **DV 2.2.3** WPs and TKs researchers identified and described which predisposing factor is important for the two categories of submarine ground instability consisting of rapid and slow submarine landslides (Table 5.5 extracted from the **DV 2.2.3**).

Subsequently, the RETURN research group of marine geologists has assigned a class to each predisposing factor representing the importance of the factor for the type of ground instability based on their experience and existing bibliography (Table 5.6).

The classes of importance assigned are: a) Negligible when the predisposing factor is considered irrelevant in predisposing slope to instability; b) Relevant: the predisposing factor is considered relevant for the instability process; c) Determinant: when the predisposing factor plays a very important role in the destabilization and d) Unknown/Not measured: when available information does not permit the exclusion but neither the consideration of the parameter.

Macro-category	Main Factors	Rapid Submarine landslide	Slow Submarine landslide
		Flows, Avalanches, Slides	*Creep, DsGSD*
Geology	Lithology	X	X
	Stratigraphic features		X
	Progradational stacking pattern	X	
	Weak layer	X	X
	Sedimentation rate	X	X
Geomorphology	Slope morphology	X	X
	Hyperpicnal flow and drainage basin character	X	
	Previous events/undercutting	X	
Physical and mechanical properties	Shear strength	X	
	Hydraulic Properties	X	X
Seismotectonics/Volcanism	Structural features	X	X
	Seismic activity	X	X
	Vertical movements	X	X
	Volcanic activity	X	
	Site effects (amplification/resonance)	X	X
Groundwater/Fluid	Presence of pressurized fluid/gas		X
Oceanographic	Littoral transport	X	

Table 5.5 Extract from the shared Predisposing Factors/Process-LE table of WP2 and their related influence for rapid and slow submarine landslide (correspond to Table 6 in **DV 2.2.3**).

Predisposing factors	Rapid landslide	Slow landslide
LEs number	8	4
Principal instability process type	Disintegrative landslide	DGPV
Geology	Lithology	Lithology
	Statigraphic features	Statigraphic features
	Progradational staking pattern	Progradational staking pattern
	Weak Layer	Weak Layer
	Sedimentation rate	Sedimentation rate
Geomorphology	Slope morphology	Slope morphology
	Hyperpycnal flow and drainage basin character	Hyperpycnal flow and drainage basin character
	Previous events/undercutting	Previous events/undercutting
Physical and mechanical properties	Shear strenght	Shear strenght
	Hydraulic properties	Hydraulic properties
Seismotectonics/ Volcanism	Structural features	Structural features
	Seismic activity	Seismic activity
	Vertical movement	Vertical movement
	Volcanic activity (in volcanic context)	Volcanic activity (in volcanic context)
	Site effects (amplification/resonance)	Site effects (amplification/resonance)
Groundwater/Fluid	Presence/effect of fluid/gas	Presence/effect of fluid/gas
Oceanographic	Littoral transport	Littoral transport

	Negligible	the factor is considered as irrelevant for the instability process
	Relevant	the factor is relevant for the instability process
	Determinant	the factor plays a very important role in the destabilization
	Unknown/Not measured	available information does not permit the quantification of the parameter

Table 5.6 Classification of the predisposing factor according to the degree of importance (this classification derives from the analysis of the learning examples presented in the RETURN project).

About all the relevant/very important predisponent factor recognized the for the susceptibility map we recognized that only part can be easily represented in a raster format. The basic prerequisite for creating a susceptibility map is the DEM (Digital Elevation Model), from which a series of important information about slope morphology, considered one of the determinant predisposing factors can be extracted (Table 3). The most important information that can be extracted from DEM: Slope, Curvature, Plan Curvature. The slope map contains information regarding other predisposing factors such as: the progradational staking pattern (as those characterizing terraces in nearshore, mid-shelf or the shelf edge portion) and previous events/undercutting.

Through the coastline and the hydrographic network, it is possible to create a raster depicting the distance from rivers through the Euclidean distance tool available in GIS. The distance from river is used as a simplified indicator of the impact of hyperpycnal flows correlated with the occurrence of flash floods considered as a relevant/determinant predisponent factor.

However, significant difficulties are encountered in obtaining other types of information that can't be extracted from a DEM as the lithology, presence of weak layer, sedimentation rate, presence of fluid/gas etc. The availability of those data changes from location to location for example the lithological information strictly depends on the availability of backscatter images, samples (sediment core, grabs, dredging, and box cores) or geotechnical data. Offshore lithological information are not uniformly available across the Italian continental margins and can be derived, for small portion across the continental shelf/slope, from Italian geological maps (derived by CARG project, https://www.isprambiente.gov.it/Media/carg/) in sheets covering coastal areas (Figure 5.17). Unfortunately, only a small portion of the available sheet with a marine portion also contains the lithological interpretation of the offshore portion (red boxes in Figure 5.17). Anyway, where the lithological attribute is present, it could represent a valid integration to the dataset to create susceptibility maps.

The sedimentation rate represents a determinant factor for submarine instability processes, but the quantification of this factor is very difficult to obtain. It strictly depends on the river input to the sea and by the littoral transport. In particular, the impact of littoral transport in terms of sedimentation volume is very difficult to calculate as it requires numerous repeated bathymetric surveys or the presence of sediment traps. Anyway, a novel multidisciplinary technique proposed by Palermo University and presented in the context of **WP3** - Novel sensors and techniques (described in the **DV 2.3.2**) could represent a step forward in the computation of this factor.

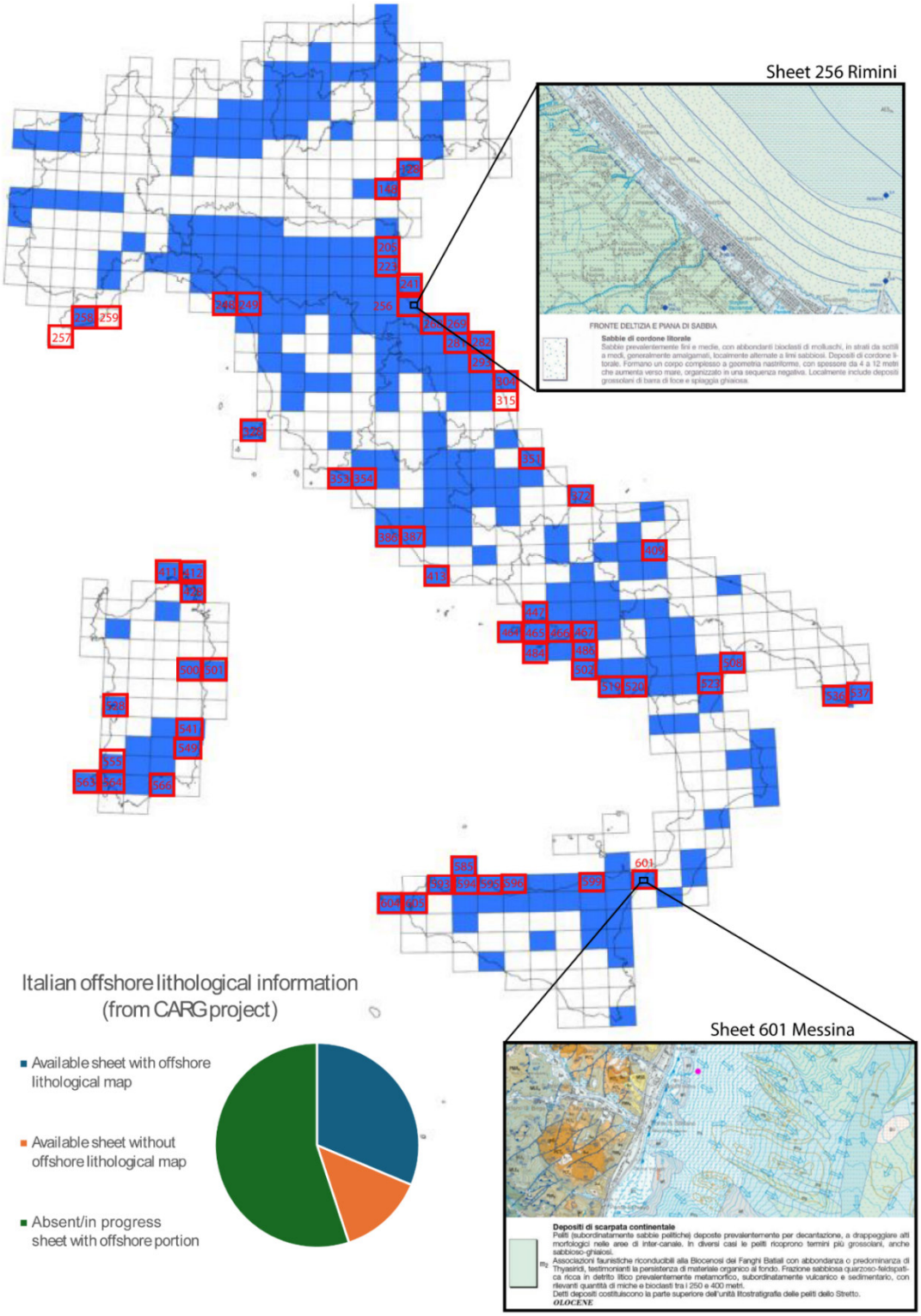

Figure 5.17 - Geological sheets of the Geological Map of Italy at a 1:50,000 scale. Sheets containing the lithological interpretation of the offshore areas are marked by red boxes. The pie chart highlights the percentage of sheets with lithological interpretation compared to the available sheets where the interpretation is missing and sheets where the offshore portion is absent or in progress.

6. Conclusions

The work undertaken as part of this **DV 2.2.4** represents a multi-faceted endeavour that builds on the initial selection of case studies or Learning Exemples (LEs) and progresses through internal validation via in-depth studies, each focusing on a specific type of ground instability. These efforts reflect a systematic approach aimed at improving our understanding of the complexity of slope dynamics and their impact on urban resilience and safety.

As part of these activities, the working group assigned to Work Package 2 (WP2), in collaboration with the Spoke Coordination and other working groups in different Work Packages (WPs), has sought to interpret the objectives set out in the Executive Working Plan as an integrated and synergistic process. This approach is particularly evident in the context of **Task 2.3** and **DV 2.2.6**, where the focus was on proposing operational solutions to define a semi-automated interface for performing GI proneness analysis using user-uploaded data to generate susceptibility maps.

These spatial datasets serve as basic building blocks for an analysis chain that aims to assess both precursory and triggering factors contributing to soil instability. By systematically investigating these factors, the project aims to provide a comprehensive understanding of slope dynamics and their potential impact on the built-up environment. Through this holistic approach, the project as a whole seeks to achieve its overarching goals of urban resilience and disaster risk reduction. The development of a semi-automated interface represents a significant advance in streamlining the ground instabilities analysis process. By utilizing user-generated data, the interface allows to contribute to the creation of susceptibility maps, improving the accuracy and relevance of the analysis. This collaborative approach not only encourages greater stakeholder engagement, but also provides to the communities the opportunity to actively participate in the identification of geological hazards, and mitigation of the related risks, in their respective areas. Furthermore, the proposed operational solution underlines the project's commitment to innovation and technological advancement. By harnessing the power of automation and data-driven analysis, the project aims to overcome the traditional barriers associated with manual vulnerability mapping. This not only speeds up the analysis process, but also improves its scalability and replicability in different geographical contexts.

By integrating susceptibility mapping into a broader risk assessment and management framework, the project also aims to improve the resilience of urban areas to ground instability hazards. By identifying vulnerable areas and implementing targeted mitigation measures, stakeholders can reduce the potential impact of land instability on infrastructure, livelihoods and communities. This pro-active approach is in line with global efforts to build more resilient cities that can withstand the challenges of natural disasters and climate change. The work described in this DV represents the first and fundamental step for the creation of a chain of analysis that, by studying also the preparatory and triggering factors, allows the VS2 as a whole to achieve the PE3 general objectives.

In this framework, the joint process carried out within **TK 2.2** and **TK 2.3** and described both by this DV and by **DV 2.2.6**, can be considered as summarized in three phases (Figure 7.1).

Stage 1. Expert-based identification of ground instability processes

Stage 2. Susceptibility analysis

Stage 3. Connection to **WP3** and **WP4**

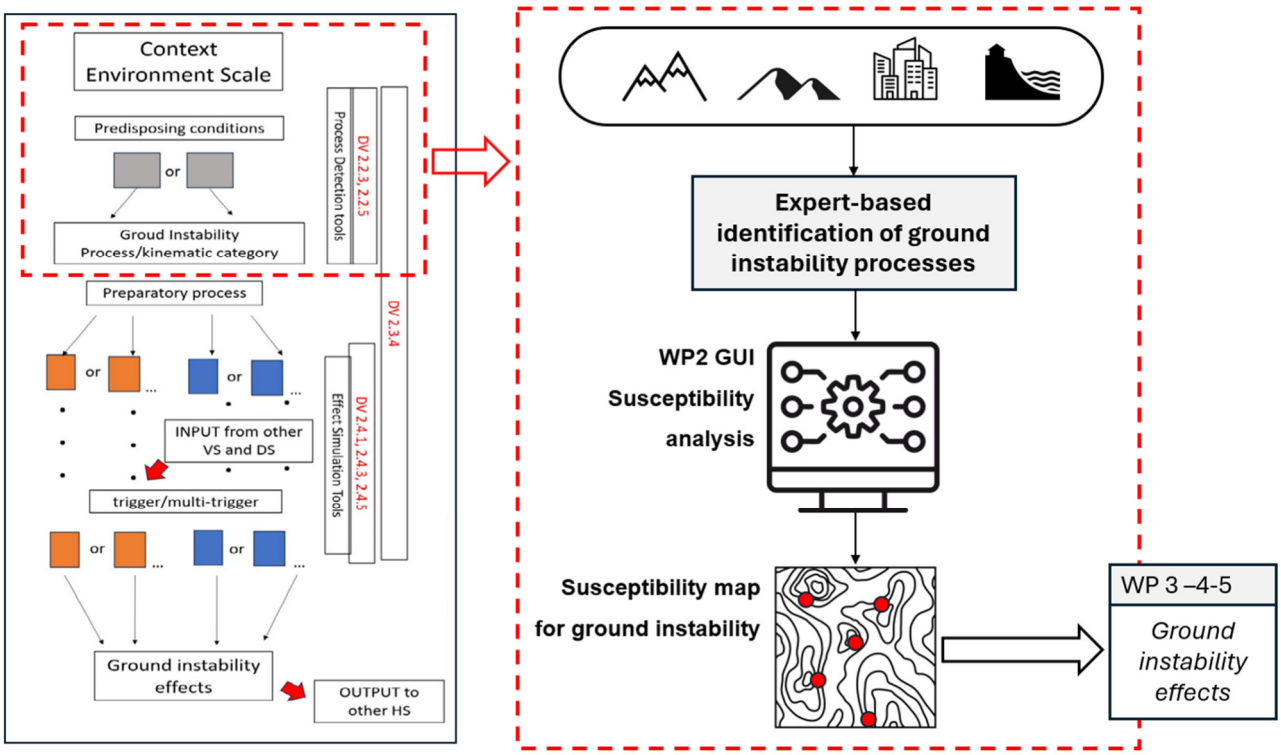

Figure 6.1: Overview of the synergistic approach of **TK 2.2** and **TK 2.3** (see also **DV 2.2.6**)

The validation cases presented in this DV are to be understood as a summary of the Stage 1 process.

In this first phase, the predominant types of instability processes affecting the area are identified in detail. This critical first step is the basis for the subsequent analysis and mitigation strategies, including the selection of appropriate tools to analyze preparation, initiation and propagation (**WP3** and **WP4**).

The initial assessment of ground instability hazards extensively relies on expert judgment to interpret data from various sources. Professional geologists conduct thorough evaluations of the geological and geomorphological settings, including rock types, soil properties, landforms, and structural landscape features, all vital for determining susceptibility to different instability processes. Historical data is also crucial; by examining past instability events, experts can discern patterns, frequencies, and triggers, which are essential for predicting future occurrences and assessing potential risks. Additionally, maps and remote sensing data, including land use data and satellite imagery, are crucial for identifying signs of potential instability.

These analyses enable experts to determine the types of ground instabilities prevalent in the area and identify the primary predisposing factors to be considered in the susceptibility assessment.

Stages 2 and 3, described in **DV 2.2.6** (document to which please refer for further information), complete the process and represent the contribution of **WP2** to the entire process of building a PoC for ground instability, as envisaged by the Project.

In the same **DV 2.2.6** and in subsequent Spoke DVs, the theme will be the subject of developments and insights.

7. References

Avdievitch, N. N., & Coe, J. A. (2022). Submarine Landslide Susceptibility Mapping in Recently Deglaciated Terrain, Glacier Bay, Alaska. Frontiers in Earth Science, 10(March), 1–21. https://doi.org/10.3389/feart.2022.821188

Bianchini S., Confuorto P., Intrieri E., Sbarra P., Di Martire D., Calcaterra D. & Fanti R. (2022). Machine learning for sinkhole risk mapping in Guidonia-Bagni di Tivoli plain (Rome), Italy. Geocarto International 37 (27), 16687-16715, doi: 10.1080/10106049.2022.2113455.

Billi, A., De Filippis, L., Poncia, P. P., Sella, P., Faccenna, C. (2016). Hidden sinkholes and karst cavities in the travertine plateau of a highly-populated geothermal seismic territory (Tivoli, central Italy). Geomorphology, 255, 63-80.

Borges, R. G., de Lima, A. C., & Kowsmann, R. O. (2016). Areas Susceptible to Landsliding on the Continental Slope. In Geology and Geomorphology (1st ed.). Elsevier Ltd. https://doi.org/10.1016/b978-85-352-8444-7.50013-5

Borrell, N., Somoza, L., León, R., Medialdea, T., Gonzalez, F. J., & Gimenez-Moreno, C. J. (2016). GIS catalogue of submarine landslides in the Spanish continental shelf: Potential and difficulties for susceptibility assessment. Advances in Natural and Technological Hazards Research, 41(July), 499–508. https://doi.org/10.1007/978-3-319-20979-1_50

Bozzano F., Esposito C., Franchi S., Mazzanti P., Perissin D., Rocca A. & Romano E. (2015). Understanding the subsidence process of a quaternary plain by combining geological and hydrogeological modelling with satellite InSAR data: The Aquae Albule Plain case study. Remote Sensing of Environment 16, 219-238. https://doi.org/10.1016/j.rse.2015.07.010.

Brunetti E., Jones J. P., Petitta M. & Rudolph D. L. (2013). Assessing the impact of large- scale dewatering on fault-controlled aquifer systems: A case study in the Acque Albule basin (Tivoli, central Italy). Hydrogeology Journal, 21 (2), 401–423.

Calcaterra, D., & Parise, M. (2010). Weathering as a predisposing factor to slope movements: an introduction. Geological society, London, Engineering Geology Special Publications, 23(1), 1-4.

Caramanna, G., Ciotoli, G., Nisio, S. (2008). A review of natural sinkhole phenomena in Italian plain areas. Natural hazards, 45(2), 145-172.

Carlton, B., Vanneste, M., Forsberg, C. F., Knudsen, S., Løvholt, F., Kvalstad, T., Holm, S., Kjennbakken, H., Mazhar, M. A., Degago, S., & Haflidason, H. (2019). Geohazard assessment related to submarine instabilities in bjørnafjorden, norway. Geological Society Special Publication, 477(1), 549 – 566. https://doi.org/10.1144/SP477.39

Casalbore, D., Bosman, A., Casas, D., Chiocci, F., Martorelli, E., Ridente, D. (2019) Morphological Variability of Submarine Mass Movements in the Tectonically–Controlled Calabro–Tyrrhenian Continental Margin (Southern Italy). Geosciences, 9, 43. https://doi.org/10.3390/geosciences9010043.

Catani, F., Casagli, N., Ermini, L., Righini, G., & Menduni, G. (2005). Landslide hazard and risk mapping at catchment scale in the Arno River basin. Landslides, 2, 329-342.

Catani, F., Lagomarsino, D., Segoni, S., & Tofani, V. (2013). Landslide susceptibility estimation by random forests technique: sensitivity and scaling issues. Natural Hazards and Earth System Sciences, 13 (11), 2815-2831.

Centamore, E., Nisio, S., Rossi, D. (2009). The San Vittorino Sinkhole Plain: relationships between bedrock structure, sinking processes, seismic events and hydrothermal springs. Bollettino della Società Geologica Italiana, 128(3), 629-639.

Ceramicola, S., Praeg, D., Cova, A., Accettella, D., Zecchin, M. (2014). Seafloor distribution and last glacial to postglacial activity of mud volcanoes on the Calabrian accretionary prism, Ionian Sea. Geo-Marine Letters, 34 (2-3), 111-129. DOI: 10.1007/s00367-013-0354-y.

Ceramicola, S., Tinti, S., Zaniboni, F., Praeg, D., Planinsek, P., Pagnoni, G., Forlin, E. (2014). Reconstruction and tsunami modeling of a submarine landslide on the ionian margin of Calabria (Mediterranean sea). In: Landslide Science for a Safer Geoenvironment: Volume 3: Targeted Landslides, 557-562. DOI: 10.1007/978-3-319-04996-0_85.

Chiaradonna A., Tropeano G., d'Onofrio A. & Silvestri F. (2019). Interpreting the deformation phenomena of a levee damaged during the 2012 Emilia earthquake. Soil Dynamics and Earthquake Engineering, 124, 389-398.

Chiaradonna, A., Özcebe, A. G., Bozzoni, F., Fama, A., Zuccolo, E., Lai, C. G., Flora, A., Cosentini, M.R., d'Onofrio, A., Bilotta, E. and Silvestri, F. (2018). Numerical simulation of soil liquefaction during the 20 May 2012 M6. 1 Emilia Earthquake in Northern Italy: the case study of Pieve di Cento. In Proceedings of the 16th European Conference on Earthquake Engineering, 16ECEE, Thessaloniki, Greece, 18-21 June 2018. Paper (Vol. 11234).

Ciotoli, G., Di Loreto, E., Finoia, M. G., Liperi, L., Meloni, F., Nisio, S., Sericola, A. (2016). Sinkhole susceptibility, Lazio region, central Italy. Journal of Maps, 12(2), 287-294.

Colantoni, P., Gennesseaux, M., Vanney, J.R., Ulzega, A. (1992). Melegari, G.; Trombetta, A. Processi dinamici del canyon sottomarino di gioia tauro (Mare Tirreno). Giorn. Geol., 3, 199–213.

Collico, S., Arroyo, M., Urgeles, R., Gràcia, E., Devincenzi, M., & Peréz, N. (2020). Probabilistic mapping of earthquake-induced submarine landslide susceptibility in the South-West Iberian margin. Marine Geology, 429(December 2019), 106296. https://doi.org/10.1016/j.margeo.2020.106296

Convertino, M., Troccoli, A., Catani, F. (2013). Detecting fingerprints of landslide drivers: a MaxEnt model. Journal of Geophysical Research: Earth Surface, 118(3), 1367-1386.

De Ritis, R., Nardi, A., Materni, V., Venuti, A., Stefanelli, P., Rotella, G., Chiappini, M. (2020). Multidisciplinary study of subsidence and sinkhole occurrences in the Acque Albule Basin (Roma, Italy). Earth and Space Science, 7(7), e2019EA000870.

Del Prete S., Iovine G., Parise M. & Santo A. (2010). Origin and distribution of different types of sinkholes in the plain areas of Southern Italy. Geodinamica Acta, 23 (1/3), 113-127.

Du, X., Sun, Y., Song, Y., Xiu, Z., & Su, Z. (2022). Submarine Landslide Susceptibility and Spatial Distribution Using Different Unsupervised Machine Learning Models. Applied Sciences (Switzerland), 12(20). https://doi.org/10.3390/app122010544

Dyer, A. S., Mark-Moser, M., Duran, R., & Bauer, J. R. (2024). Offshore application of landslide susceptibility mapping using gradient-boosted decision trees: a Gulf of Mexico case study. Natural Hazards, 0123456789. https://doi.org/10.1007/s11069-024-06492-6

Faccenna C., Soligo M., Billi A., De Filippis L., Funiciello R., Rossetti C., et al. (2008). Late Pleistocene depositional cycles of the Lapis Tiburtinus travertine (Tivoli, Central Italy): Possible influence of climate and fault activity. Global and planetary change, 63 (4), 299–308.

Fiore A. (2006). Pericolosità geologica connessa alla presenza di cavità sotterranee. Atto di indirizzo dell'Autorità di Bacino della Puglia. Geologi & Territorio, 1-2-3, 3-11.

Fiore, A., Parise, M. (2013). Cronologia degli eventi di sprofondamento in Puglia, con particolare riferimento alle interazioni con l'ambiente antropizzato. Memorie Descrittive della Carta Geologica d'Italia, 93, 239-252.

Floris M., Bozzano F., Strappaveccia C., Baiocchi V. & Prestininzi A. (2014). Qualitative and quantitative evaluation of the influence of anthropic pressure on subsidence in a sedimentary basin near Rome. Environmental Earth Sciences. http://dx.doi.org/10. 1007/s12665-014-3317-3.

Galeazzi C. (2013). The typological tree of artificial cavities: a contribution by the Commission of the Italian Speleological Society. Opera Ipogea, 1, 9-18.

Gomes, V. H., IJff, S. D., Raes, N., Amaral, I. L., Salomão, R. P., de Souza Coelho, L., Ramos, J. F. (2018). Species Distribution Modelling: Contrasting presence-only models with plot abundance data. Scientific Reports, 8(1), 1003.

Gutierrez F., Parise M., De Waele J. & Jourde H. (2014). A review on natural and human-induced geohazards and impacts in karst. Earth Science Reviews, vol. 138, p. 61-88, doi: 10.1016/j.earscirev.2014.08.002.

Guzzetti, F., Ardizzone, F., Cardinali, M., Galli, M., Reichenbach, P., & Rossi, M. (2008). Distribution of landslides in the Upper Tiber River basin, central Italy. Geomorphology, 96(1-2), 105-122.

Innocenti, C., Battaglini, L., D'angelo, S., & Fiorentino, A. (2020). Submarine landslides: Mapping the susceptibility in european seas. Quarterly Journal of Engineering Geology and Hydrogeology, 54(1). https://doi.org/10.1144/qjegh2020-027

Ioualalen, M., Migeon, S., Sardoux, O., 2010. Landslide tsunami vulnerability in the Ligurian Sea: case study of the 1979 October 16 Nice international airport submarine landslide and of identified geologicalmass failures. Geophysical Journal International 181, 724–740. http://dx.doi.org/10.1111/j.1365-246X.2010.04572.x.

Ishihara K. (1993). Liquefaction and flow failure during earthquakes. Geotechnique, 43(3), 351-451.

Ishihara, K., Yoshimine, M. (1992). Evaluation of settlements in sand deposits following liquefaction during earthquakes. Soils and Foundations, 32 (1), 173–188.

Iwasaki, T., Arakawa, T. and Tokida, K.I. (1984). Simplified procedures for assessing soil liquefaction during earthquakes. International Journal of Soil Dynamics and Earthquake Engineering, 3 (1), 49-58.

Kaky, E., Nolan, V., Alatawi, A., Gilbert, F. (2020). A comparison between Ensemble and MaxEnt species distribution modelling approaches for conservation: A case study with Egyptian medicinal plants. Ecological Informatics, 60, 101150.

Kornejady, A., Ownegh, M., Bahremand, A. (2017). Landslide susceptibility assessment using maximum entropy model with two different data sampling methods. Catena, 152, 144-162.

Koseki J., Wakamatsu K., Sawada S. & Matsushita K. (2015). Liquefaction-induced damage to houses and its countermeasures at Minami-Kurihashi in Kuki City during the 2011 Tohoku Earthquake, Japan. Soil Dynamics and Earthquake Engineering, 79, 391-400.

Lai, C. G., Bozzoni, F., Mangriotis, M. D., Martinelli, M. (2015). Soil Liquefaction during the 20 May 2012 M5. 9 Emilia Earthquake, Northern Italy: Field Reconnaissance and Post-Event Assessment. Earthquake Spectra, 31(4), 2351-2373.

Lapa, N., Marques, F. M. F. S., & Rodrigues, A. (2020). Aveiro canyon head (Portugal) submarine slope instability assessment. Applied Sciences (Switzerland), 10(24), 1–17. https://doi.org/10.3390/app10249038

León, R., & Somoza, L. (2011). GIS-based mapping for marine geohazards in seabed fluid leakage areas (Gulf of Cadiz, Spain). Marine Geophysical Research, 32(1), 207–223. https://doi.org/10.1007/s11001-011-9135-z

Lirer S., Chiaradonna A. & Mele L. (2020). Soil liquefaction: from mechanisms to effects on the built environment. Rivista Italiana di Geotecnica, 3, 2020.

Liso I.S. & Parise M. (2023). Sinkhole development at the freshwater-saltwater interface in Apulia (southern Italy). In: Land L., Kromhout C. & Suter S. (Eds.), Proceedings of the 17th Multidisciplinary Conference on Sinkholes and the Engineering and Environmental Impacts of Karst, Tampa (Florida, USA), 27-31 March 2023, NCKRI Symposium no. 9, p. 229-238.

Lombardi, D., Bhattacharya, S. (2014). Liquefaction of soil in the Emilia-Romagna region after the 2012 Northern Italy earthquake sequence. Natural Hazards, 73 (3), 1749-1770.

Luti, T., Segoni, S., Catani, F., Munafò, M., & Casagli, N. (2020). Integration of remotely sensed soil sealing data in landslide susceptibility mapping. Remote Sensing, 12 (9), 1486.

Nian, T., Guo, X., Zheng, D., Xiu, Z., & Jiang, Z. (2019). Susceptibility assessment of regional submarine landslides triggered by seismic actions. Applied Ocean Research, 93. https://doi.org/10.1016/j.apor.2019.101964

Nisio S., Caramanna G. & Ciotoli G. (2007). Sinkholes hazard in Italy: first results on the inventory and analysis of some case studies. In: Parise M. & Gunn J. (eds.) Natural and anthropogenic hazards in karst: Recognition, Analysis and Mitigation. Geological Society of London, special publication 279, 23–45.

NTC (2018) - Aggiornamento delle norme tecniche per le costruzioni. Ministero delle infrastrutture e dei trasporti.

Ozdemir, A. (2016). Sinkhole susceptibility mapping using logistic regression in Karapınar (Konya, Turkey). Bulletin of Engineering Geology and the Environment, 75, 681-707.

Parise M. (2011). Surface and subsurface karst geomorphology in the Murge (Apulia, southern Italy). Acta Carsologica 40 (1), 79-93.

Parise M. (2019). Sinkholes. In: White W.B., Culver D.C. & Pipan T. (Eds.), Encyclopedia of Caves. Academic Press, Elsevier, 3rd edition, ISBN ISBN 978-0-12-814124-3, p. 934-942.

Parise M. (2022). Sinkholes, Subsidence and Related Mass Movements. In: Shroder J.J.F. (Ed.), Treatise on Geomorphology, vol. 5. Elsevier, Academic Press, pp. 200–220. https://dx.doi.org/10.1016/B978-0-12-818234- 5.00029-8. ISBN: 9780128182345.

Parise M., Galeazzi C., Bixio R., Dixon M. (2013). Classification of artificial cavities: a first contribution by the UIS Commission. In: Filippi M. & Bosak P. (Eds.), Proc. 16th Int. Congr. Speleology, Brno, 21-28 July 2013, 2, pp. 230-235.

Parise, M., Vennari, C. (2017). Distribution and features of natural and anthropogenic sinkholes in Apulia. In: Renard P. & Bertrand C. (Eds.), EuroKarst 2016, Neuchatel. Advances in the hydrogeology of karst and carbonate reservoirs. Springer, ISBN 978-3-319-45464-1, p. 27-34.

Pepe P., Pentimone N., Garziano G., Martimucci V. & Parise M. (2013a). Lessons learned from occurrence of sinkholes related to man-made cavities in a town of southern Italy. In: Land L., Doctor D.H. & Stephenson B. (Eds.), Proceedings of the 13th Multidisciplinary Conference on Sinkholes and the Engineering and Environmental Impacts of Karst, Carlsbad (New Mexico, USA), 6-10 May 2013, National Cave and Karst Research Institute, p. 393-401.

Pepe, P., Garziano, G., Parise, M. (2013b). L'utilizzo delle tecniche GIS per la valutazione della suscettibilità a sprofondamenti: il caso di studio di Altamura (BA). Memorie Descrittive della Carta Geologica d'Italia, 93, 365-380.

Pepe, P., Pentimone, N., Garziano, G., Parise, M., Martimucci, V., Lorusso, G. (2013c). Le cave sotterranee di Altamura. Fasi operative per la mappatura e per il supporto alle attività di bonifica. Atti del Convegno "Studi ed interventi per il risanamento delle cavità antropiche e naturali. Aspetti geologici, geotecnici e sismici", Geologia dell'Ambiente, suppl. 2/2013, 33-40.

Perrotti M., Lollino P., Fazio N.L. & Parise M. (2019). Stability charts based on the finite element method for underground cavities in soft carbonate rocks: validation through case-study applications. Natural Hazards and Earth System Sciences, 19, 2079-2095.

Perrotti M., Lollino P., Fazio N.L., Pisano L., Vessia G., Parise M., Fiore A. & Luisi M. (2018). Finite Element–based stability charts for underground cavities in soft calcarenites. ASCE International Journal of Geomechanics, 18 (7), 04018071.

Phillips S.J., Dudík M., Schapire R.E. (2021). Maxent software for modeling species niches and distributions (Version 3.4.1). [accessed 2018 May 21]. ttps://biodiversityinformatics.amnh.org/open_source/maxent/.

Phillips, S.J., Anderson, R.P., Schapire, R.E. (2006). Maximum entropy modeling of species geographic distributions. Ecological modelling, 190(3-4), 231-259.

Rosi, A., Tofani, V., Tanteri, L., Tacconi Stefanelli, C., Agostini, A., Catani, F., & Casagli, N. (2018). The new landslide inventory of Tuscany (Italy) updated with PS-InSAR: geomorphological features and landslide distribution. Landslides, 15, 5-19.

Sciarra, A., Cantucci, B., Buttinelli, M., Galli, G., Nazzari, M., Pizzino, L., Quattrocchi, F. (2012). Soil-gas survey of liquefaction and collapsed caves during the Emilia seismic sequence. Annals of Geophysics, 55(4).

Shan, Z., Guo, F., Lai, X., & Xiao, J. (2021). Assessment of Submarine Landslide Susceptibility in the Sea Area of Zhoushan. IOP Conference Series: Earth and Environmental Science, 734(1). https://doi.org/10.1088/1755-1315/734/1/012023

Sinharay S. (2010). Jackknife methods. In: Peterson P, Baker E, McGaw B editors, International encyclopedia of education: Elsevier Ltd; p. 229–231. https://doi.org/10.1016/B978-0-08-044894-7.01338-5.

Strasser, M., Hilbe, M., & Anselmetti, F. S. (2011). Mapping basin-wide subaquatic slope failure susceptibility as a tool to assess regional seismic and tsunami hazards. Marine Geophysical Research, 32(1), 331 – 347. https://doi.org/10.1007/s11001-010-9100-2

Tan, L., Liu, F., Huang, Y., Wang, R., Geng, J., Crosta, G., & Frattini, P. (2023). Mapping submarine landslides susceptibility in continental slopes with rich gas hydrates. Gas Science and Engineering, 116. https://doi.org/10.1016/j.jgsce.2023.205054

Tan, L., Zhou, M., & Wang, F. (2023). A Probabilistic Assessment Framework for Submarine Landslide Susceptibility in Continental Slopes with Rich Gas Hydrates. Journal of Marine Science and Engineering, 11(7). https://doi.org/10.3390/jmse11071366

Tarazona, D. M., Prieto, J., Murphy, W., Vesga, J. N., Rincon, D., Munoz, C. H., Pinzon, H. M., Mora, A. M., & Acuña-Uribe, M. (2023). Submarine landslide susceptibility assessment along the southern convergent margin of the Colombian Caribbean. Leading Edge, 42(5), 344 – 359. https://doi.org/10.1190/tle42050344.1

Tinti, S., Pagnoni, G., Zaniboni, F. (2006). The landslides and tsunamis of 30th December 2002 in Stromboli analysed through numerical simulations. Bulletin of Volcanology, 68, 462-479, doi: 10.1007/s00445-005-0022-9.

Tonkin, Taylor. (2013). Canterbury Earthquakes 2010 and 2011. Land report as at 29 February 2012. 108 pp. Earthquake Commission.

Tonni L., Gottardi G., Amoroso S., Bardotti R., Bonzi L., Chiaradonna A., d'Onofrio A., Fioravante V., Ghinelli A., Giretti D., Lanzo G., Madiai C., Marchi M., Martelli L., Monaco P., Porcino D., Razzano R., Rosselli S., Severi P., Silvestri F., Simeoni L., Vannucchi G., Aversa S. (2015). Analisi dei fenomeni deformativi indotti dalla sequenza sismica emiliana del 2012 su un tratto di argine del Canale Diversivo di Burana (FE). Rivista Italiana di Geotecnica, 49, 28-58.

Townsend Peterson A., Papeş M., Eaton M. (2007). Transferability and model evaluation in ecological niche modeling: a comparison of GARP and Maxent. Ecography. 30(4):550–560.

Vannucchi, G., Crespellani, T., Facciorusso, J., Ghinelli, A., Madiai, C., Puliti, A., & Renzi, S. (2012). Soil liquefaction phenomena observed in recent seismic events in Emilia-Romagna Region, Italy. International Journal of Earthquake Engineering, 2(3).

Vennari C. & Parise M. (2022). A chronological database about natural and anthropogenic sinkholes in Italy. Geosciences, vol. 12, 200, https://doi.org/10.3390/geosciences12050200.

Vennari C., Salvati P., Bianchi C., Casarano D., Parise M., Basso A. & Marchesini I. (2022). AReGeoDatHa: Apulian Regional GeoDatabase for geo-hydrological Hazards. Journal of Environmental Management 322, 116051. https://doi.org/10.1016/j.jenvman.2022.116051.

Waltham T., Bell F. & Culshaw M. (2005). Sinkholes and subsidence. Karst and cavernous rocks in engineering and construction. Springer Praxis, 382 pp.

Zaniboni F., Armigliato A. and Tinti S. (2016). A numerical investigation of the 1783 landslide-induced catastrophic tsunami in Scilla, Italy. Natural Hazards 84, S455–S470, doi: 10.1007/s11069-016-2461-3.

Zecchin, M., Accaino, F., Ceramicola, S., Civile, D., Critelli, S., Da Lio, C., Mangano, G., Prosser, G., Teatini, P., Tosi, L. (2018). The Crotone Megalandslide, southern Italy: architecture, timing and tectonic control. Scientific Reports 8, 7778. https://doi.org/10.1038/S41598.

Finanziato dall'Unione europea NextGenerationEU | Ministero dell'Università e della Ricerca | Italiadomani PIANO NAZIONALE DI RIPRESA E RESILIENZA

multi-Risk sciEnce for resilienT commUnities undeR a changiNgclimate

Codice progetto MUR: **PE00000005** – CUP LEAD PARTNER UNIPD C93C22005160002

Addendum to Deliverable:

Data processing and analysis by the implementation of a geodatabase in advanced computing cloud systems.

AUTHORS

Filippo Catani (UNIPD), Carlo Esposito (UNIROMA), Silvia Ceramicola (OGS), Giovanni Forte (UNINA), Elena Scacchia (UNIROMA) Maria Lia Napoli (POLITO), Rita Tufano (UNINA), Andrea Brenna (UNIPD), Ascanio Rosi (UNIPD)

1. Technical references

Project Acronym	RETURN
Project Title	multi-Risk sciEnce for resilienT commUnities undeR a changiNg climate
Project Coordinator	Domenico Calcaterra UNIVERSITA DEGLI STUDI DI NAPOLI FEDERICO II domcalca@unina.it
Project Duration	December 2022 – November 2025 (36 months)

Deliverable No.	DV2.2.4
Dissemination level*	PU
Work Package	WP4 - Trigger-based multiple geohazard scenarios
Task	T2.4.1, T2.4.2, T2.4.3
Lead beneficiary	UNIPD
Contributing beneficiary/ies	UNIROMA1, UNIFI, UNIBA, UNINA, UNIBO, OGS, UNIPA.

* PU = Public

PP = Restricted to other programme participants (including the Commission Services)

RE = Restricted to a group specified by the consortium (including the Commission Services)

CO = Confidential, only for members of the consortium (including the Commission Services)

Document history

Version	Date	Lead contributor	Description
0.1	15/05/2024	Carlo Esposito, Silvia Ceramicola, Giovanni Forte	First draft
0.2	20/05/2024	Ascanio Rosi, Filippo Catani	First review
0.3	29/05/2024	Carlo Esposito, Silvia Ceramicola, Giovanni Forte	Edits for approval
0.4	30/05/2024	Salvatore Martino	Spoke leader review
1.0	30/05/2024	Participants to WP4	Final version

2. Abstract

This document represents an integration of the previous deliverables to deepen aspects concerning the limits of applicability of the tools identified and rationalized from the learning examples (LE) that have been proposed, screened and adopted in the first phase. The first phase, in fact, was basically dedicated to an in-depth analysis, albeit preliminary, of the numerous cases proposed for the extraction of operational tools. The operation carried out in the first phase can be defined as preliminary because it envisaged first of all the setting up of a methodological framework (logical criteria) to be followed in order to extract the useful information. Proceeding by successive approximations (summary sheets of each case issued in versions gradually more and more tailored to the needs of the project), it was possible to arrive at an initial rationalization of the learning cases with a view to the generalizability of the tools contained therein. Subsequently, efforts were first devoted to finding a stable criterion for classifying and codifying the information deduced and deducible from each LE and then, with a view to the construction of the PoC, to devising an architecture for the systemization of the various operational tools extracted in complete processing chains referring to specific environments and instability processes. After this phase it was possible to critically review what had been done and, once the shortcomings and/or weaknesses had been identified, to proceed with the in-depth studies necessary to move from a feasibility project of the toolchains to a definitive design of the same in view of the PoC. This addendum therefore aims to summarize the in-depth studies carried out by: i) defining the conceptual framework, ii) exemplifying the upgrade of the toolchains and iii) illustrating a real application. For easily understandable reasons, it was necessary to work transversally with respect to the WP Tasks at this stage; therefore, a single document was produced, in which the different environments focused on in the respective Tasks still find their place.

3. Table of contents

Technical references 57
Document history 58
ABSTRACT....60
3. Table of contents 62
List of Tables....62
List of Figures 62
4. Conceptual framework of toolchains usage....64
5. Toolchain workflow for the coastal areas....67
5.1 Proposed Tool chains (TC) scheme 67
5.2 Summary of Tool chains (TC) submitted in DV2.4.1 68
5.2 TC Rapid submarine landslides and volcanic islands at local scales in nearshore areas (offshore) 70
5.3 What have we learned from the rationale for near shores, coastal areas and volcanic islands?....72
6. Example of tool application....74
6.1 Liquefaction triggering assessment 74
6.2 Tool chain for liquefaction....77
6.3. Test site and data availability 82
6.4 Tool chain application....84
7. References 86
Appendix 1: list of toolchain 88

List of Tables

Table 1 - Analyses for liquefaction triggering assessment modified after (Silvestri and D'Onofrio, 2014)….75

List of Figures

Figure 1: Graphic illustration of general and local filters activated depending on boundary conditions; ellipses in different shades of green represent zones or sub-zones with specific characteristics and subject to different G.I. processes. The same shades of green in the DB table indicate the tools that can be activated for that specific (sub-)zone 65
Figure 2: Graphic illustration of general and local filters activated depending on input data availability (and for a specific trigger category, which implies a further reduction of available tools) 65
Figure 3: Simplified sketch of the procedural framework for the construction of toolchains 66

Figure 4: Proposed conceptual framework (flow charts) for G.I.s occurring at nearshore and coastal areas, volcanic islands. 68
Figure 5: Toolchains (TCs) related to ground instabilities in coastal areas (onshore) conceived for G.Is in Tasks 2.4.2 and 2.4.3. 69
Figure 6: Example of toolchains (TCs) related to rapid ground instabilities in coastal areas at basin scales 70
Figure 7: Upgrade of toolchain for submarine landslides in nearshore environments 71
Figure 8: Stress state in a liquefiable layer before (t=0) and during an earthquake of duration t_e and after the earthquake, during the post-seismic consolidation of duration t_c. (Flora et al., 2023). 74
Figure 9: Particle size ranges of soils susceptible to liquefaction (adapted from NTC (2008) with uniform coefficient Uc< 3.5 (a) and Uc> 3.5 (b). 75
Figure 10: Liquefaction Susceptibility of Sedimentary Deposits from Youd and Perkins (1978)..... 78
Figure 11: Scheme to evaluate the susceptibility liquefaction of level 1, considering geology/geomorphology and water table. 79
Figure 12: Scheme to evaluate the susceptibility liquefaction of level 1, considering geology/geomorphology, water table and PGA. 80
Figure 13: Procedure to calculate FS(z) based on the knowledge of (a) q_{c1Ncs} or (b) $(N_1)_{60cs}$ 81
Figure 14. Liquefaction evidences at San Carlo: main roads covered by grey silty sand ejected from the ground in San Carlo (a); garage (b); sand boils (c) and a private house (d) (Vannucchi et al., 2012). 83
Figure 15. Geological/geomorphological setting following Youd & Perkins (1978) and mean water table depth. 84
Figure 16. PGA map referred to 2012 Emilia earthquake with magnitude of 5.8 84
Figure 17. Susceptibility map of level 1 (with geological/geomorphological data and water table) and liquefaction evidence 85
Figure 18. Susceptibility map of level 1(with geological/geomorphological data, water table and PGA) and liquefaction evidence 85
Figure 19. CPT investigations distribution for LPI index evaluation 85
Figure 20. LPI index classes distribution 85

4. Conceptual framework of toolchains usage

The implementation of toolchains consists of a query sequence - according to if-then(-else) logic - on attributes stored in a specially structured database containing the rationalized information. In fact, the usability of a tool must be verified according to two different perspectives. The first relates to the applicability constraints of a tool in terms of the "boundary conditions" under which the tool was developed and tested, in relation to:

- scale of analysis;
- litho-morphological-climatic (and seismotectonic) settings.

The second perspective deals with the "internal" limits of each tool (data dependency), understood mainly as requirements of thematic content and the relative quantification/qualification log.

The “if” operator can thus represent:

- a switch that includes/excludes upstream a tool according to both "boundary" and "internal" validity;
- a thematic filter that drives towards the use of one or more tools depending on the type of trigger (or preparatory factor) to be considered;
- a spatial filter which, especially for large-scale studies (basin - regional), activates a tool locally, where the conditions for its operability exist.

The first switch is easily activated according to the scale of analysis required and/or needed, based on the instructions already contained in the rationalization tables.

The second step (site characterization) is instead more complex and, especially in the case of large areas, requires a decision-support analysis that can be carried out in a GIS environment and making use of institutional databases (environmental characterization) and project results (characterization of G.I. processes, derived from the output of WP2). The objective is to define the characteristics of the territory, and then compare them with the operational characteristics of the tool according to a conditional logic approach, in terms of:

- Physiographic features.
- Geomorphological setting.
- Geolithological and lithotechnical features.
- Seismotectonic structure (also useful for assessing the significance of seismic input).
- Climatic features (also useful for assessing the significance of meteo-climatic forcing as both preparatory and triggering factors).

As previously mentioned, conventional overlay operations in a GIS environment (e.g. zonal statistics, using the study area as an analysis mask) allow us to attribute to a given area a set of thematic information useful for the application of switches and filters for “external” operating conditions (and expected trigger type), pointing to institutional databases with information about elevation, slope, lithology, land cover, physiographic features, rainfall, seismic hazard.

Site characteristics will then be compared with information associated with each tool and nested in parent tables produced for the previous deliverable. With a similar procedure, the information derived from WP2 must be extracted, which is useful to define the expected G.I. type(s) and, therefore, to activate only the tools that manage this(these) process(es). It is important to emphasize that in the case of large areas and/or with highly variable geo-environmental conditions (and/or trigger/preparation process) it would be advisable to subdivide the territory into homogeneous sub-areas (unique combinations of litho-morpho-structural conditions and, if necessary, intensity of the forcing agents), thus guaranteeing the application of localized spatial filters that do not exclude locally useful tools.

The tools that have passed the various switches and filters will then be subject to verification of the correspondence between the input requirements (type, quantity and quality of information) and the actual availability of data that meet such requirements.

In summary, the methodological framework, sketched in Figure 1 and in Figure 2, is as follows:

1. After having selected the requested scale, identification of "environments" and GIs: possible subdivision of the area into several sub-areas by combination of morpho-litho-climatic conditions and G.I. type(s).
2. In each area (or sub-area) only those tools are selected that meet the multi-criteria condition, also in terms of data requirements.

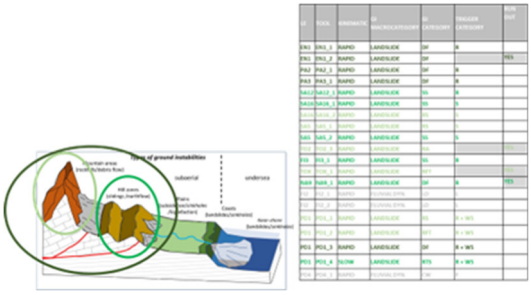

Figure 1: Graphic illustration of general and local filters activated depending on boundary conditions; ellipses in different shades of green represent zones or sub-zones with specific characteristics and subject to different G.I. processes. The same shades of green in the DB table indicate the tools that can be activated for that specific (sub-)zone

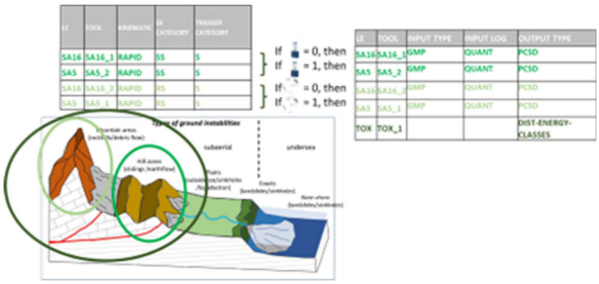

Figure 2: Graphic illustration of general and local filters activated depending on input data availability (and for a specific trigger category, which implies a further reduction of available tools)

3. The generic process/environment "toolchains" thus become operational for the specific requirements of the application case, until the scenario(s) are returned. The latter will have a degree of completeness and output register linked to the "pruning" (i.e., the exclusion of tools that do not meet the selection criteria) of the toolchains and, therefore, to the tools remaining available. It should be noted that the results may be differentiated in the case of subdivision into sub-areas and, thus, selective spatial exclusion.
4. The repetition of the operations for different levels of intensity and trigger categories (and preparatory factors) for each G.I. type leads to the production of “single-hazard” information layers which in combination (according to methods to be evaluated depending on the type of result, with particular reference to the output registers) may give rise to a combined “multi-hazard” result.

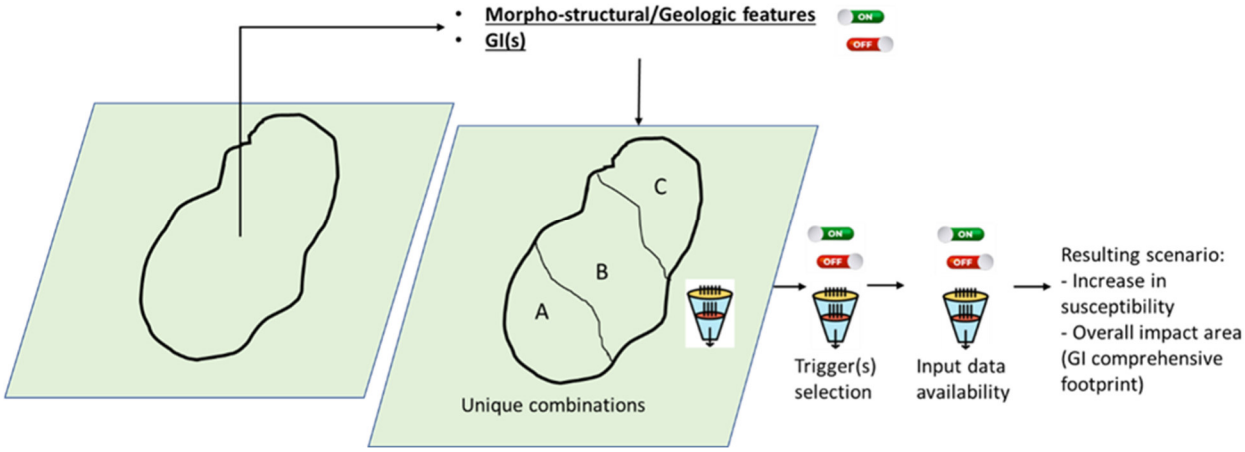

Figure 3: Simplified sketch of the procedural framework for the construction of toolchains

The main limitation lies in the "pruning" operations, that may significantly reduce the cases in which toolchains can be exploited to their full potential. Another, more practical issue concerns how to verify the actual availability of data.

5. Toolchain workflow for the coastal areas

Nearshore and coastal areas as well as volcanic islands face complex geohazard challenges, often subjected to single or multiple ground instabilities. These regions experience a number of different geological processes, including volcanic activity, seismicity, coastal erosion subsidence and vertical uplift. Understanding the interplay of these processes is crucial for assessing geohazards and implementing effective coastal mitigation strategies.

In addition coastal areas are peculiar areas of the continental margins for several reasons:

- They are among the most important areas for G.I's occurrence as they are important hotspots for living communities and infrastructures (railways, harbors, pipelines) especially in the Mediterranean Sea (active geodynamics setting!).
- In coastal areas both subaerial and submarine G.I.'s occur and often interact (multi-hazards) but we 'observe' them with different methods scale and resolutions.
- Investigation and monitoring underwater G.I.'s is very costly and time consuming, often requiring underwater vehicles or marine observatory systems (no direct methods)

There is a gap in knowledge in G.I.'s assessment of marine landslides, as we miss real-time and in-situ monitoring systems, as well as long-term initiatives to carry out repeated surveys (high-resolution multibeam)

5.1 Proposed Tool chains (TC) scheme

The aim of RETURN Task 2.4.1 is to analyze different occurrences and types of on land and submarine ground instabilities, observed by the two scientific communities using different methods, scale and resolutions and address them developing a conformal approach. This is done by identifying triggers and multihazard occurrences in both realms (subaerial and submarine) in relation to specific predisposing and preparatory factors, in order to identify criticalities and gaps in knowledge.

To achieve that, we have selected and analyzed specific learning examples (LEs), extracted the working tools (algorithms, numerical calculator used to model the different geological processes), built toolchains (sequence of connected interoperable tools) in a conceptual way so as to provide a suitable framework able to summarize all possible processes responsible to ground instabilities occurring in these critical areas of the continental margins. This conceptual framework (flow charts) will constitute the kernel of the PoC for grounded instabilities occurring at nearshore and coastal areas, volcanic islands.

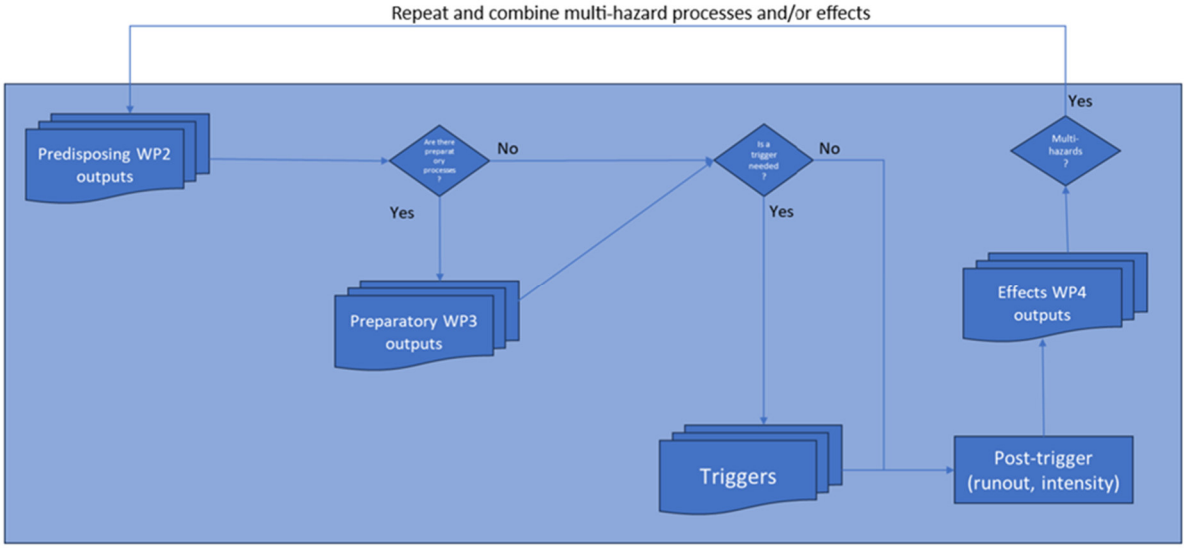

Figure 4: Proposed conceptual framework (flow charts) for G.I.s occurring at nearshore and coastal areas, volcanic islands.

5.2 Summary of Tool chains (TC) submitted in DV2.4.1

When drafting DV2.4.1. it was decided to use the flow chart showed in Figure 4 for all tasks. However, considering the existing criticalities enhanced for the coastal areas (different resolution and different scale of observation for onland and onshore G.I.s), it was decided to apply the flow charts conceived for G.I.s in onshore environment (tasks 2.4.2 and 2.4.3.) also for the G.Is. (task 2.4.1) that were located on land along the coast (see Figure 5).

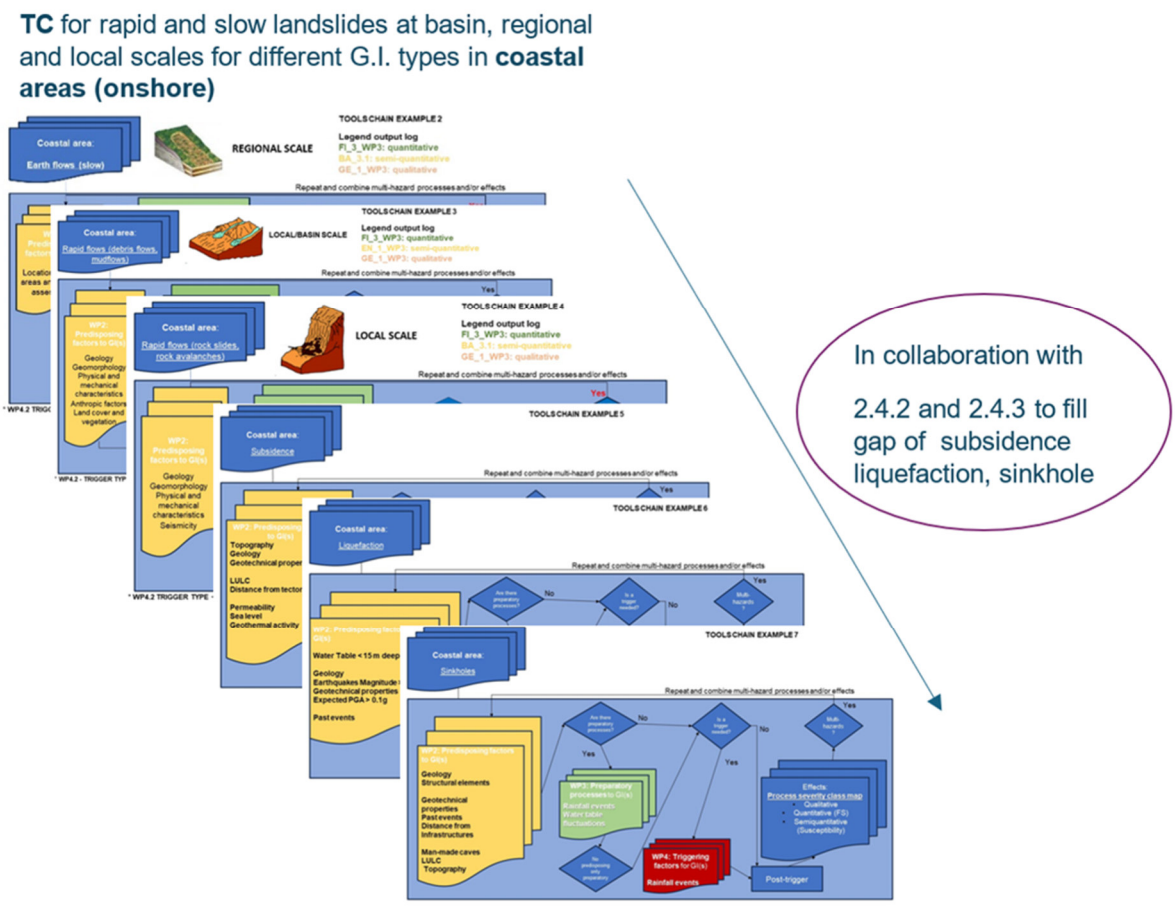

Figure 5: Toolchains (TCs) related to ground instabilities in coastal areas (onshore) conceived for G.Is in Tasks 2.4.2 and 2.4.3.

All the tool chains require some predisposing factors to be assessed, for the most probable ground instability to be identified. For instance, if the area under study is characterized by a rock lithology (i.e., ground instabilities such as mud flows, liquefaction, sinkhole, earthflow, and subsidence are excluded) and a significant slope inclination without (erosion) channels (i.e., debris flows, therefore, are also excluded) the instabilities that can potentially occur within the selected area are rock falls, topples or avalanches (i.e., rapid landslides). The presence of further predisposing factors, such as geological, geomorphological, physical and mechanical characteristics, can help selecting the most probable ground instability and defining its spatial susceptibility to failure.

Once the ground instability has been defined, if at least a preparatory process related to that phenomenon is available for the area of interest, reference can be made to the specific tool linked to this process (if no preparatory factors can be estimated, it is possible to move to the next step related to triggers). For instance, if the "falls and topples" ground instability typology is considered, as shown in Figure 6 , "weathering" is the only preparatory process that can be considered, since one tool is available for that specific factor only.

Then, similarly to preparatory factors, available triggering processes can be analyzed. For instance, for the "falls and topples" ground instability typology, as shown in Figure 6, "rainfall intensity", "wave height", "wind intensity", "cumulated monthly rainfall", "uprooting and vegetation impact" and "ground motion parameters" are possible factors that can be considered (if no triggering factors can be estimated, it is possible to move to the next step related to the runout).

The last step is the G.I. activation, through a run-out simulation, for the assessment of the kinetic energy and/or velocity (and/or bounce height in the case of a rock fall) of the unstable mass along the slope. For the "falls and topples" ground instability typology, as shown in Figure 6, the plugin QPROTO can be used.

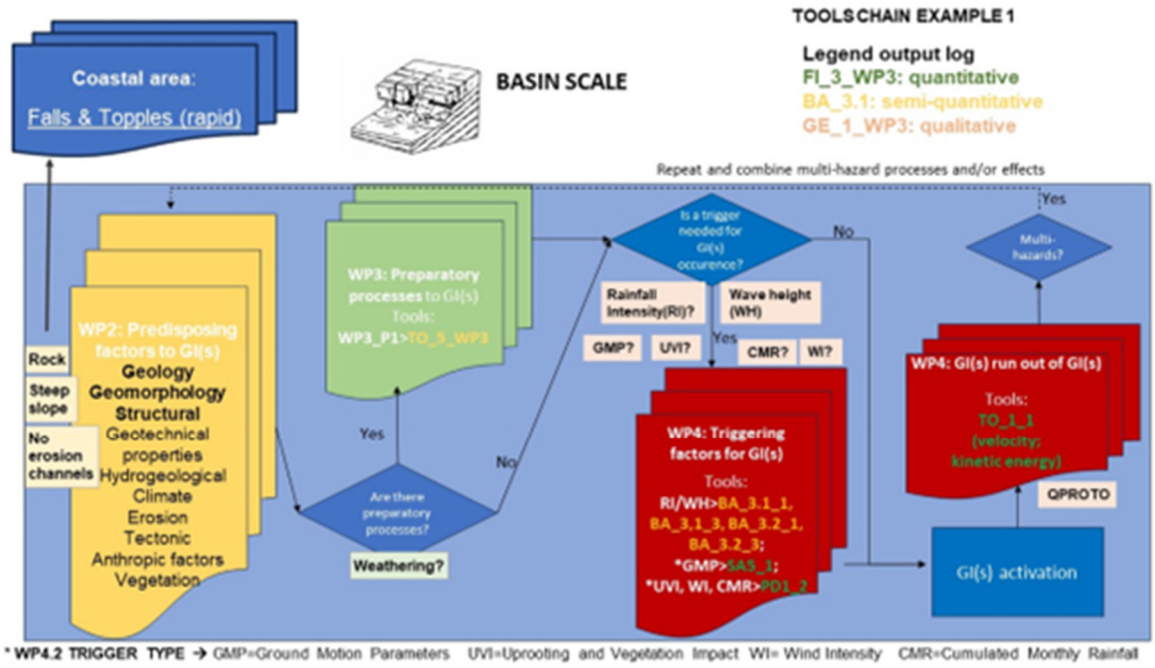

Figure 6: Example of toolchains (TCs) related to rapid ground instabilities in coastal areas at basin scales

5.2 TC Rapid submarine landslides and volcanic islands at local scales in nearshore areas (offshore)

Regarding submarine landslides in nearshore environments, an upgrade to the tool chain presented in deliverable DV 2.4.1 has been produced. This upgrade involves adding a binary system to the previous framework, which relies on the presence/absence of data to provide screening in the number of available tools that can be applied to the specific case study.

Specifically, the chosen implementation relies on the availability of high-resolution bathymetric data, which effectively allows for scaling down the data analysis and choosing the local, basin or regional scale. This approach is related to the uneven availability of high-resolution data (in the order of tens of meters) in marine environments across Italian seas, where there is instead a full coverage provided by the European Marine Observation and Data Network (EMODnet). The "EMODnet Digital Bathymetry (DTM)" is a multilayer bathymetric product covering Europe's sea basins in gridded form on a DTM grid of 1/16 * 1/16 arc minute of longitude and latitude (approximately 115 * 115 meters), enabling a regional or basin scale instability analysis.

If high-resolution data are available (in the order of tens of meters), it is possible to conduct instability analysis at the local scale. The specific case developed for rapid submarine instabilities at the local scale is reported in Figure 7.

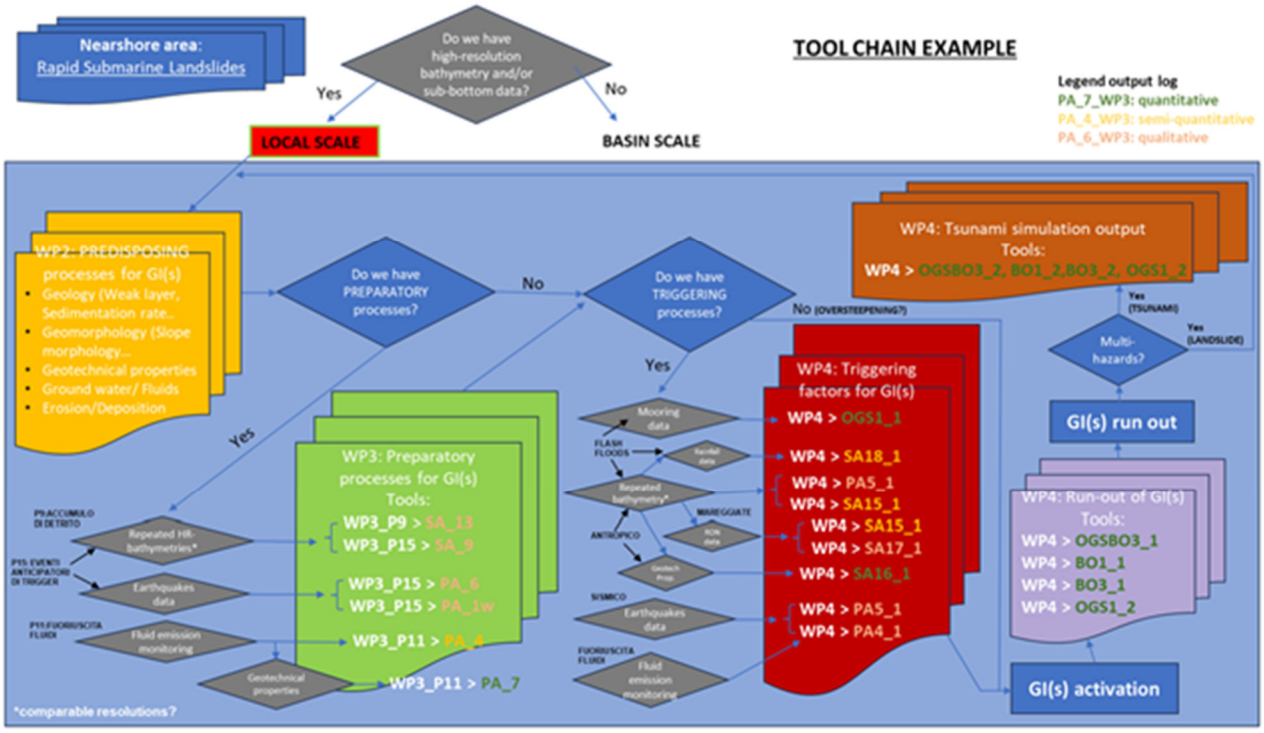

Figure 7: Upgrade of toolchain for submarine landslides in nearshore environments

The toolchain begins with defining the susceptibility of the selected study area using the investigation methodologies developed within WP2. Following the susceptibility analysis, which highlights the most susceptible areas based on different types of instabilities (rapid or slow landslides), it will be necessary to determine if preparatory processes are present in the study area.

If data characterizing some preparatory processes are not available, the analysis proceeds directly to the step concerning triggering processes. Otherwise, the analysis continues by selecting tools developed within WP3 regarding preparatory processes.

The tools presented within WP3 require various types of data to be applied; therefore, the system will rely on the data availability in the study area to present the user with a series of tools to choose from. Specifically, within the context of WP3, tools have been introduced that allow for the qualitative, semi-quantitative and quantitative analysis of preparatory processes related to:

1. P9: *The preparation for coastal landslides or at canyon heads and/or continental margins related to debris accumulation from riverbeds (deltaic systems) or fiumare (flash floods) and subaerial processes (e.g. coastal landslides, lava flows)* through the use of repeated bathymetries (Qualitative tools).
2. P15: *The preparation related to pre-trigger events (e.g., seismic sequences, recurrent storm surges, cumulative intense rainfall events, landslide succession, creep and rock mass damaging)* through seismic data. (Qualitative tools).
3. P11: *Preparation for detachment of submarine sediments related to outgassing phenomena* requiring monitoring data related to fluid seepage (via systems like pockmarks or mud volcanoes) (Semi-quantitative tool). If geotechnical data are also available alongside these, a quantitative tool option will be available.

Once the tools related to preparatory processes have been applied, the process moves on to triggering processes. In the context of WP4, various types of triggers for submarine landslides in nearshore environments have been defined (Figure 7) (for further details, reference is made to deliverable DV 2.4.1). Through the same approach, depending on data availability, different tools will be available according to the type of trigger:

1. *Flash floods*: If mooring data (quantitative tool) or repeated bathymetries (quantitative/semi-quantitative tools) are available. If rainfall data are available in addition to repeated bathymetries, a semi-quantitative tool can be applied.

2. *Storm events*: If repeated bathymetries and wave data (qualitative and semi-quantitative tools) are available.
3. *Anthropic factors*: If repeated bathymetries (qualitative and semi-quantitative tools) and geotechnical data (quantitative tool) are available.
4. *Earthquake*: If seismic data is available (qualitative tools).
5. *Piping/Fluids in sediments*: If seismic subbottom data indicative of fluid flow in sediments is available (qualitative tools) or if monitoring data from fluid flow events are available (quantitative tools).

If none of the mentioned data is available, the landslide can be directly activated. It is plausible that in marine environments, submarine landslides can occur without a specific trigger if the slope undergoes oversteepening, and thus gravitational instability will primarily be driven by seafloor geomorphology.

Once the tools related to triggers are applied (or not), it is possible to calculate the run-out of instabilities and maximum velocity attained by the failed mass using various quantitative tools.

The last available step concerns multihazard. Once the run-out of the landslide is calculated, it is possible to apply various quantitative tools that allow for the calculation of the maximum water amplitude (in meters) for different locations along the coast, at increasing distances from the source, to understand if the instability can generate tsunamis potentially damaging for coastal areas.

5.3 What have we learned from the rationale for near shores, coastal areas and volcanic islands?

The learning examples (LEs) from project partners provide genuine insights and the latest state-of-the-art information about ground instabilities in coastal areas (GIs). However, the available LEs might not fully encompass the entire spectrum of GI scenarios, particularly since most examples are concentrated in the South of Italy. Additionally, the majority of nearshore LEs are focused on local scales, leading to an underrepresentation of various GI types in nearshore areas.

This underrepresentation is primarily due to the challenges associated with observing and monitoring GIs in the marine environment. There is also an overrepresentation of a specific type of nearshore GI, namely retrogressive landslides at canyon heads. Moreover, there is a notable gap in tools for addressing slow kinematic landslides in nearshore areas. To address this, we plan to include two Deep-Seated Gravitational Slope Deformations (DSGSDs) from the Ionian Calabria margin: the Megaslide of Crotone and the Squillace gravitational complex. Furthermore, there is a need to consider the phenomenon of creeping in the context of slow kinematic landslides.

6. Example of tool application

Earthquake induced liquefaction can be simply defined as the temporary transition of a granular soil from the solid to a fluid state as a consequence of the increased pore-water pressures. The detrimental effects on structures and infrastructures put soil liquefaction among the most serious consequences of earthquakes and in the last years, there has been an increasing demand for developing liquefaction hazard maps to reduce risk for the built environment.

Liquefaction typically occurs on loose saturated sandy deposits, being their contractive tendency upon cyclic shearing inhibited by water with the onset of positive excess pore pressures (Δu).

If the net excess pore pressures build up is positive, the normal effective stresses will reduce during the seismic action, eventually increasing back during the post-seismic consolidation phase. Since the soil shear strength $\tau(\sigma')$ and stiffness $G(\sigma')$ directly depend on the effective stresses, they will progressively reduce during the seismic action on liquefiable soils, becoming nihil when the effective stresses tend to zero (full liquefaction, theoretically at ru=1). At the end of cyclic action, consolidation will take place due to the excess pore pressure drainage.

Figure 8 summarizes the phases before earthquake and after when liquefaction occurs (Flora et al., 2023).

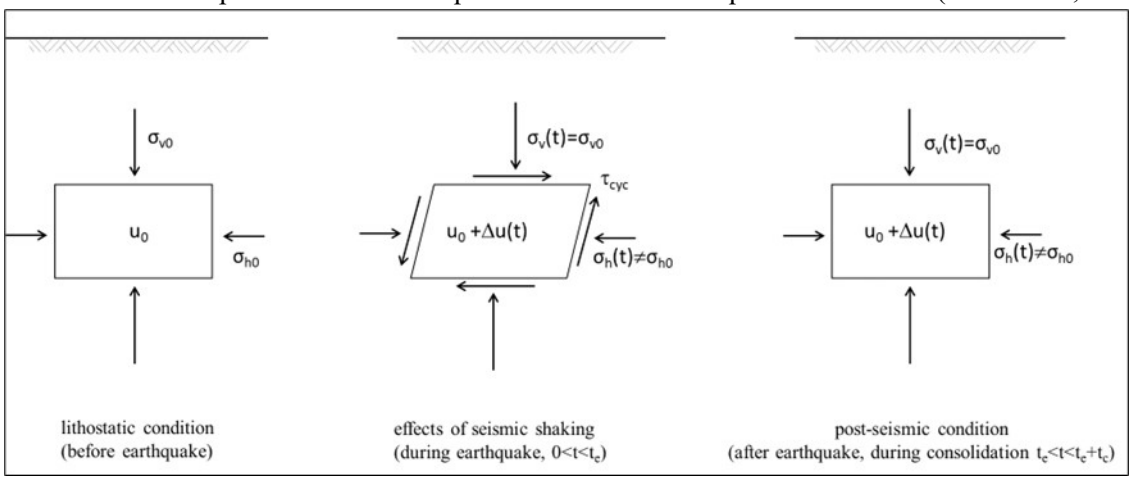

Figure 8: Stress state in a liquefiable layer before (t=0) and during an earthquake of duration t_e and after the earthquake, during the post-seismic consolidation of duration t_c. (Flora et al., 2023).

6.1 Liquefaction triggering assessment

The assessment of liquefaction triggering and, more generally the response of a soil deposit in terms of pore pressure increments, can be carried out with approaches of increasing complexity, as briefly reported in Table 2.

Table 2 - Analyses for liquefaction triggering assessment modified after (Silvestri and D'Onofrio, 2014).

Level of analysis	Type of analysis	Constitutive model	Calculation approach	Output
Level 1	Screening criteria (qualitative)	-	Evaluation of some parameters (grain size distribution, ground water table and expected maximum acceleration)	Liquefaction yes, no
Level 2	Semi-empirical methods	Elementary	Simplified stress-based	Actions (demand) vs. Resistance (capacity)
Level 2	Simplified dynamic analyses	Simplified (mostly visco-elastic, uncoupled)	Dynamic (with simplified geometry)	Total stresses, shear strains, pore pressure increments*
Level 4	Advanced dynamic analyses	Advanced (elasto-plastic with hardening, coupled)	Dynamic (with complex 3D geometry)	Total and effective stresses, shear strains, pore pressure increments, residual displacements

*Calculated through analytical correlations.

Level 1 is based on the Italian Technical Standards for Constructions (NTC, 2008).

According to the NTC (2008) (Section 7.11.3.4.2), the likelihood of liquefaction occurring in saturated sandy soils is low or zero if at least one of the following conditions occurs:

1. maximum expected accelerations at ground level in the absence of artefacts (free field conditions) less than 0.1g;
2. average seasonal depth of the water table greater than 15 m from ground level, for sub-horizontal ground level with superficial foundations;
3. deposits consisting of clean sands with normalised penetrometer resistance (N1)60> 30 or qc1N> 180;
4. particle size distribution outside the zones shown in Figure 9a in the case of soils with uniformity coefficient Uc< 3.5 and in Figure 9b in the case of soils with uniformity coefficient Uc> 3.5.

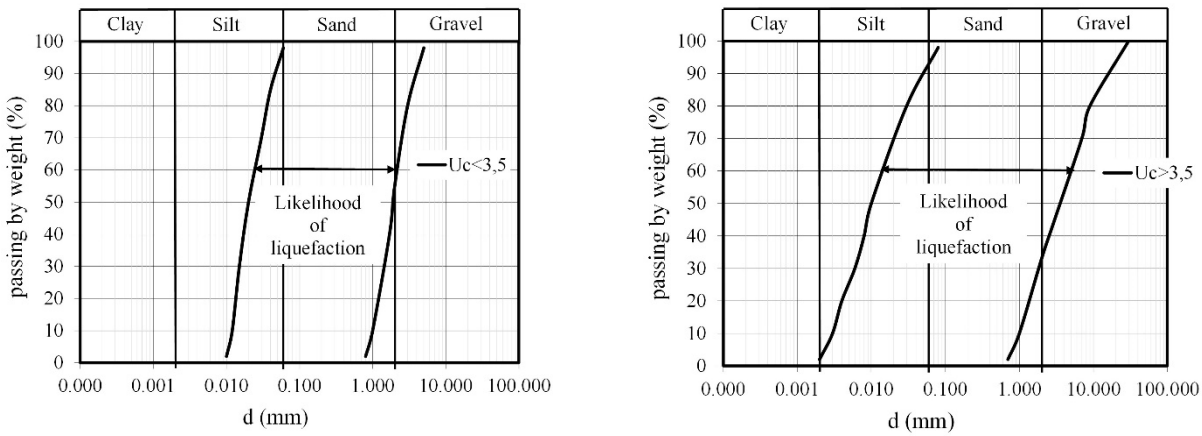

(1) U_c<3.5 (2) U_c>3.5

Figure 9: Particle size ranges of soils susceptible to liquefaction (adapted from NTC (2008) with uniform coefficient Uc< 3.5 (a) and Uc> 3.5 (b).

If the first condition is not verified and, therefore, the maximum acceleration expected at ground level is higher than 0.1 g, the geotechnical investigations must be aimed at determining the parameters necessary to verify the other three conditions.

When none of the four abovementioned conditions is satisfied, NTC (2008) say that the site is potentially susceptible to liquefy (i.e., vulnerable, due to the presence of predisposing elements) and therefore potentially at risk (due to the non-negligible seismic hazard). It is therefore

necessary to assess the liquefaction safety factor at the depths where potentially liquefiable soils are present.

Quite often in engineering practice, liquefaction triggering assessment is carried out using the semi-empirical stress-based analysis (level 2). With this approach, a factor of safety FS(z) is defined for free-field conditions (i.e. without buildings and structures) as the ratio between the normalized shear stress required to induce liquefaction (CRR=soil capacity) and the normalized equivalent stress induced by the design earthquake (CSR=demand) (Boulanger and Idriss, 2014; Seed and Idriss, 1971):

$$FS(z) = \frac{CRR(z)}{CSR(z)} = \frac{CRR_{M=7,5,\sigma' v=1}}{CSR} \cdot MSF \cdot K_\sigma \cdot K_\alpha \qquad \text{Eq. 1}$$

where soil capacity CRRM=7.5, σ'v=1 is calculated with reference to a seismic event of magnitude M=7.5 and a vertical effective stress state of one atmosphere (101 kPa). The parameter MSF (Magnitude Scaling Factor) is a factor accounting for the effect of earthquake magnitude, and the two corrective coefficients Kσ and Kα respectively take into account the effects of vertical stress and of a possible pre-existing static shear stress on horizontal planes (e.g. sloping ground or state of stress under existing structures) (see Fig. 3 for their expressions). Literature data (e.g. Tomasello and Porcino (2022); Vaid et al. (2001) indicate that, in loose or medium dense sands (Dr < 50%), pre-existing shear stresses reduce soil capacity. In this density range, from a practical point of view, this detrimental effect can be considered assuming Kα = 0.8.

Liquefaction resistance can be evaluated interpreting the results of in-situ or laboratory tests. Usually, in situ tests are more commonly adopted for the following shortcomings of laboratory tests:

i) it is extremely difficult to retrieve granular undisturbed samples on site: therefore, tested specimens may not represent the true in situ conditions;

ii) laboratory tests are carried out using constant amplitude cycles; as a consequence, for their interpretation a correlation has to be introduced between the irregular seismic action and the equivalent number of constant amplitude cycles, N;

iii) even using very sophisticated laboratory apparatuses, the stresses applied in laboratory cannot represent the true stress path experienced by the soil in situ during the earthquake.

Therefore, the values of CRR are generally derived from historic-empirical correlations based on CPT and SPT results (Boulanger and Idriss, 2014) as:

$$CRR_{M=7.5,\sigma' v=1} = exp\left(\frac{q_{c1Ncs}}{113} + \left(\frac{q_{c1Ncs}}{1000}\right)^2 - \left(\frac{q_{c1Ncs}}{140}\right)^3 + \left(\frac{q_{c1Ncs}}{137}\right)^4 - 2.8\right) \qquad \text{Eq. 2}$$

$$CRR_{M=7.5,\sigma' v=1} = exp\left(\frac{N_{1,60cs}}{14.1} + \left(\frac{N_{1,60cs}}{126}\right)^2 - \left(\frac{N_{1,60cs}}{23.6}\right)^3 + \left(\frac{N_{1,60cs}}{25.4}\right)^4 - 2.8\right) \qquad \text{Eq. 3}$$

where qc1Ncs and (N1)60cs are respectively the normalized values of the tip resistance CPT and the number of blows (NSPT) corrected for the fines content (FC, defined as the percentage by weight passing at the 0.075 mm sieve).

It has to be emphasized that Eq. 1 and Eq. 3 have no mechanical origin and are just analytical correlations empirically set up to separate historical data of liquefied from non-liquefied cases in a capacity vs. demand plane. Generally, they correspond to a conservative lower bound of the observed values of CRR, and thus lead to a conservative estimate of FS(z).

With the semi-empirical approach, the stress state induced by the seismic action is estimated through the knowledge of the maximum horizontal acceleration expected at ground level (PGA, amax) according to a well-established empirical procedure, or as a(z) at the generic depth of

interest, if the results of local seismic response analyses are used. Typically, with this approach the cyclic stress ratio CSR is calculated as (Seed and Idriss, 1971):

$$CSR(z) = 0.65 \frac{a_{max}}{g} \frac{\sigma_v}{\sigma'_v} r_d \qquad \text{Eq. 4}$$

where σ_v and σ'_v are the total and effective lithostatic stress at the generic depth (z), a_{max} is the peak value of the expected horizontal acceleration at the surface, g is the earth's gravitational acceleration and r_d is a reductive factor of the acceleration to take into account the deformability of the soil column and can be estimated empirically or calculated numerically through a local seismic response analysis. In this calculation, if remediation actions have to be implemented, the effects of ground improvement should be taken into account considering their effect in terms of stiffness increase.

6.2 Tool chain for liquefaction.

Following the Literature collection described in DV2.4.5, the tool chain for liquefaction phenomena can consider several predisposing factors with different degree of importance: water table < 15 m deep (very high), geology, geotechnical properties, expected PGA > 0.1g (high).

Liquefaction susceptibility can be evaluated in four levels as reported in table 1 but to define susceptibility in large areas, levels 1 and 2 are more suitable. In particular, knowing the geological and geomorphological characteristics of the area and the groundwater table depth, it is possible to develop a basic susceptibility map (level 1) also called as "screening map" to assess which macro sectors are more susceptible than others.

It is based on the definition of geological categories mostly susceptible to liquefaction, e.g., Youd and Perkins (1978) proposed liquefaction susceptibility categories of various types of soil deposits by assigning a qualitative score based on general depositional environment and geologic age of the deposit. The relative susceptibility degree shown in Figure 10 indicates that unconsolidated soils recently deposited such as Holocene age river channel, floodplain, and delta deposits have high to very high liquefaction susceptibility. Such deposits as an alluvial fan and plain, beach, glacial till, talus, residual soils, tuff and compacted fill are, in general, not susceptible to liquefaction. For each deposit type, the liquefaction susceptibility is decreasing by the ages, from young (< 500 years) to old (Pre-Pleistocene), except for the loess, which is always susceptible to liquefaction during strong earthquakes no matter the age is of Holocene or Pleistocene. The Holocene sediments are more susceptible to liquefaction than the Pleistocene ones, and the Pre-Pleistocene sediments are rarely susceptible.

Type of deposit (1)	General distribution of cohesionless sediments in deposits (2)	Likelihood that Cohesionless Sediments, When Saturated, Would Be Susceptible to Liquefaction (by Age of Deposit)			
		<500 yr (3)	Holocene (4)	Pleistocene (5)	Pre-pleistocene (6)
(a) Continental Deposits					
River channel	Locally variable	Very high	High	Low	Very low
Flood plain	Locally variable	High	Moderate	Low	Very low
Alluvial fan and plain	Widespread	Moderate	Low	Low	Very low
Marine terraces and plains	Widespread	—	Low	Very low	Very low
Delta and fan-delta	Widespread	High	Moderate	Low	Very low
Lacustrine and playa	Variable	High	Moderate	Low	Very low
Colluvium	Variable	High	Moderate	Low	Very low
Talus	Widespread	Low	Low	Very low	Very low
Dunes	Widespread	High	Moderate	Low	Very low
Loess	Variable	High	High	High	Unknown
Glacial till	Variable	Low	Low	Very low	Very low
Tuff	Rare	Low	Low	Very low	Very low
Tephra	Widespread	High	High	?	?
Residual soils	Rare	Low	Low	Very low	Very low
Sebka	Locally variable	High	Moderate	Low	Very low
(b) Coastal Zone					
Delta	Widespread	Very high	High	Low	Very low
Esturine	Locally variable	High	Moderate	Low	Very low
Beach					
High wave energy	Widespread	Moderate	Low	Very low	Very low
Low wave energy	Widespread	High	Moderate	Low	Very low
Lagoonal	Locally variable	High	Moderate	Low	Very low
Fore shore	Locally variable	High	Moderate	Low	Very low
(c) Artificial					
Uncompacted fill	Variable	Very high	—	—	—
Compacted fill	Variable	Low	—	—	—

Figure 10: Liquefaction Susceptibility of Sedimentary Deposits from Youd and Perkins (1978)

According to Youd and Perkins (1978), and considering the water table depth, the susceptibility of level 1 was performed using the "if/then (else)" logic Boolean scheme (Figure 11).

Following the scheme the low susceptibility is obtained if the deposits belong to river channel, flood/alluvial plain, beach plain and lacustrine of pre-Pleistocene age and the water table is < 15 meters deep. Susceptibility is medium if deposits belong to Holocene floodplain, beach or delta/fan-delta or Pleistocene lacustrine with water table < 15 meters, while a high degree of susceptibility occurs if the deposits belong to Holocene river channel and pyroclastic soils or Pleistocene/Holocene loess.

Liquefaction events in mountain, foothill and hill environments do not occur, as well as in plain areas where the PGA is very low (< 0.01g) or the water table depth is deeper than 15 meters, then the susceptibility is null.

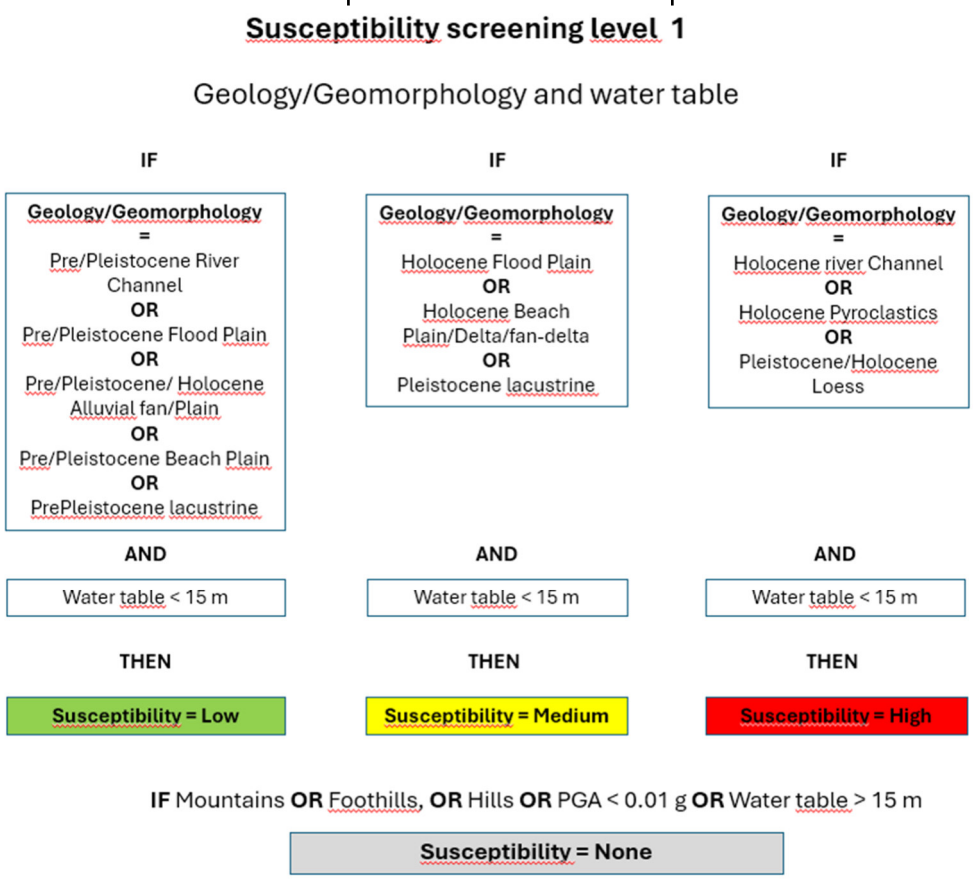

Figure 11: Scheme to evaluate the susceptibility liquefaction of level 1, considering geology/geomorphology and water table.

Considering that liquefaction is never witnessed where seismicity is low, the distribution of PGA values can be considered both a predisposing and a triggering factor.

For these reasons, the scheme for assessing liquefaction susceptibility can be updated also adopting this parameter. According to NTC (2018), the value of PGA must be higher than 0.1g to have liquefaction.

PGA values can be obtained from simulation of earthquake scenario following a suitable GMPE (e.g., Bindi et al., 2011, Lanzano at al. 2020) or simply importing the results of the National Seismic Hazard Map for a defined return period. In the latter approach the results will be more cautionary.

Thus, by intersecting the geological and geomorphological features of the deposits, the depth of the water table and the PGA, susceptibility classes obtained with the previous approach can be enhanced from low to very high. In particular, as shown in Figure 12, susceptibility is low if pre-Pleistocene/Pleistocene deposits with water table depth less than 15 meters and low PGA values are observed. The level of susceptibility is very high when Holocene river channel or pyroclastic soils or loess deposits are present together with a water table depth < 15 meters and PGA values > 0.1g.

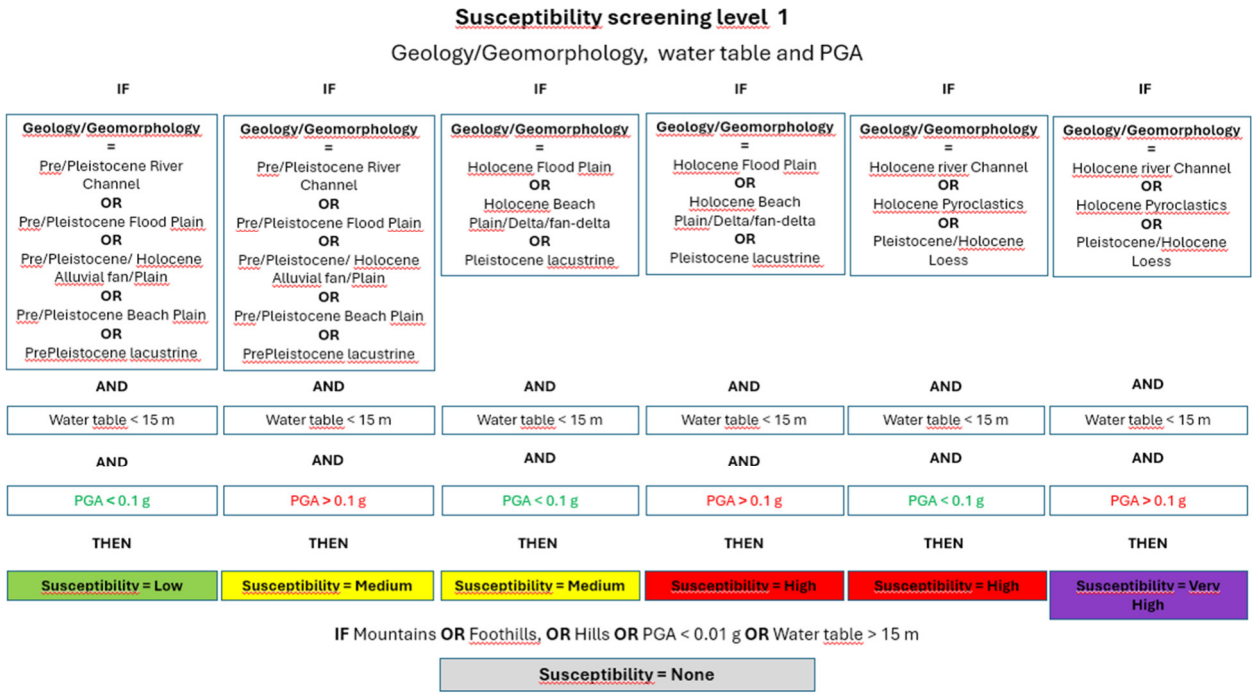

Figure 12: Scheme to evaluate the susceptibility liquefaction of level 1, considering geology/geomorphology, water table and PGA

If the analyses should be carried out at level 2, the estimate of a Factor of Safety (FS) is mandatory. Figure 13 summarizes the steps necessary to calculate FS(z) with the semi-empirical stress-based approach (Boulanger and Idriss, 2014; Idriss and Boulanger, 2008).

It has to be highlighted that, even though the normalized values qc1Ncs and (N1)60cs take into account the fines content, sometimes they may lead to a misprediction of soil capacity: this is for instance the case of pyroclastic soils, which may have a relevant fines content FC with no plasticity (which means that the normalized resistance overestimates the beneficial effect of FC on CRR), and their fragile grains may be easily crushed by the testing tool (especially during SPT) (which means that soil shear strength may be underestimated). The combined effect of these two peculiarities cannot be theoretically assessed, but some experimental evidence (i.e. Anderson et al. (2019)) indicate that the use of the semi-empirical stress-based approach for pyroclastic soils is largely conservative, because of an overall underestimate of soil capacity.

Moreover, it should be stressed that the simplified approach just described does not consider peculiar site mechanisms that may affect the overall behaviour, like for instance the so called “system response” in layered deposits, smartly identified by Cubrinovski et al. (2019) in well documented case histories in Christchurch.

CPT

$$q_{c1} = C_N \cdot q_c$$

$$q_{c1N} = \frac{q_{c1}}{P_a} \quad (P_a = 101kPa)$$

$$C_N = \left(\frac{P_a}{\sigma'_v}\right)^m \leq 1.7 m = 1.338 - 0.249 \cdot (q_{c1N})^{0.264}$$

SPT

$$(N_1)_{60} = C_N \cdot N_{60}$$

$$C_N = \left(\frac{P_a}{\sigma'_v}\right)^m \leq 1.7 \qquad m = 0.784 - 0.0768 \cdot \sqrt{(N_1)_{60cs}}$$

Fines content evaluation

$$FC = 80 \cdot (I_c + C_{FC}) - 137 \qquad -0.29 \leq C_{FC} \leq 0.29$$

$$I_c = [(3.47 - logQ)^2 + (1.22 + logF)^2]^{0.5} \quad \begin{cases} Q = \left(\frac{q_c - \sigma_{vc}}{P_a}\right) \cdot \left(\frac{P_a}{\sigma'_{vc}}\right)^n \\ F = \left(\frac{f_s}{q_c - \sigma_{vc}}\right) \cdot 100 \end{cases}$$

Fines content evaluation

$$FC = 80 \cdot (I_c + C_{FC}) - 137 \qquad -0.29 \leq C_{FC} \leq 0.29$$

$$I_c = -0.717 \cdot ln\left(\frac{V_s^2}{9.81 \cdot z}\right) + 6.3211 \quad \begin{cases} V_s = 100.59 \cdot N_{SPT}^{0.302} \end{cases}$$

$$\Delta q_{c1N} = \left(11.9 + \frac{q_{c1N}}{14.6}\right) \cdot exp\left[1.63 - \frac{9.7}{FC+2} - \left(\frac{15.7}{FC+2}\right)^2\right]$$

$$q_{c1Ncs} = q_{c1N} + \Delta q_{c1N}$$

$$\Delta(N_1)_{60} = exp\left[1.63 + \frac{9.7}{FC+0.01} - \left(\frac{15.7}{FC+0.01}\right)^2\right]$$

$$(N_1)_{60cs} = (N_1)_{60} + \Delta(N_1)_{60}$$

$$CRR_{M=7.5,\sigma'v=1} = \exp\left[\frac{q_{c1Ncs}}{113} + \left(\frac{q_{c1Ncs}}{1000}\right)^2 - \left(\frac{q_{c1Ncs}}{140}\right)^3 + \left(\frac{q_{c1Ncs}}{137}\right)^4 - 2.8\right]$$

$$CRR_{M=7.5,\sigma'v=1} = \exp\left[\frac{(N_1)_{60cs}}{14.1} + \left(\frac{(N_1)_{60cs}}{126}\right)^2 - \left(\frac{(N_1)_{60cs}}{23.6}\right)^3 + \left(\frac{(N_1)_{60cs}}{25.4}\right)^4 - 2.8\right]$$

$$\boldsymbol{FS = \frac{CRR}{CSR}}$$

$$CSR = 0.65 \cdot \frac{a_{max}}{g} \cdot \frac{\sigma_v}{\sigma'_v} \cdot r_d \cdot \frac{1}{MSF} \cdot \frac{1}{K_\sigma} \cdot \frac{1}{K_\alpha}$$

$$\ln(r_d) = \alpha + \beta \cdot M \quad \begin{cases} \alpha = -1.012 - 1.26 \cdot sen\left(\frac{z}{11.73} + 5.133\right) \\ \beta = 0.106 - 0.118 \cdot sen\left(\frac{z}{11.28} + 5.142\right) \end{cases}$$

$$C_\sigma = \frac{1}{37.3 - 8.27 \cdot q_{c1Ncs}^{0.264}} \leq 0.3 \qquad K_\sigma = 1 - C_\sigma \cdot ln\frac{\sigma'_v}{P_a} \leq 1.1 \qquad C_\sigma = \frac{1}{18.9 - 2.55 \cdot (N_1)_{60cs}^{0.5}} \leq 0.3$$

$$MSF = 6.9 \cdot exp\left(-\frac{M}{4}\right) - 0.058$$

$$K_\alpha = a + b \cdot exp\left(-\frac{\xi_R}{c}\right) \quad \begin{cases} a = 1267 + 636 \cdot \alpha^2 - 634 \cdot \exp(\alpha) - 632 \cdot \exp(-\alpha) \\ b = \exp(-1.11 + 12.3 \cdot \alpha^2 + 1.31 \cdot ln(\alpha + 0.0001)) \\ c = 0.138 + 0.126 \cdot \alpha + 2.52 \cdot \alpha^3 \end{cases} \qquad \alpha = \frac{\tau_s}{\sigma'_{vc}}$$

$$\xi_R = \frac{1}{Q - ln\left[\frac{100 \cdot (1 + 2 \cdot K_0) \cdot \sigma'_{vc}}{3 \cdot P_a}\right]} - (0.478 \cdot q_{c1Ncs}^{0.264} - 1.063) \qquad \xi_R = \frac{1}{Q - ln\left[\frac{100 \cdot (1 + 2 \cdot K_0) \cdot \sigma'_{vc}}{3 \cdot P_a}\right]} - \sqrt{\frac{(N_1)_{60}}{46}}$$

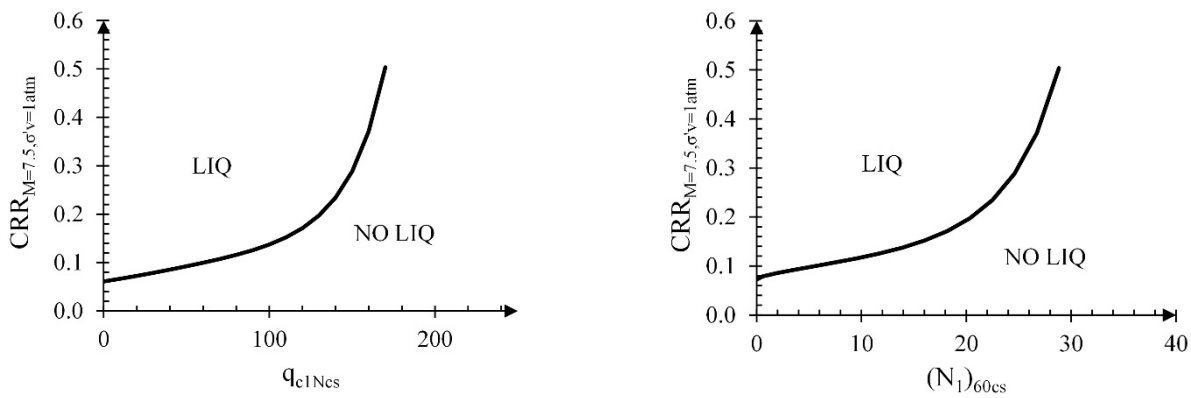

Figure 13: Procedure to calculate FS(z) based on the knowledge of (a) q_{c1Ncs} or (b) $(N_1)_{60cs}$

This mechanism, that can be quantitatively taken into account only using fully coupled advanced dynamic analyses, is related to the hydraulic interaction between contiguous granular layers, i.e. to the change in their pore pressure regime during the earthquake (or immediately after it) caused by transient inter-layer flows that may lead to the liquefaction of layers initially far from it.

FS values lower than 1 imply the liquefaction susceptibility of site. In this case, the potential consequences of liquefaction can be evaluated with the integral response of the deposit, through the simplified liquefaction index LSN (Tonkin and Taylor, 2012), defined as:

$$LSN = 1000 \int_0^{20} \frac{\varepsilon_v}{z} dz \qquad \text{Eq. 5}$$

where z is the depth in meters and ε_v is the post-liquefaction volumetric reconsolidation strain (entered as a decimal) that can be calculated according to existing charts (see (Ishihara and Yoshimine, 1992). Degree of damage can be estimated as:

0<LSN<20: minor;
20<LSN<40: major;
LSN>40: severe.

It is worth mentioning that LSN is not the only indicator proposed in literature, and many alternatives have been suggested in time. From a historical point of view, the first (and most popular) integral indicator is the Liquefaction Potential Index, LPI (Iwasaki et al., 1984), which represents a measure of the vulnerability of a site as a single value, ranging between 0 (very low risk) and values over 15 (very high risk), defined as:

$$LPI = \int_0^{20} F(z) \cdot W(z) dz \qquad \text{Eq. 6}$$

where z is the depth in meters, while F(z) and W (z) are respectively:

$$F(z) = \begin{cases} 1 - FS & for \;\; FS < 1 \\ 0 & for \;\; FS \geq 1 \end{cases} \qquad \text{Eq. 7}$$

$$W(z) = 10 - 0.5z \qquad \text{Eq. 8}$$

in which FS is computed by Eq. 1.

6.3. Test site and data availability

In the following an application of the described tool chains for liquefaction phenomena is shown. The chosen test site is an area of Emilia Romagna Region. Indeed, in May 2012, Northen Italy was struck by an important seismic sequence. The main shock occurred on 20 May 2012 (Mw=6.1) and caused extensive liquefaction phenomena. The part of the country which was affected by these violent shakes was the area of the Po River Valley, in the foreland basin of two mountain chains constituted by the Alps and the northern Apennine, in the Emilia-Romagna Region (Northern-Italy). Since 19 May 2012, Emilia Romagna and surrounding Regions of Veneto and Lombardia are hit by a long seismic sequence characterized by about two thousands of shakes. Many buildings collapsed and 27 victims were recorded. The epicentre of the 20 May event

(44.89°N latitude and 11.23°E longitude) was located between the provinces of Modena and Ferrara, while the hypocentre was at a depth of 6.3 km, owing to that it is considered a shallow earthquake (Lai et al., 2015). This event is relevant because it demonstrated that Italy is also a Country where soil liquefaction can occur. The most evident effects of liquefaction phenomena following the 2012 earthquake were found in San Carlo (Municipality of Sant'Agostino) and Mirabello, whose subsoil was characterized by alluvial sediments of river and levee depositional environment, which consists of alternated layers of silty-clayey deposits and sandy soils (Chiaradonna et al., 2018, Lai et al., 2015; Lombardi and Bhattacharya, 2014; Sciarra et al., 2012; Vannucchi et al., 2012). As an example, some photos have been reported in Figure 14 (Vannucchi et al., 2012), where the typical effects of liquefaction may be noted, such as sand boils, vents, sinkholes, craters, surface ruptures, extensional fissures. Many open spaces, as courtyards, gardens and roads, were completely covered by the ejected sand, mud and water.

(a) (b) (c) (d)

Figure 14. Liquefaction evidences at San Carlo: main roads covered by grey silty sand ejected from the ground in San Carlo (a); garage (b); sand boils (c) and a private house (d) (Vannucchi et al., 2012).

The test area for the application of liquefaction tool chain was selected considering a sector with the highest density of events. In addition, data for developing the tool chain were collected, such as geological and geotechnical investigations, water table depth, and PGA values.

In particular, geological and geotechnical investigations were obtained from the database created by the Geology, Soil, and Seismic Area of the Emilia-Romagna Region. The water table depth

values were obtained by interpolating the average groundwater levels from point data downloaded from the ARPAE database (Regional Agency for Prevention, Environment, and Energy of Emilia-Romagna). This data refers to the monitoring conducted from 2009 to 2022 at the groundwater stations belonging to the regional network for environmental quality.

Finally, the PGA (Peak Ground Acceleration) values related to the 2012 Emilia earthquake with a magnitude of 5.8 were obtained from the INGV archive.

By using these data two levels of tool chain were developed.

6.4 Tool chain application

The first susceptibility map of level 1 was elaborated applying a GIS intersection of geological/geomorphological information and the water table maps following the Boolean logical scheme of Figure 4. In particular, by means of some studies of Literature (Civico et al., 2015; Minarelli et al., 2022; Priolo et al., 2012; Stefani et al., 2018) and boreholes available in the area, a map was drawn complying with the Youd and Perkins's classification (Figure 15).

The water table level was obtained by interpolation of water table depth point values among the monitoring database of ARPAE (Regional Agency for Prevention, Environment and Energy of Emilia-Romagna) stations (Figure 15).

On the other hand, the updated susceptibility map of level 1, was elaborated applying a GIS intersection of geological/geomorphological data, the water table and PGA maps. The latter is related to the 2012 Emilia earthquake with a magnitude of 5.8 and shows that the liquefaction evidence is within the range of 0.18 - 0.30 g. Few points are present for PGA values less than 0.18 g (Figure 16).

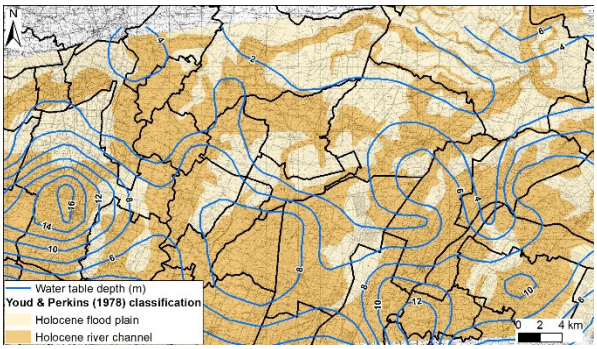

Figure 15. Geological/geomorphological setting following Youd & Perkins (1978) and mean water table depth.

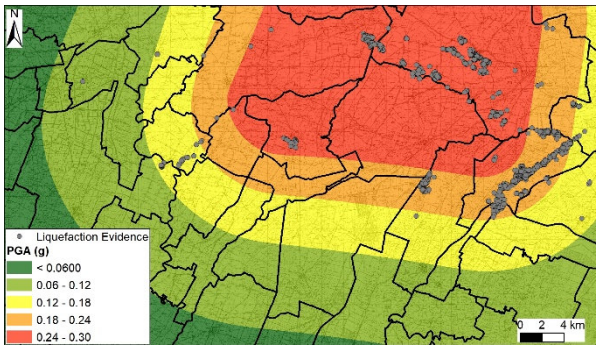

Figure 16. PGA map referred to 2012 Emilia earthquake with magnitude of 5.8

The susceptibility maps of two levels for liquefaction phenomena were shown respectively in Figure 17 and Figure 18. The water table depth of the area is always less than 15 meters, therefore in the first scenario the result class zonation depends on the distribution of Holocene flood plain and river channel deposits, while in the second one it is evident also the contribution of the PGA. The majority of liquefaction events fall within the high and very high susceptibility class.

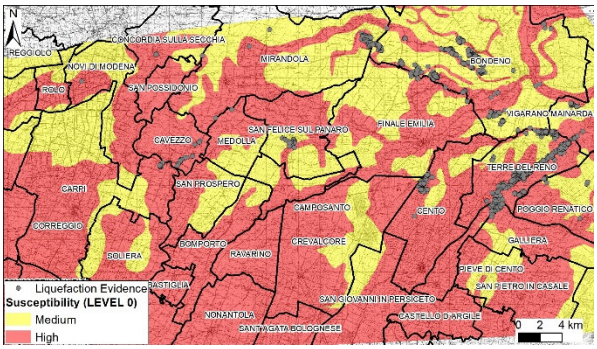

Figure 17. Susceptibility map of level 1 (with geological/geomorphological data and water table) and liquefaction evidence

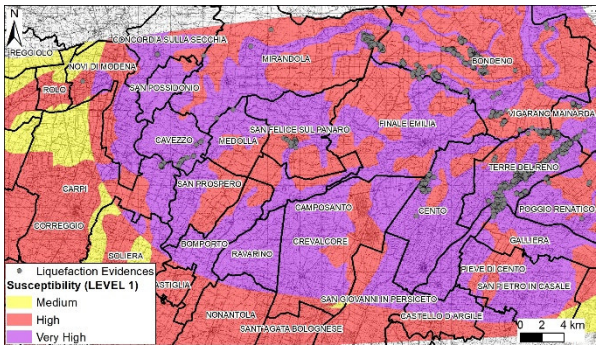

Figure 18. Susceptibility map of level 1(with geological/geomorphological data, water table and PGA) and liquefaction evidence

In order to obtain a liquefaction map at level 2, based on the semi-empirical stress-based approach of Idriss and Boulanger (2008), (Boulanger and Idriss, 2014), geotechnical investigations (CPT or SPT) are necessary. For the study area more than two thousand points representing CPT investigations are available that could be interpolated and used to elaborate a susceptibility map.

A first attempt was made to estimate the LPI index for 12 CPT points localized neighboring the high concentration of liquefaction events and close to boreholes with evidence of sand layers interbedded to silt and clay (Figure 19).

Following the procedure described in figure 3 and using equation 5 the LPI (Liquefaction potential index) was estimated. For 11 examined points the LPI values ranged from 6.8 and 14 with a high potential failure index, while one data shows LPI value of 21.9 with very high potential failure index (Figure 20).

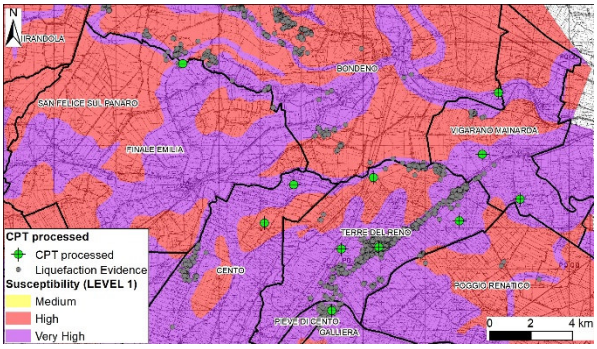

Figure 19. CPT investigations distribution for LPI index evaluation

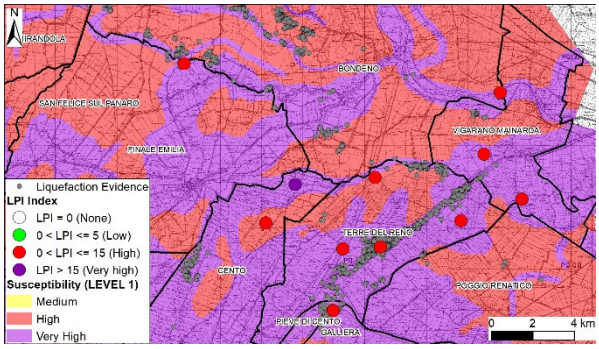

Figure 20. LPI index classes distribution

7. References

Anderson, D., Franke, K.W., Dashti, S., Badanagki, M., Kayen, R., 2019. The over-prediction of liquefaction in alluvially deposited volcanic sediments, Earthquake Geotechnical Engineering for Protection and Development of Environment and Constructions. CRC Press, pp. 1122-1129.

Anderson, K., Nelson, S., Mayo, A., Tingey, D., 2006. Interbasin flow revisited: The contribution of local recharge to high-discharge springs, Death Valley, CA. Journal of Hydrology, 323, 276-302.

Bindi, D., Pacor, F., Luzi, L., Puglia, R., Massa, M., Ameri, G., & Paolucci, R., 2011. Ground motion prediction equations derived from the Italian strong motion database. Bulletin of Earthquake Engineering, 9, 1899-1920.

Boulanger, R.W., Idriss, I.M., 2014. CPT and SPT based liquefaction triggering procedures. Report No. UCD/CGM -14, 1, 134.

Chiaradonna, A. et al., 2018. Numerical simulation of soil liquefaction during the 20 May 2012 M6. 1 Emilia Earthquake in Northern Italy: the case study of Pieve di Cento, pp. 18-21.

Civico, R. et al., 2015. Liquefaction susceptibility assessment in fluvial plains using airborne lidar: the case of the 2012 Emilia earthquake sequence area (Italy). Natural Hazards and Earth System Sciences, 15, 2473-2483.

Cubrinovski, M., Rhodes, A., Ntritsos, N., Van Ballegooy, S., 2019. System response of liquefiable deposits. Soil Dynamics and Earthquake Engineering, 124, 212-229.

Flora, A., Bilotta, E., Lirer, S., Mele, L., Madoni, G., 2023. Liquefaction mechanisms and mitigation techniques. Rivista Italiana di Geotecnica, 2/2023, 33-88.

Idriss, I.M., Boulanger, R.W., 2008. Soil liquefaction during earthquakes. Earthquake Engineering Research Institute. Oakland, CA.

Ishihara, K., Yoshimine, M., 1992. Evaluation of settlements in sand deposits following liquefaction during earthquakes. Soils and foundations, 32, 173-188.

Iwasaki, T., Arakawa, T., Tokida, K.-I., 1984. Simplified procedures for assessing soil liquefaction during earthquakes. International Journal of Soil Dynamics and Earthquake Engineering, 3, 49-58.

Lai, C.G., Bozzoni, F., Mangriotis, M.-D., Martinelli, M., 2015. Soil liquefaction during the 20 May 2012 M5. 9 Emilia earthquake, northern Italy: Field reconnaissance and post-event assessment. Earthquake Spectra, 31, 2351-2373.

Lanzano, G., Luzi, L., D'Amico, V., Pacor, F., Meletti, C., Marzocchi, W., ... & Varini, E., 2020. Ground motion models for the new seismic hazard model of Italy (MPS19): selection for active shallow crustal regions and subduction zones. Bulletin of Earthquake Engineering, 18, 3487-3516.

Lombardi, D., Bhattacharya, S., 2014. Liquefaction of soil in the Emilia-Romagna region after the 2012 Northern Italy earthquake sequence. Natural hazards, 73, 1749-1770.

Minarelli, L. et al., 2022. Liquefied sites of the 2012 Emilia earthquake: a comprehensive database of the geological and geotechnical features (Quaternary alluvial Po plain, Italy). Bulletin of Earthquake Engineering, 20, 3659-3697.

NTC, 2008. Norme tecniche per le costruzioni. Decree of the Minister of the Infrastructures, 14.

Priolo, E. et al., 2012. The Ferrara thrust earthquakes of May-June 2012: preliminary site response analysis at the sites of the OGS temporary network. Annals of Geophysics, 55.

Sciarra, A. et al., 2012. Soil-gas survey of liquefaction and collapsed caves during the Emilia seismic sequence. Annals of Geophysics.

Seed, H.B., Idriss, I.M., 1971. Simplified procedure for evaluating soil liquefaction potential. Journal of the Soil Mechanics and Foundations division, 97, 1249-1273.

Silvestri, F., D'Onofrio, A., 2014. Risposta sismica e stabilità di centri abitati e infrastrutture, La Geotecnica nella difesa del territorio e delle infrastrutture dalle calamità naturali. AGI, pp. 5-60.

Stefani, M., Minarelli, L., Fontana, A., Hajdas, I., 2018. Regional deformation of late Quaternary fluvial sediments in the Apennines foreland basin (Emilia, Italy). International Journal of Earth Sciences, 107, 2433-2447.

Tomasello, G., Porcino, D.D., 2022. Influence of sloping ground conditions on cyclic liquefaction behavior of sand under simple shear loading. Soil Dynamics and Earthquake Engineering, 163, 107516.

Tonkin, Taylor, 2012. Canterbury Earthquakes 2010 and 2011: Land Report as at 29 February 2012. . Earthquake, Commission.

Vaid, Y.P., Stedman, J.D., Sivathayalan, S., 2001. Confining stress and static shear effects in cyclic liquefaction. Canadian Geotechnical Journal, 38, 580-591.

Vannucchi, G. et al., 2012. Soil liquefaction phenomena observed in recent seismic events in Emilia-Romagna Region, Italy. Ingegneria sismica, 2016, 20-30.

Youd, T.L., Perkins, D.M., 1978. Mapping liquefaction-induced ground failure potential. Journal of the Geotechnical Engineering Division, 104, 433-446.

Appendix 1: list of toolchain

Landslide

1.1.1. Coastal and volcanic island (T2.41)

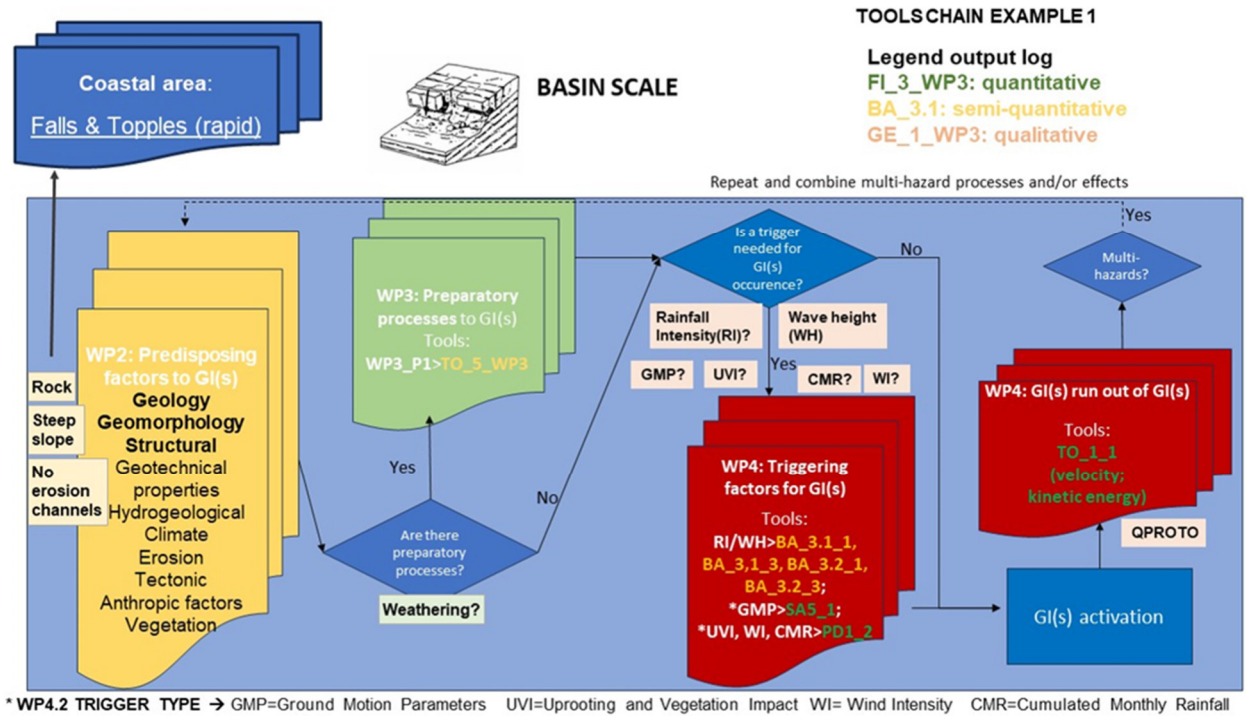

Figure 21 Tool chain for Rapid rock landslides (rockfall) occurring at basin scales. The tools with the asterisk refer to TK2

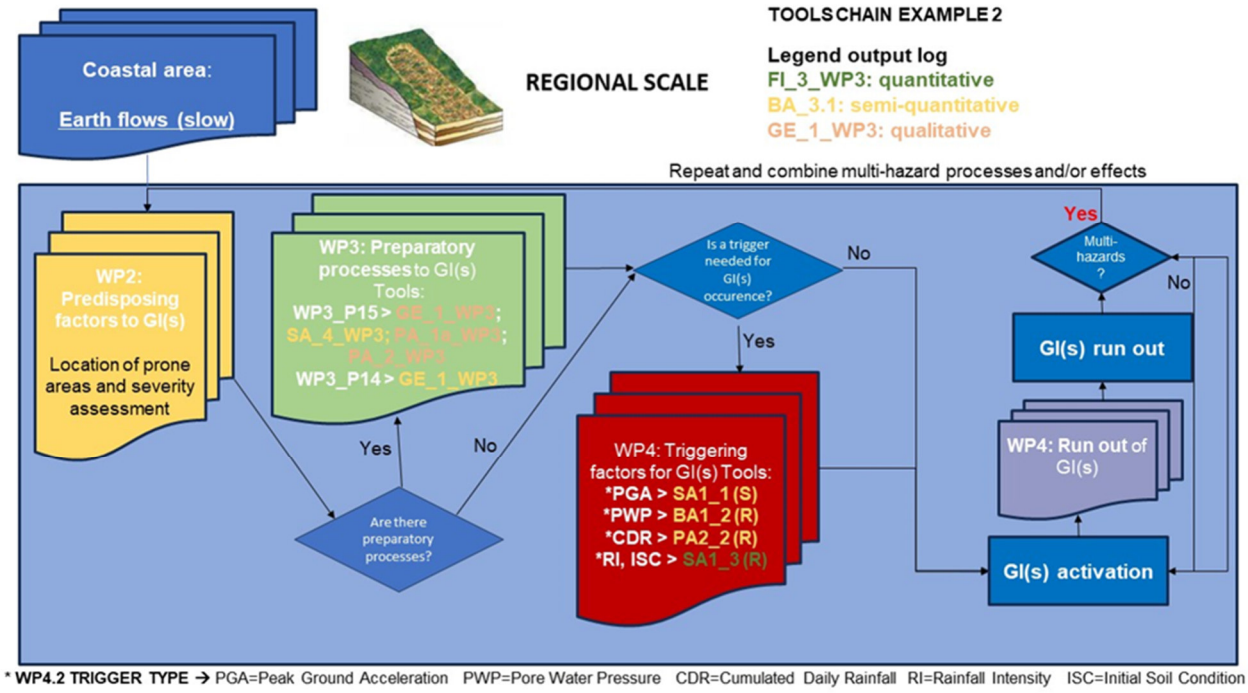

Figure 22: Tool chain for Slow earth flows occurring at regional scales. The tools with the asterisk refer to TK2.

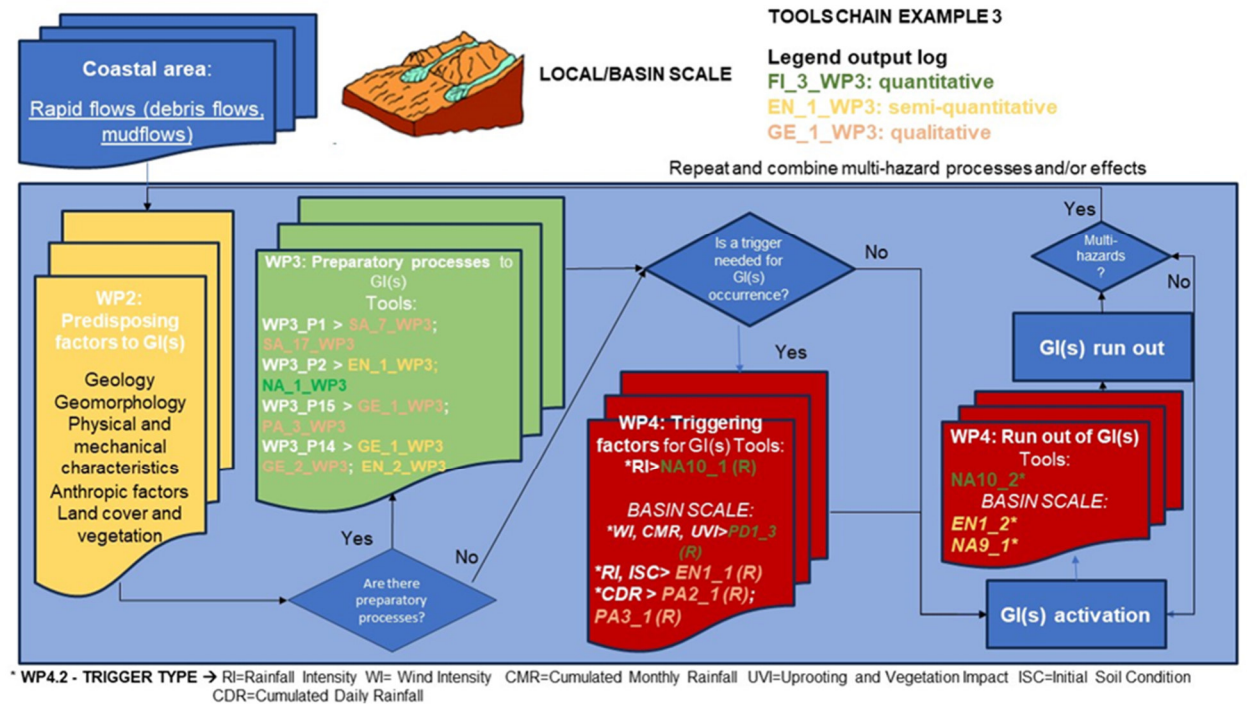

Figure 23: Tool chain for rapid flows, such as debris flows and mudflows, occurring at local/basin scales. The tools with the asterisk refer to TK2.

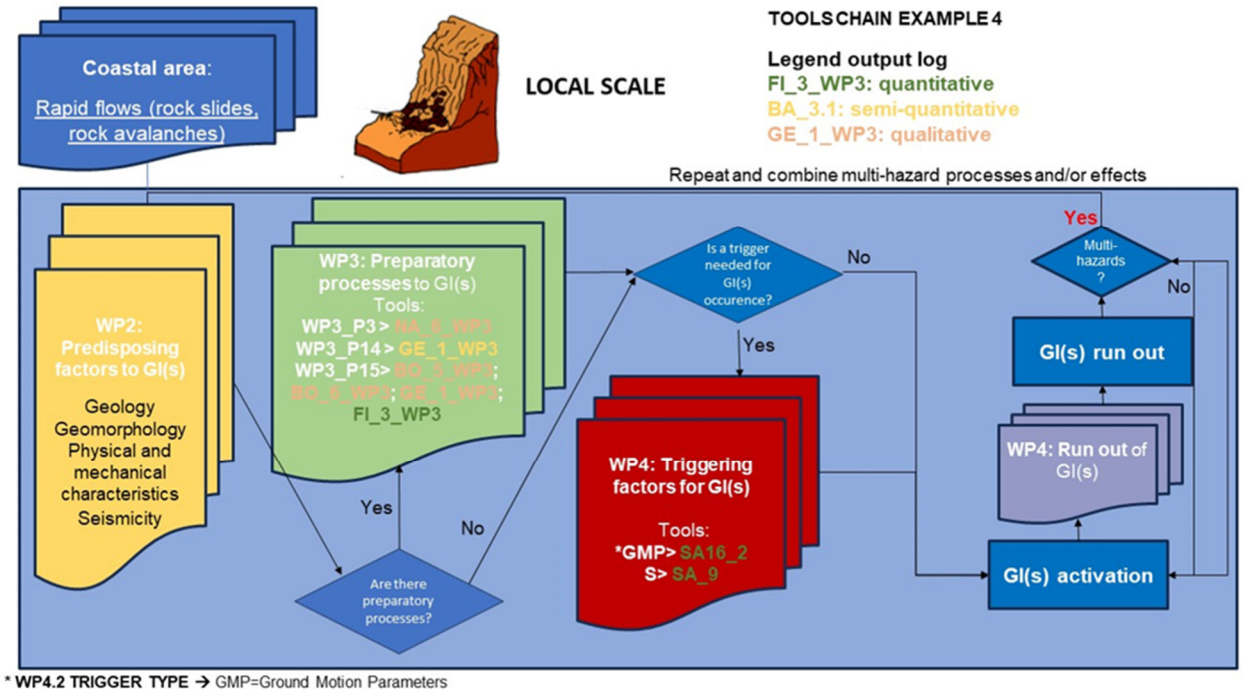

Figure 24 Tool chain for rapid flows, such as rockslides and rock avalanches, occurring at local scales. The tools with the asterisk refer to TK2.

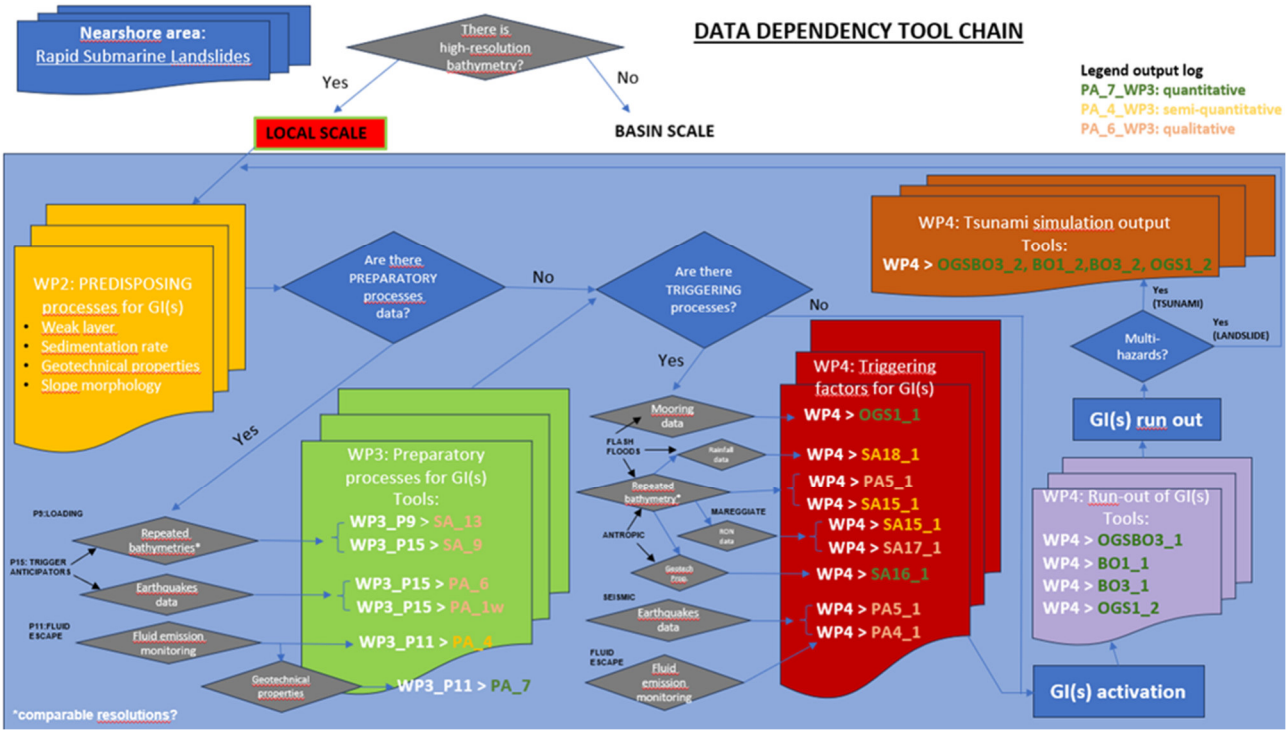

Figure 25 Tool chain for rapid submarine landslides at the local scale in nearshore areas.

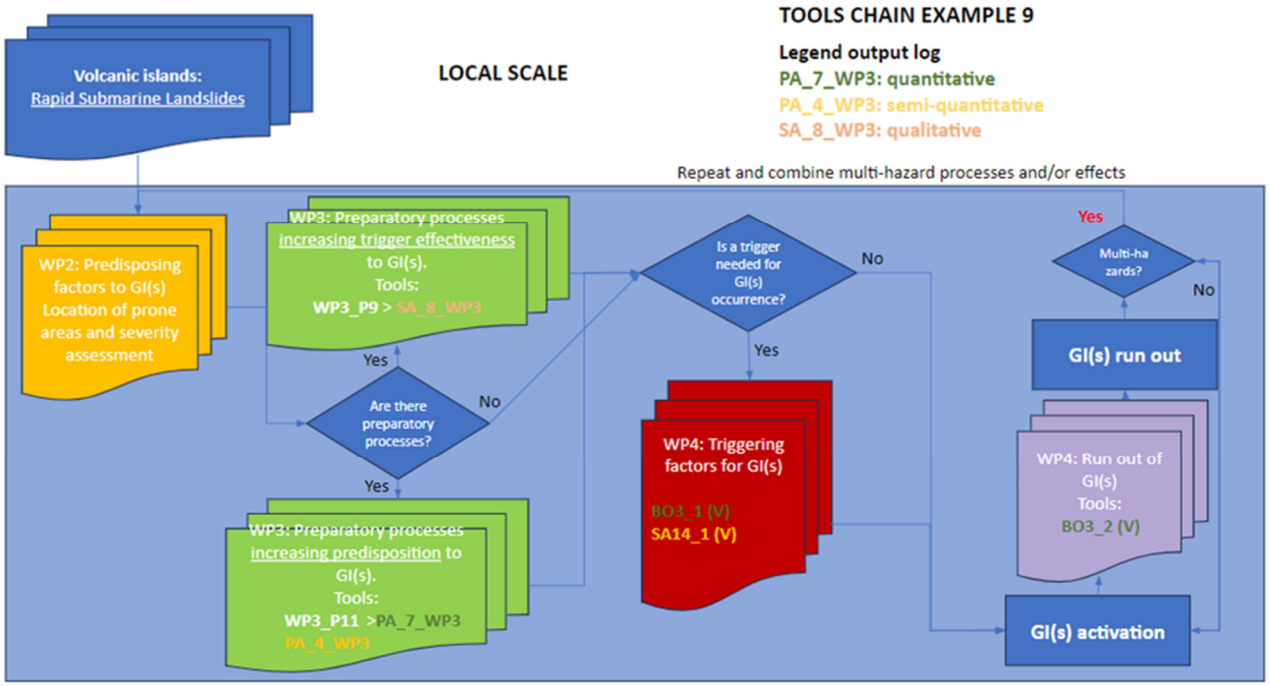

Figure 26 Tool chain for rapid submarine landslides at the local scale in volcanic islands.

1.1.2. Hilly and mountain areas (T2.4.2)

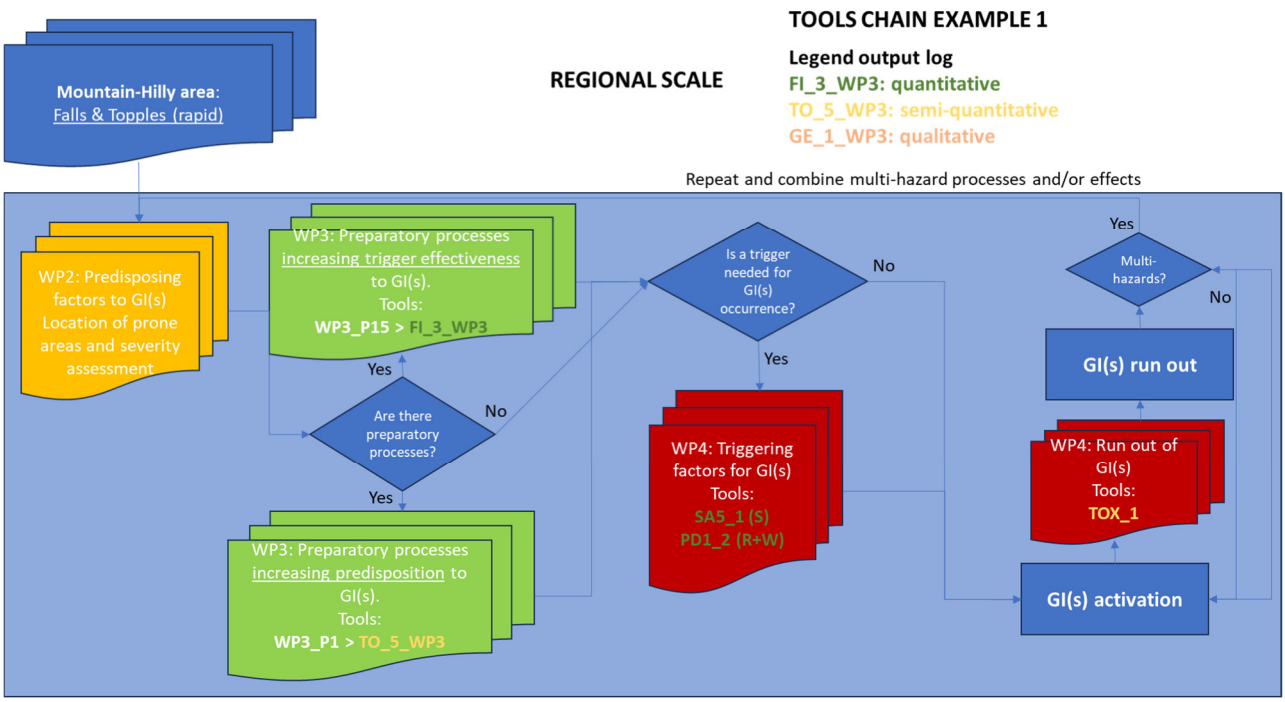

Figure 27: Tools chain for Falls & Topples at regional scale of analysis.

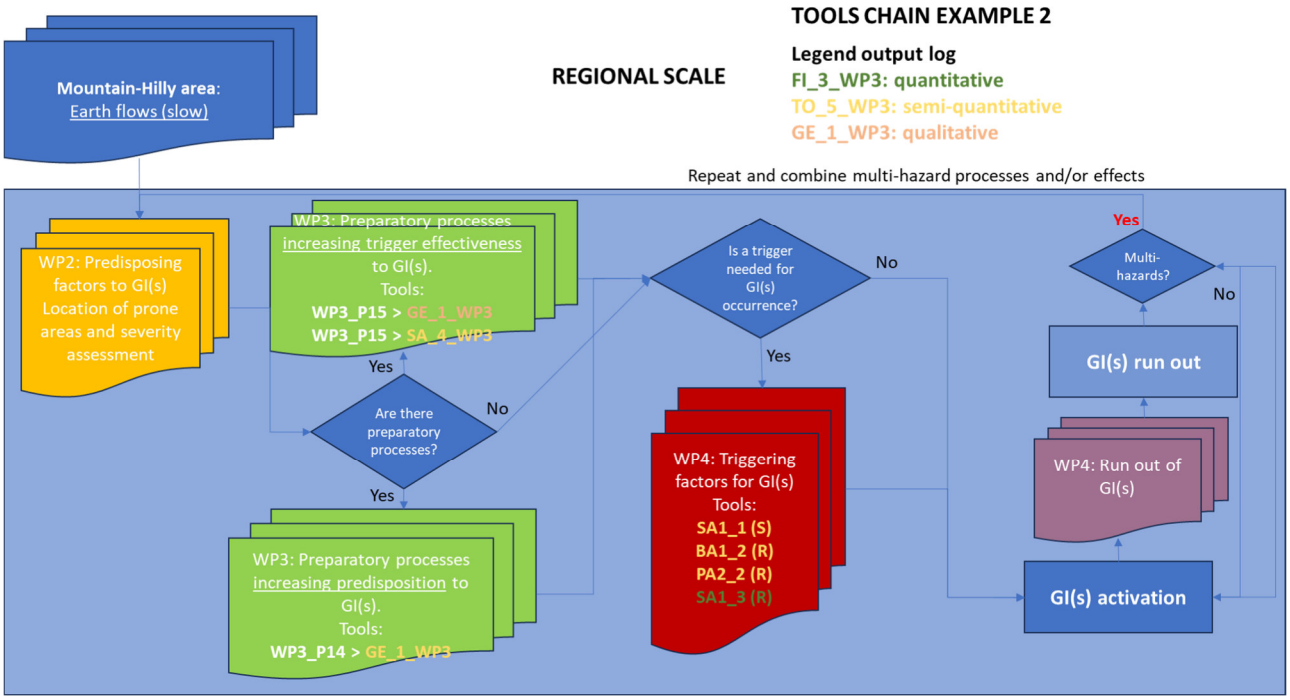

Figure 28: Tools chain for Earth flows at regional scale of analysis.

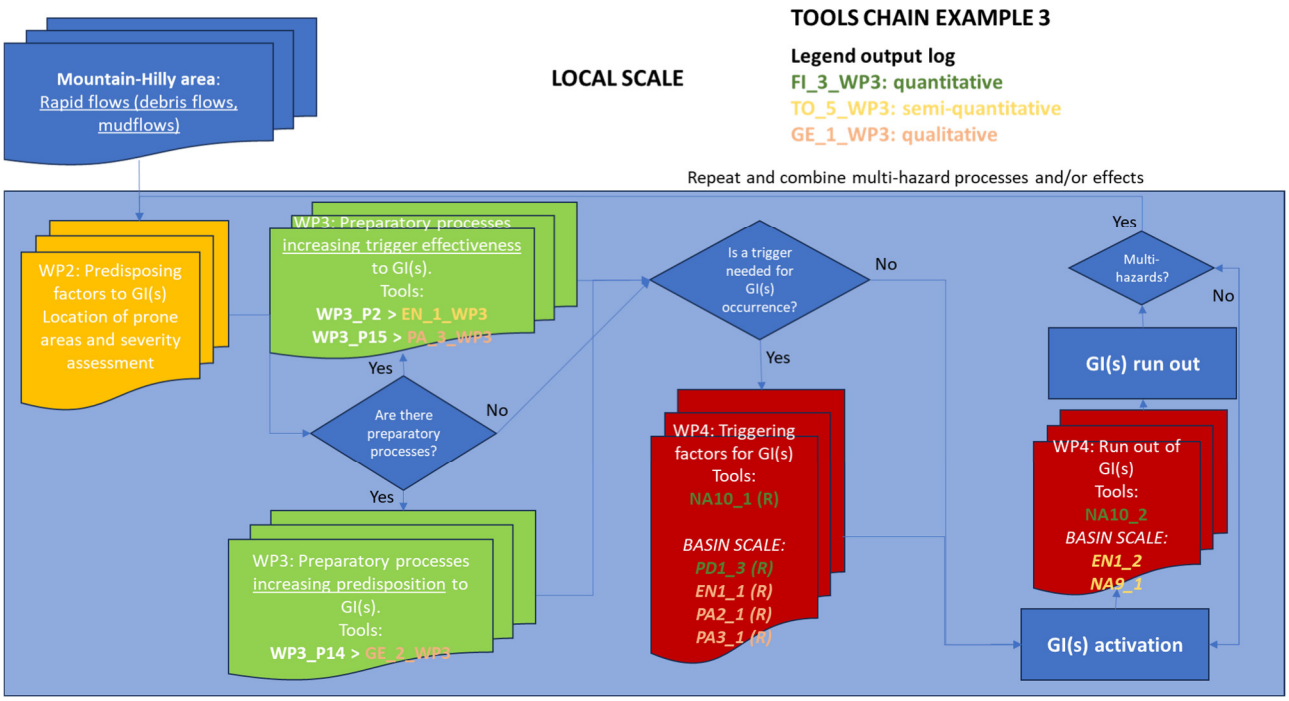

Figure 29: Tools chain for Rapid flows at local scale of analysis.

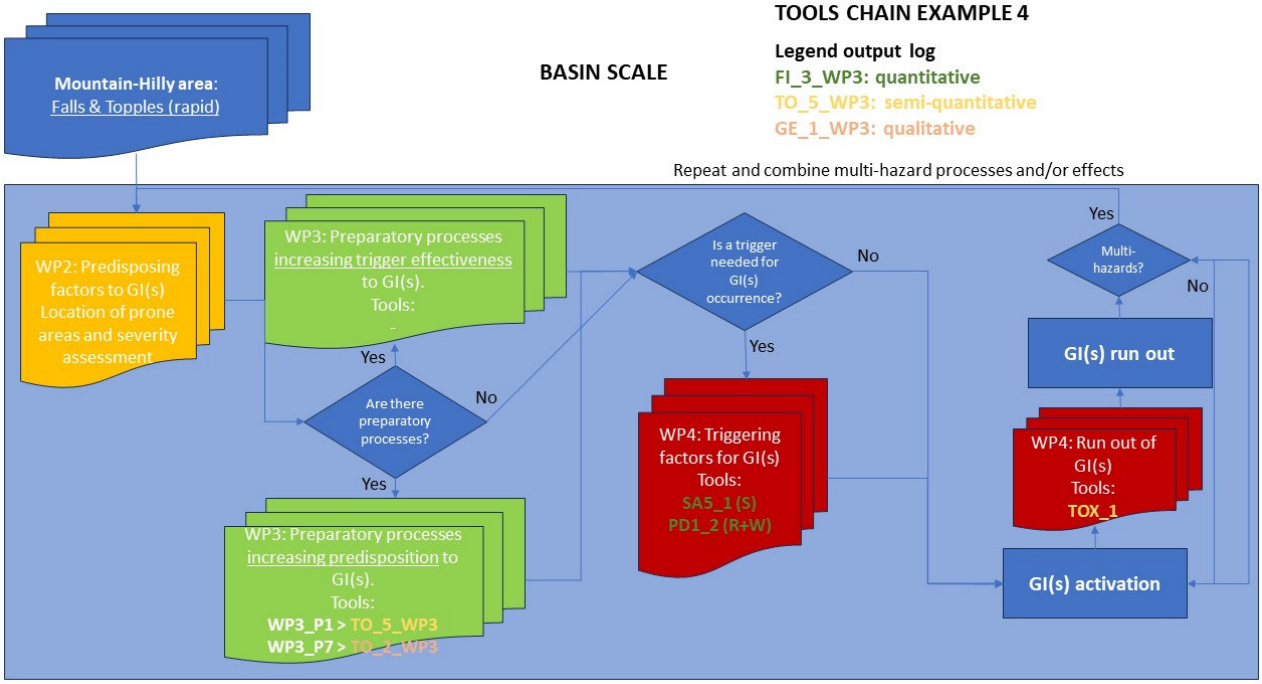

Figure 30: Tools chain for Falls and Topples at basin scale of analysis.

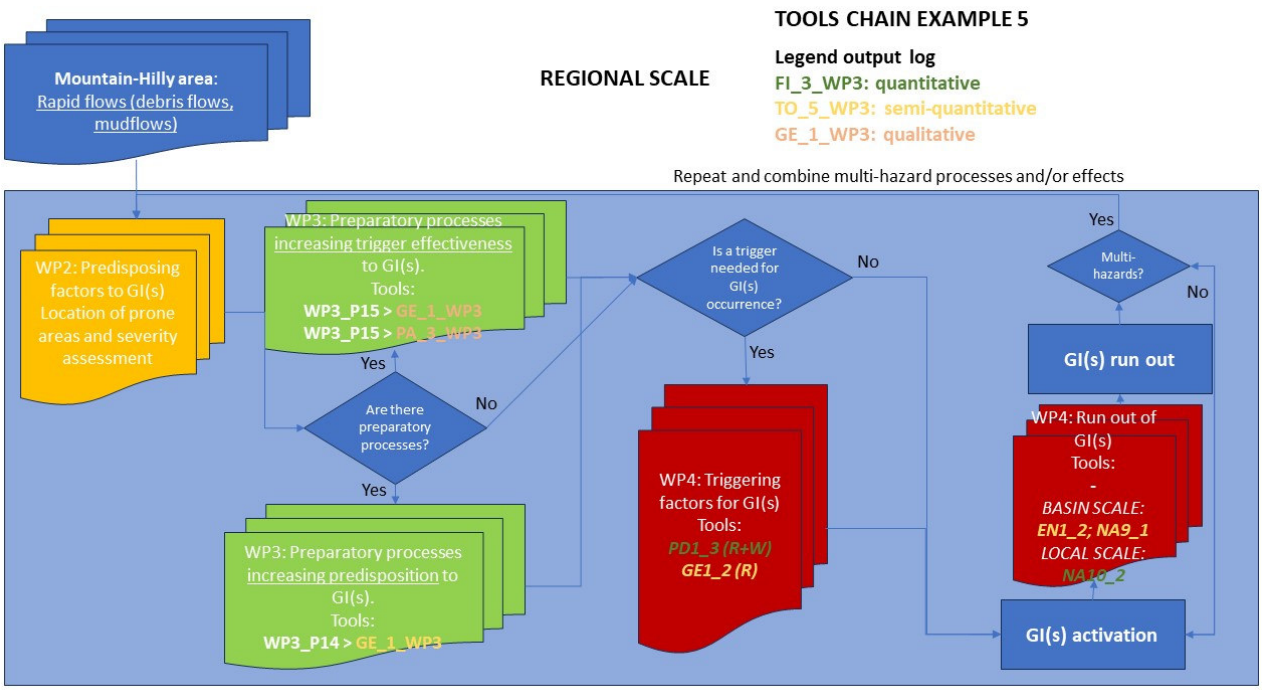

Figure 31: Tools chain for Rapid flows at regional scale of analysis.

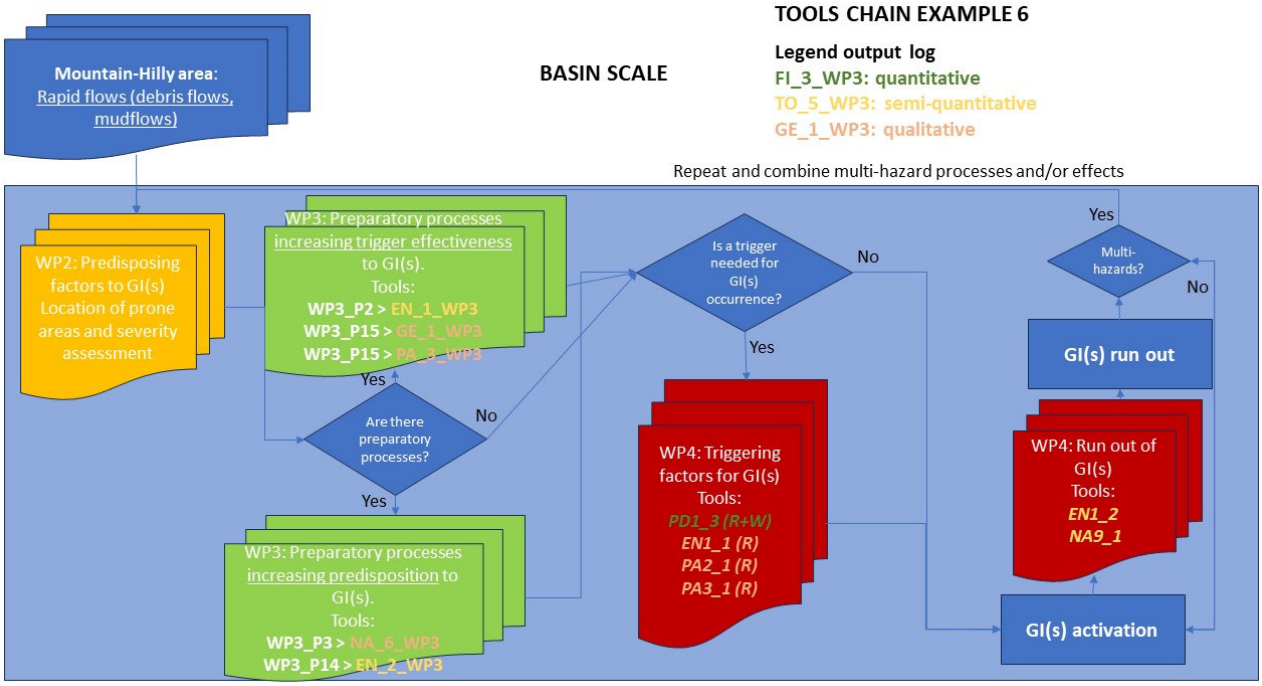

Figure 32: Tools chain for Rapid flows at basin scale of analysis.

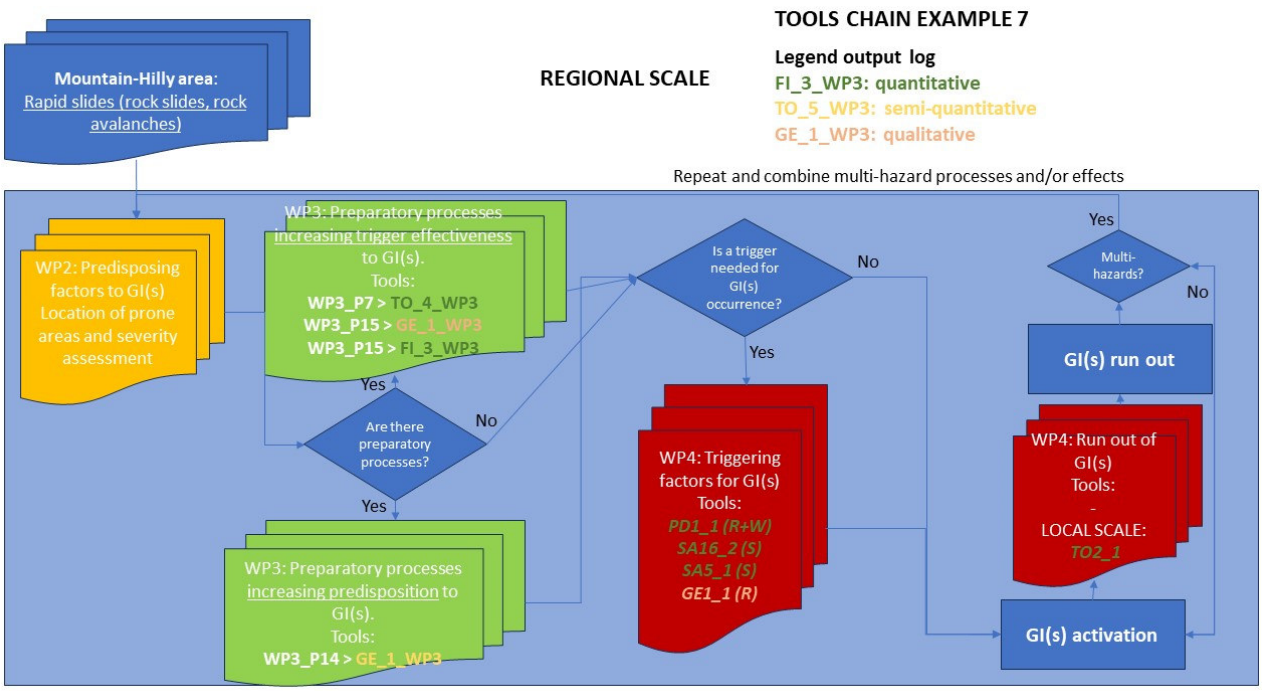

Figure 33: Tools chain for Rapid slides at regional scale of analysis.

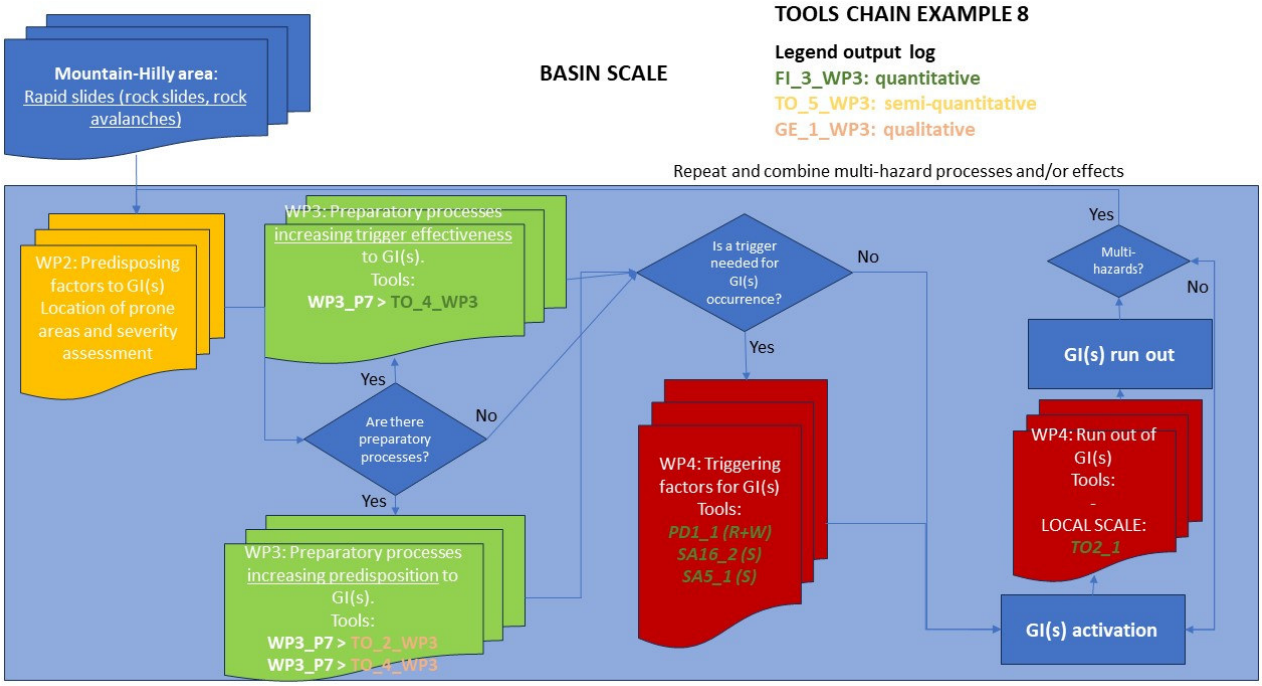

Figure 34: Tools chain for Rapid slides at basin scale of analysis.

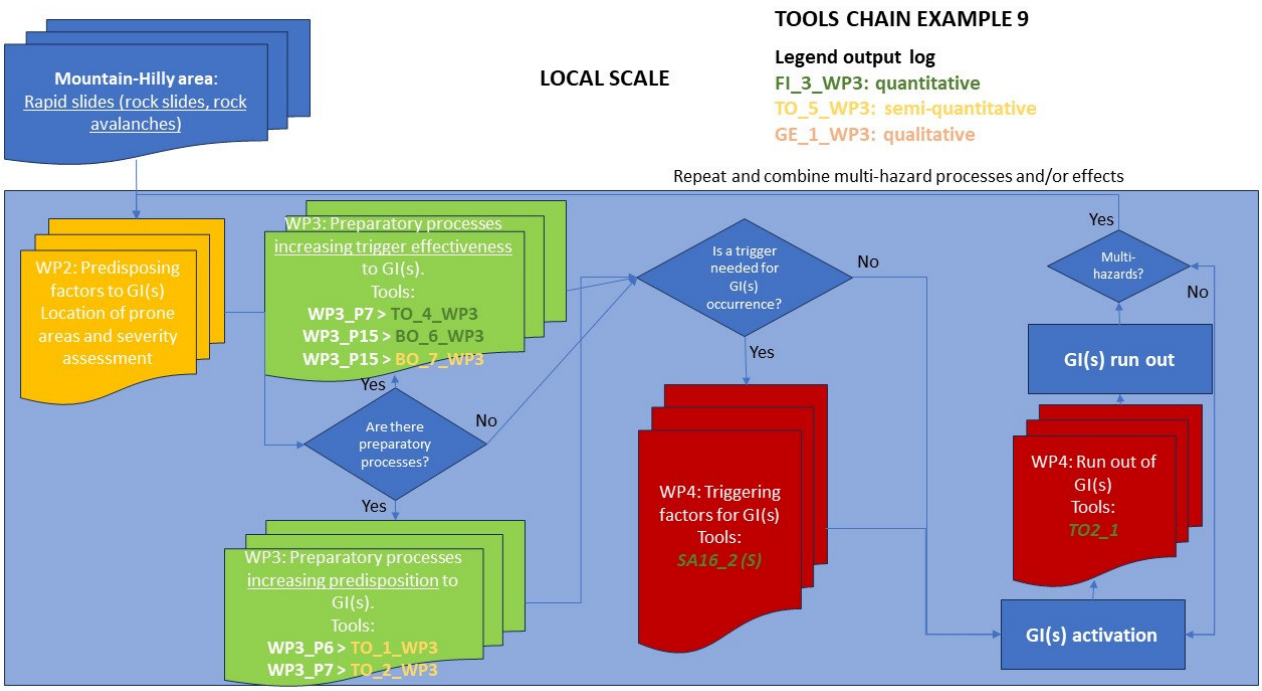

Figure 35: Tools chain example 9 Rapid slides at local scale of analysis.

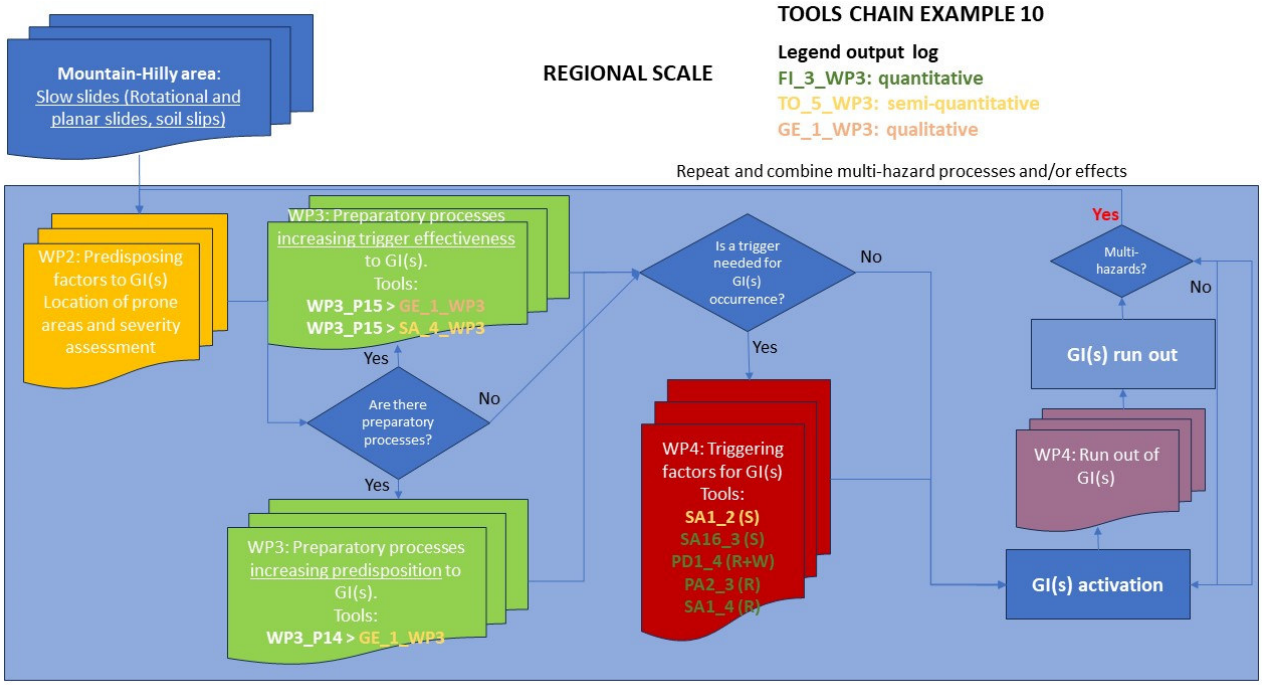

Figure 36: Tools chain for Slow slides at regional scale of analysis.

Subsidence

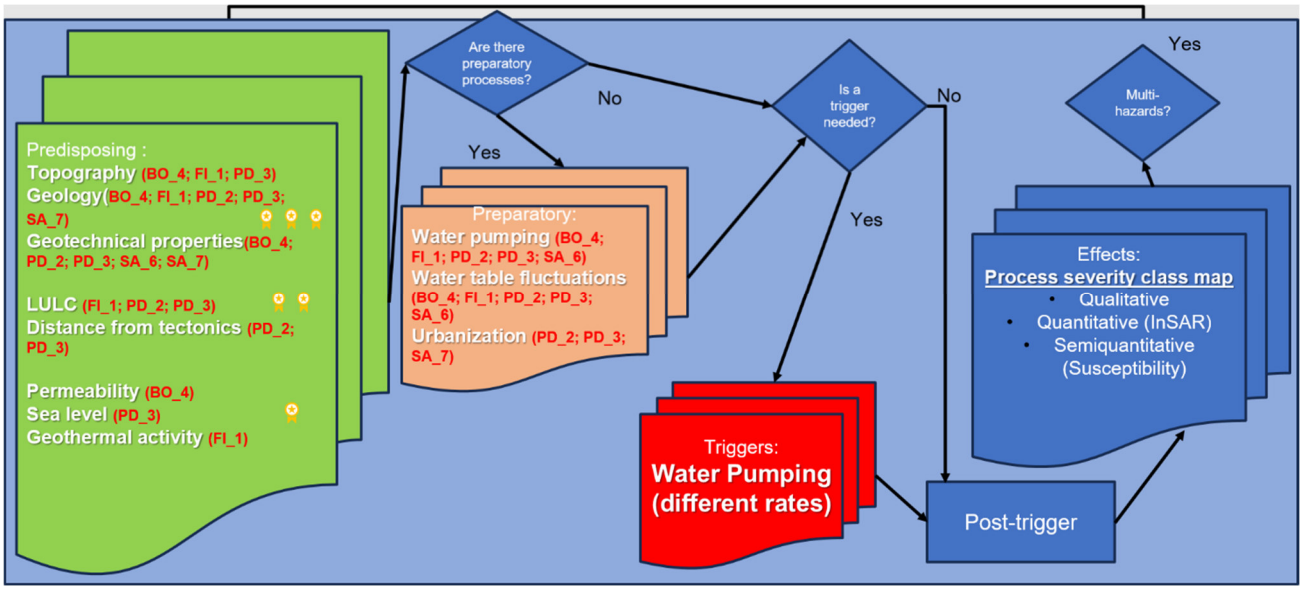

Figure 37 Tool chain for subsidence

Sinkholes

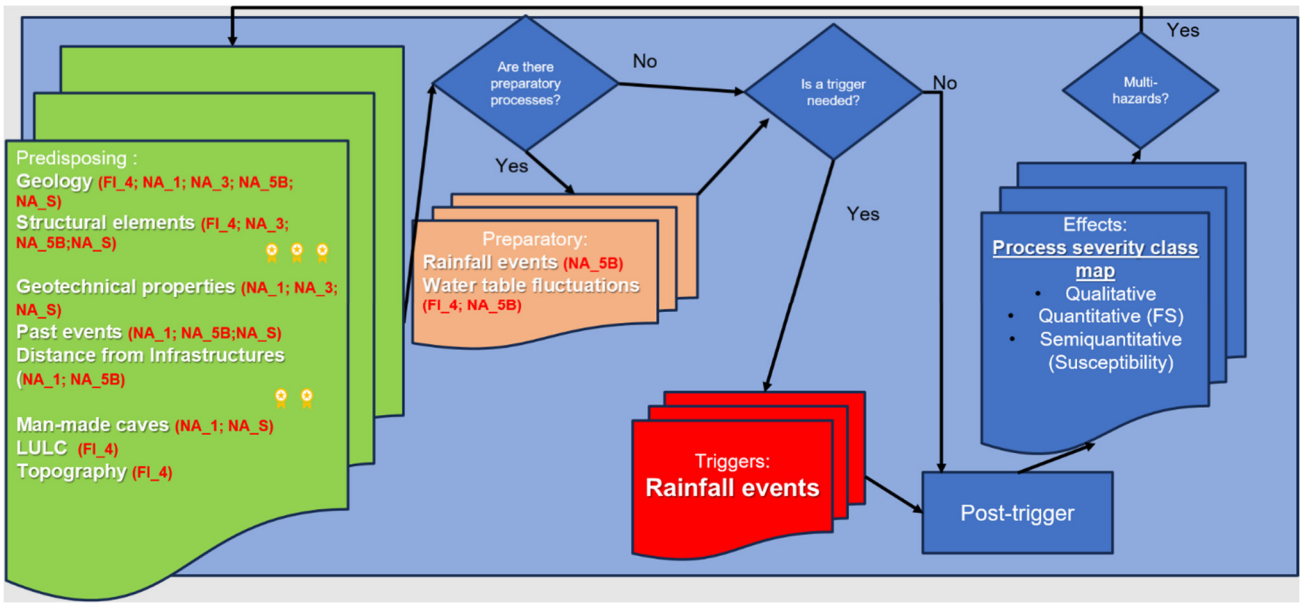

Figure 38 Tool chain for sinkholes

Liquefaction

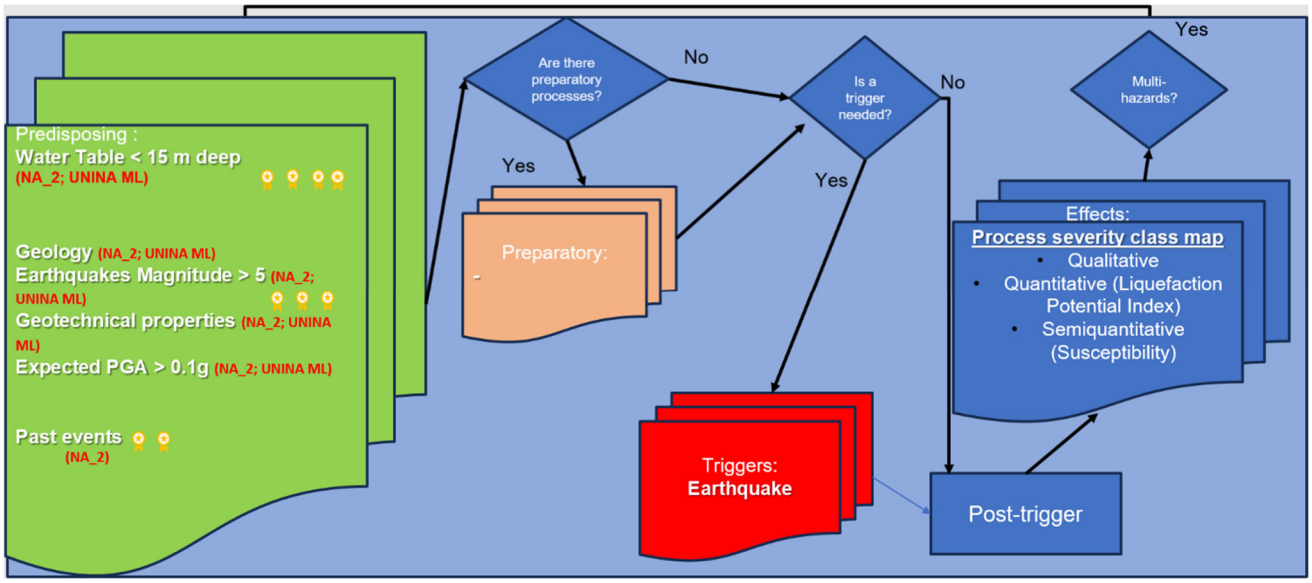

Figure 39 Tool chain for liquefaction